Schweizerische Eidgenossenschaft
Confédération suisse
Confederazione Svizzera
Confederaziun svizra

Federal Department of the Environment, Transport, Energy and Communications DETEC

Swiss Federal Office of Energy SFOE
Energy Research and Cleantech

Final Report March 6, 2025

Ice-Grid

Implementation of ice storage tanks into 5GDHC networks as seasonal storage or load shifting element

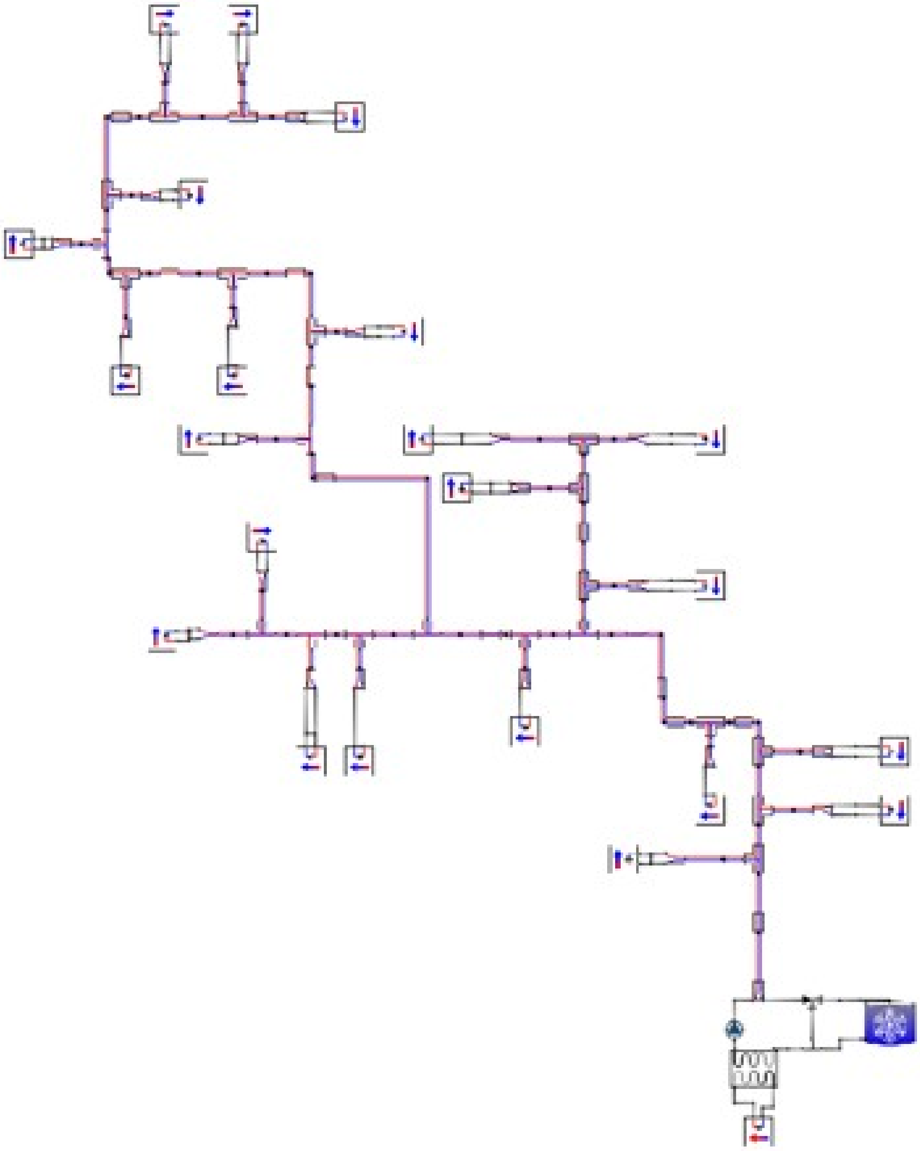

INSTITUT FÜR SOLARTECHNIK

OST Ostschweizer Fachhochschule

Date: March 6, 2025

Place: Rapperswil

Publisher:

Swiss Federal Office of Energy SFOE
Research Programme Solar Heat and Heat Storages
CH-3003 Bern
www.bfe.admin.ch
energieforschung@bfe.admin.ch

Agent:

Institut für Solartechnik SPF, Ostschweizer Fachhochschule OST
Oberseestr. 10
CH-8640 Rapperswil
www.spf.ch

Authors:

Dr. Daniel Carbonell, extern.carbonell@ost.ch, daniel.carbonell@dcarbo.es
Damian Birchler, damian.birchler@ost.ch
Dr. Alex Hobé, alex.hobe@ost.ch
Florian Ruesch, florian.ruesch@ost.ch

Collaborators:

Maike Schubert
Dr. Martin Neugebauer

SFOE Head of domain: Andreas Eckmanns, andreas.eckmanns@bfe.admin.ch
SFOE Programme manager: Stephan A. Mathez, stephan.a.mathez@solarcampus.ch
SFOE Contract number: SI/502280-01

Contents

List of abbreviations and acronyms

AWHX Air-to-Water Heat Exchanger
CTS Constant Temperature Source
DH District Heating
5GDHC 5th Generation of District Heating and Cooling
DHW Domestic Hot Water
EZL Energie Zürichsee Linth
FLH Full Load Hours
GUI Graphical User Interface
HP Heat Pump
HX Heat Exchanger
HTF Heat Transfer Fluid
SH Space Heating
SPF Seasonal Performance Factor
SOC State-Of-Charge
WW Waste Water
WWTP Waste Water Treatment Plant
WWHX Waste Water Heat Exchanger
WWHS Waste Water Heat Source
CTS Constant Temperature Source
CTS Constant Temperature Source
DHW/SH ratio between DHW and SH demands
$\mathbf{M_{fice}}$ mass ice fraction
$\mathbf{M_{fice,max}}$ maximum mass ice fraction
$\mathbf{V_{ice,lat}}$ scaling factor for latent ice storage volume

Abstract

According to the Energy Strategy 2050+, the share of district heating (DH) in Switzerland's heat supply is set to rise sharply to around 30 %. An increasingly popular type of district heating (DH) network is the anergy network, which distributes energy from a low-temperature source to decentralized heat pumps installed in buildings. Many low-temperature energy sources available in Switzerland have limitations, either in their power output (e.g., waste heat from sewage treatment plants) or in their availability during cold winter days, if at all (e.g., solar thermal energy). Due to the high amount of energy released (or absorbed) during the liquid/solid phase transition of water, ice storage are suitable for storing large amounts of energy at temperatures near 0 °C. For this reason, ice storages are being used in buildings as an energy source for heat pumps in Switzerland, in so-called solar-ice systems. However, until now, there has been a lack of analysis on integrating large-scale ice storage into district heating networks. In IceGrids, we explored the energetic feasibility and economic viability of integrating ice storages into low-temperature district heating networks, also known as 5th generation district heating and cooling (5GDHC). As a case study, our investigation focused on the Jona energy network, which utilizes waste heat from a waste water treatment plant (WWTP) to supply decentralized heat pumps, making the heat usable. Ice storage tanks can be easily integrated into 5GDHC networks that employ an antifreeze heat transfer fluid, as the Jona network. However, freezing of the heat exchanger on the sewage treatment plant side must be prevented by a partial re-circulation from the flow pipe. Based on the results in this study, the following findings emmerge: In combination with power limited waste heat sources, even small ice storage volumes are sufficient to bridge power peaks in winter. As a lot of surplus waste heat is readily available for regenerating ice storage systems during the transition period, ice storage systems can more than double the capacity of such sources. When combining ice storage tanks with scalable seasonal heat sources (e.g.outdoor air or solarthermal energy), ice storage sizes of approx. 0.6 m^3/MWh are required to enable year-round operation of the network at 0 °C.

Zusammenfassung

Gemäss der Energiestrategie 2050+ soll der Anteil der Fernwärme an der Wärmeversorgung in der Schweiz auf rund 30% stark ansteigen. Dabei werden vermehrt sogenannte Anergienetze erstellt, welche die Energie einer Niedertemperaturquelle auf deren Temperaturniveau an dezentral in den Gebäuden installierte Wärmepumpen verteilen. Viele der in der Schweiz verfügbaren Niedertemperaturquellen, wie z.B. Abwärme aus Kläranlagen, sind in ihrer Leistung begrenzt oder stehen im Falle der Solarthermie an kalten Wintertagen nur eingeschränkt oder gar nicht zur Verfügung. In diesem Projekt wird untersucht, inwieweit Eisspeicher in Wärmenetze integriert werden können, um solche Leistungsengpässe oder Lücken zu überbrücken. Aufgrund des hohen Energieinhalts beim Phasenübergang eignen sich Eisspeicher zur Speicherung großer Energiemengen bei tiefen Temperaturen von null Grad Celsius. Aus diesem Grund werden auch in der Schweiz immer mehr und immer grössere Eisspeicher als Energiequelle für Wärmepumpen eingesetzt. Als Beispiel für die Untersuchungen diente der Energieverbund Jona, der die Abwärme der ARA in einem an dezentrale Wärmepumpen verteilt und damit nutzbar macht. In frostschutzgefüllten Netzen können Eisspeicher einfach und direkt eingebunden werden. Das Einfrieren des Wärmetauschers auf der Kläranlagenseite muss dabei durch eine Beimischung aus dem Vorlauf verhindert werden. In Ergänzung zu derartigen, leistungsbegrenzten Abwärmequellen reichen bereits kleine Eisspeichervolumina aus, um Leistungsspitzen im Winter zu überbrücken. Da aber in der Übergangszeit bereits viel überschüssige Abwärme zur Regeneration von Eisspeichern zur Verfügung steht, können grössere Eisspeicher die Kapazität solcher Quellen mehr als verdoppeln. Eisspeicher können ebenfalls mit skalierbaren saisonealen Wärmequellen wei der Aussenlust oder Solarthermie kombiniert werden. Bei einer grosszügigen Dimensionierung dieser Quellen sind Eisspeichergrössen von ca. 0.6 m^3/MWh Bedarf erforderlich, um einen ganzjährigen Betrieb des Netzes bei 0 °C zu ermögliche

Résumé

Selon la stratégie énergétique 2050+, la part du chauffage à distance dans l'approvisionnement en chaleur en Suisse doit fortement augmenter pour atteindre environ 30%. Dans ce contexte, de plus en plus de réseaux dits d'énergie sont mis en place, qui distribuent l'énergie d'une source à basse température à son niveau de température à des pompes à chaleur installées de manière décentralisée dans les bâtiments. De nombreuses sources d'énergie à basse température disponibles en Suisse, telles que les rejets thermiques des stations d'épuration, ont une puissance limitée ou, dans le cas de l'énergie solaire thermique, ne sont disponibles que de manière restreinte, voire pas du tout, les jours d'hiver froids. Ce projet étudie dans quelle mesure les accumulateurs de glace peuvent être intégrés dans les réseaux de chaleur afin de pallier de tels goulots d'étranglement ou lacunes. En raison du contenu énergétique élevé lors de la transition de phase, les accumulateurs de glace se prêtent au stockage de grandes quantités d'énergie à des températures basses de zéro degré Celsius. C'est pour cette raison qu'en Suisse aussi, on utilise de plus en plus d'accumulateurs de glace, et de plus en plus grands, comme source d'énergie pour les pompes à chaleur. Le réseau énergétique de Jona, qui distribue la chaleur résiduelle de la STEP dans un réseau de pompes à chaleur décentralisées et la rend ainsi utilisable, a servi d'exemple pour les études. Dans les réseaux remplis d'antigel comme ce réseau exemple, les accumulateurs de glace peuvent être intégrés facilement et directement. Le gel de l'échangeur de chaleur du côté de la STEP doit cependant être évité par un mélange avec le circuit d'alimentation. En complément de telles sources de chaleur résiduelle à puissance limitée, de petits volumes d'accumulation de glace suffisent déjà pour surmonter les pics de puissance en hiver. Cependant, étant donné qu'une grande quantité de chaleur résiduelle est déjà disponible pour régénérer les accumulateurs de glace pendant la période de transition, des accumulateurs de glace plus grands peuvent plus que doubler la capacité de telles sources. Les accumulateurs de glace peuvent également être combinés avec des sources de chaleur saisonnières modulables, telles que l'air extérieur ou l'énergie solaire thermique. Si ces sources sont largement dimensionnées, des volumes de stockage de glace d'environ 0.6 m^3/MWh sont nécessaires pour permettre au réseau de fonctionner toute l'année à 0 °C.

Main findings

- The open source extensions to both TRNSYS/pytrnsys we have developed in this project simplify the modelling of 5GDHC.
- A direct integration of an ice storage in a 5GDHC network is possible when an anti-freeze heat transfer fluid is used in the network.
- The integration of an ice storage allows a significant extension of the demand met by existing sources.
- In the combination with scalable sources like ambient air or solar thermal collectors, ice storage volumes of at least 0.6 m^3_{lat}/MWh are needed, where m_{lat} refers to the volume of the ice storage that can be frozen (which depends on technology used) and the MWh refer to the total heat demand of the DH.

1 Introduction

1.1 Motivation and project idea

Traditional thermal networks deliver usable supply temperatures for Space Heating (SH) and Domestic Hot Water (DHW) with a temperature of the Heat Transfer Fluid (HTF) of 70 °C and more. However, renewable sources for high temperature heat are limited (e.g., wood, waste incineration, waste heat or renewable fuels) and many high temperature thermal networks with renewable sources cover about 10 % to 20 % of their demand with fossil burners (Nussbaumer et al., 2017). Most of the remaining renewable sources for District Heating (DH) systems are low temperature sources as lakes, rivers, groundwater, shallow geothermal or low temperature waste heat (Sres and Nussbaumer, 2014), which need heat pumps to be lifted to a usable temperature level. Large central heat pumps can be used to operate classical networks at "hot" temperatures, however their efficiency is strongly dependent on temperature lift.

Low temperature or "anergy" networks are thermal grids which distribute the energy at the temperature level of the source (25 °C and lower) to decentralised heat pumps that provide the temperature lift needed for the specific application. Modern buildings with low SH demand temperatures allow a much smaller lift compared to a centralised heat pump increasing the heat pump operation efficiency. Moreover, reducing the temperature reduces heat losses and eliminates the need of pipe insulation. However, lower temperatures in thermal networks call for higher mass flow rates which in turn increase the costs for the installation of piping due to the requirement of larger diameters. Roughly speaking the higher cost for piping is compensated by the lower need of insulation and the higher need for pumping is overcome by the higher energetic efficiency of the heat pumps. While in German speaking countries the terms "Anergienetz" (anergy network) or "Niedertemperaturnetz" (low temperature network) are common, in an international context such networks are often referred to as 5^{th} Generation District Heating and Cooling or 5GDHC networks (Buffa et al., 2019). Despite 5GDHC are a relatively new thermal network type, the number of 5GDHC networks has increased significantly since 2010. Fig. 1 shows the distribution of thermal networks in Switzerland classified by their temperature levels over time. In the future a further increase in the employment of 5GDHC networks is expected (Sres and Nussbaumer, 2014).

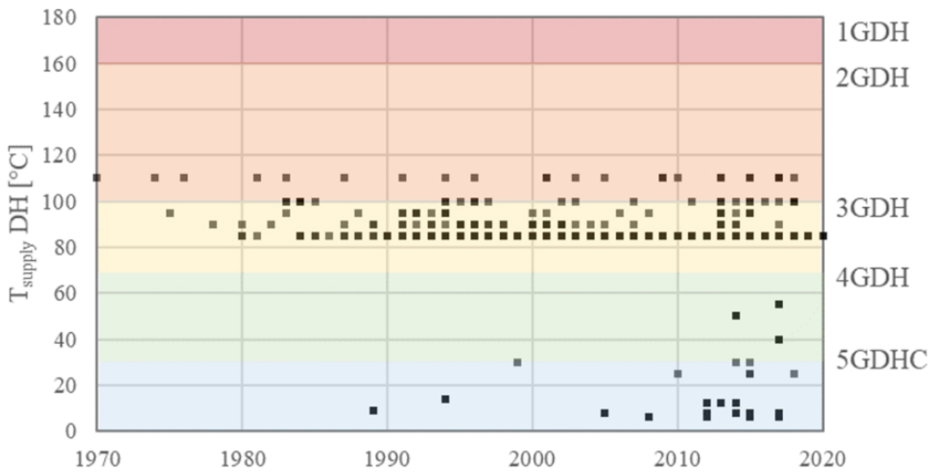

Figure 1: Distribution of Swiss thermal networks classified by estimated temperature levels (Caputo et al., 2021).

The low operational temperatures of 5GDHC networks allow to use a wide range of heat sources. However, research is needed to investigate the advantages and shortcomings of using different heat sources and analyse the synergies of combining them. Furthermore, how these DH grids will cover the winter peak loads needs to be investigated. On top of that, about 40 % of the potential of heat sources for 5GDHC come from limited sources like sewage plants, ground water, rivers, geothermal or heat rejected from cooling demands, e.g., from data centers (Sres and Nussbaumer, 2014). The use of limited heat sources in thermal networks often means a shortage in winter periods. On the other hand, excess heat is often available in summer. Therefore, seasonal thermal energy storages that can shift heat at the network level from summer to winter might become necessary to cover the high thermal demand in winter while reducing fossil fuel needs.

Different kinds of seasonal thermal energy storages are used today, including sensible, ground and aquifer thermal energy storages. Water has a sensible storage capacity of 1.17 kWh/(m^3K). Assuming a temperature difference of 30 K results in an energy storage density of 35 kWh/m^3. Pit storages filled with gravel and water, soil or rocks have a lower energy storage density (Haller and Ruesch, 2019).

By utilizing ice storage concepts, the latent heat of water, 92.4 kWh/m^3, can be effectively harnessed.. Considering that the maximum ice fraction will be limited to around 50 % to 80 %, the energy storage density is in the range of 80 kWh/m^3 to 110 kWh/m^3 considering latent and sensible heat with maximum temperature difference of 30 K. Ice storages have smaller thermal losses compared to the other options listed above as they are operated for long periods at a temperature of 0 °C. Indeed gains from the surrounding ground are expected in winter.

However, the phase transition of water at 0 °C means that heat can also be transported in the network at that temperature. To ensure this without the risk of freezing of the HTF, the network must be operated with an antifreeze solution. Even though many 5GDHC grids are operated with water, there are numerous current DH installations which are operated with ethanol-water mixtures as frost protection, e.g. the DH grids in Zug (lake water as a source), Uster and Rapperswil Jona (with waste heat from the wastewater treatment plant as a source). The use of antifreeze as a heat transfer medium in the grid enables the direct integration of ice storage tanks. However, up to date, there is not a single 5GDHC with an ice storage integrated. An ice storage within a 5GDHC network can have two main functions: i) provide peak power in winter for limited sources such as waste heat or ground water or ii) store the excess summer energy seasonally to be used in winter. The larger the seasonality of the source the larger the potential for ice storages. However, even a constant source can benefit from the us of an ice storage due to the seasonality of the heat demand. Moreover, using the short-term capacity of ice storages within thermal networks can help stabilising the heat supply in the thermal network.

1.2 Project objectives

The overall goal of this project was to quantify the potential and the effects of ice storage tanks used within 5GDHC networks. Ice storage tanks are expected to be a benefit in 5GDHC with limited heat sources. Different combinations of heat sources were analyzed using detailed dynamic system simulations with *TRNSYS*. Heat sources studied were waste heat of sewage plants and a generalised constant source (for example from data center cooling), air heat exchangers and solar thermal collectors. Different control and integration strategies have been tested and the most important factors influencing the performance of thermal networks with ice storage tanks have been identified.

The specific objectives of the project are:

- Describe typical network configurations with large potential for the implementation of ice storage tanks.
- Adapt the simulation framework "pytrnsys" in order to enable the simulation of 5GDHC networks and make it available to the research community.
- Analyse the potential of ice storages in 5GDHC networks. The focus will be on identifying the main influencing factors on the performance of thermal networks with an integrated ice storage.
- Give simple rules for the implementation and the dimensioning of ice storages in thermal networks considering both long-term as well as short-term storage concepts.
- Make our simulation framework publicly available, facilitating the further development and uptake of these concepts in the research community.

1.3 Typical 5GDHC and potentials

The use of low temperature sources for thermal networks increased by a factor of 10 between 2010 and 2020, especially in districts with low energy density, where low temperature networks are preferable to higher temperature sources (Hangartner and Ködel, 2021). Prognoses from Sres and Nussbaumer (2014) expect a use of 17 TWh per year from low temperature heat sources in the year 2050 in Switzerland. This would result in a further increase of the use of low temperature sources by a factor of 9 between 2020 and 2050 (Hangartner and Ködel, 2021). According to Hangartner and Ködel (2021), 15 % of the energy for low temperature thermal networks (1.9 TWh/a) will be supplied from sewage plants in 2050 with an additional 15 % provided from rivers. In places where no other heat source is available one can use solar thermal or an air heat exchanger for regenerating the ice storage.

In the SFOE project BigIce (Carbonell et al., 2021), the energetic potential of solar-ice systems for multi-family buildings was shown. Seasonal performance factors of about 4 can be reached all over Switzerland with well dimensioned systems. The concept of a solar-ice system was scaled and adapted to low temperature thermal networks in the project Ice-Grid. Hence, in the current project the combination of an ice storage with solar thermal collectors as the only renewable heat source for a low temperature thermal network will be explored, too. Furthermore, concepts which replace the solar thermal collectors with cheaper air heat exchangers are examined as well.

1.3.1 Network topologies

The operative temperature of district heating networks has steadily declined over the last century. This temperature reduction has the goal of meeting heating and cooling demands, while simultaneously minimising both heat losses and distribution costs. Where the First Generation District Heating (1GDH) networks had supply temperatures of more than 100 °C, the novel low-temperature networks referred to as Fifth Generation District Heating or Cooling (5GDHC) networks have network temperatures below 30 °C (Buffa et al., 2019). This development occurred in a series of steps. The steam used in the first generation was replaced in 2GDH networks by pressurized hot water with temperatures above 100 °C. The next evolution achieved in 3GDH was to use water at atmospheric pressure with temperatures between 80 °C to 90 °C.

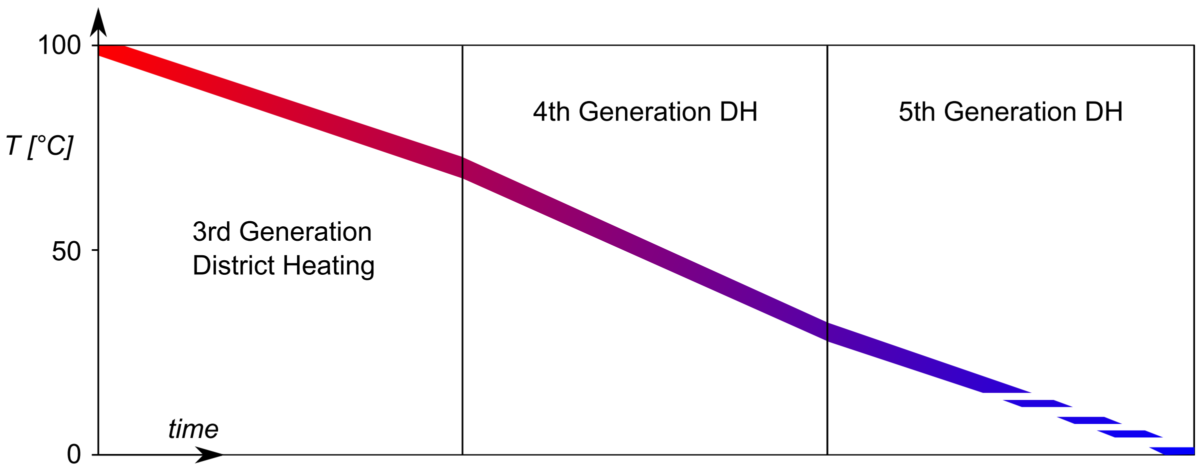

Figure 2: Operative temperature of the network in third to fifth generation district heating networks (modified from Caputo et al., 2021).

Fig. 2 illustrates how the supply temperature of heat carriers was reduced from 3GDH to 5GDHC networks. Both 4GDH and 5GDHC networks are capable of extracting waste heat from the heat sources and integrating different renewable energy sources like ground, air or lakes/rivers. Both use decentralized heat pumps to supply heat to the buildings allowing the reduction of grid losses in both systems. The key difference between 4th and 5th DH generations is that 4GDH are operated at temperature levels which are, at lest to some extent, sufficient for providing space heating of buildings directly, i.e. without the need to be boosted by heat pumps. On the other hand, 5GDHC depend on decentralized heat pumps for all heating application's and include an important cooling part. Since 5GDHC networks allow the operation of the consumer substation to be reversed, both the heating and cooling demands of the consumer are supplied through the same pipes (Buffa et al., 2019).

The inclusion of simultaneous heating and cooling has lead to radical changes in network designs. Where traditional networks had unidirectional fluid and energy flow, newer systems use bidirectional fluid flow and bidirectional energy flows (Fig 3). Accordingly, traditional district heating (DH) or cooling (DC) systems had centralised pumps to provide the fluid circulation in the network. Instead, 4GDHC and 5GDHC systems have both centralised and decentralised circulation concepts (Buffa et al., 2019).

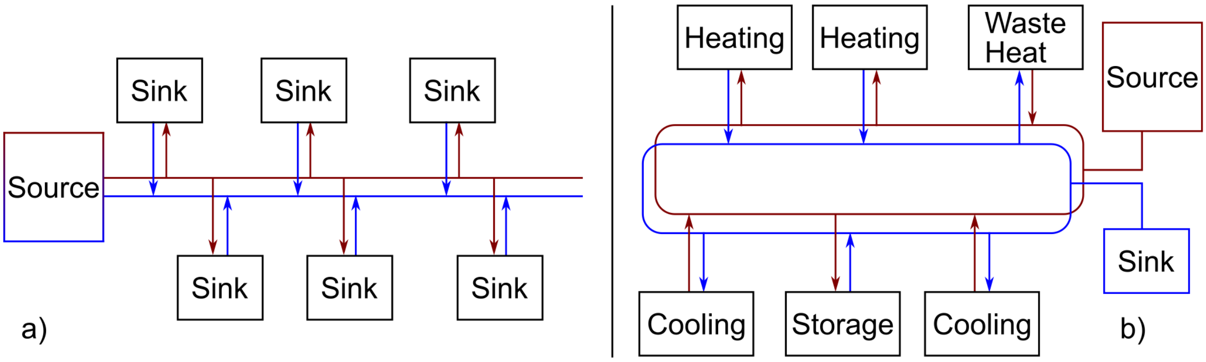

Figure 3: Schematic diagrams of **a)** unidirectional and **b)** bidirectional networks (modified from Caputo et al., 2021).

In an unidirectional network, there is only one direction of the heat-transfer fluid flow from the supplier to the consumer and the energy flow is always from the source side to the consumer side. A unidirectional network can serve for heating and cooling, but provides the same temperature for both applications.Thus, when operated in a cooling dominated mode, the energy flow can be reverted (i.e. from the users to the source). In a bidirectional network, both the fluid and energy flow can be in either direction from the supply side to the consumer side or vice-versa (Caputo et al., 2021, Nussbaumer et al., 2021). Additionally, changes of the flow direction can occur in different parts of the network. This allows each element connected to a bidirectional network to act as both heat source or heat sink. The operational mode in such configurations depends upon the flow directions that occurs between the supplier and the consumer.

Note that it is also possible to have a bidirectional energy flow in a network with a unidirectional fluid flow. As the flow direction in such systems is fixed, the energy for cooling has to be extracted from and/or supplied into the same pipe as the energy for heating (Hangartner et al., 2018).

Table 1 summarizes the different operational modes in the thermal networks. In Switzerland, the 5GDHC systems of ETH Zürich, Richti Wallisellen, Surstoffi, and Familienheim-Genossenschaft use bidirectional energy and fluid flow. The 5GDHC system of ETH Zürich, Campus Hönggerberg has an installed capacity of 5.50 MW and operates with waste heat from space cooling from the laboratories and includes seasonal geothermal storage. The temperature level varies from 8 °C to 24 °C in the warm pipe with an average temperature difference of 4 K for the cold pipe (Buffa et al., 2019).

Table 1: Operational modes in thermal networks based on Buffa et al. (2019) and Hangartner et al. (2018).

		Energy flow	
		Unidirectional energy flow	**Bidirectional energy flow**
Heat-transfer fluid flow	Unidirectional HTF flow	**Typical operational mode in traditional district heating (DH) or district cooling (DC) system (unidirectional network)** There is only one supply station All users are either in heating or cooling mode Centralized pump is pumping the HTF from the supply-side to the consumer side	**Typical operational mode for 5GDHC (bidirectional energy, unidirectional fluid flow)** Centralized pumping stations for supplying heating and cooling demands Some users could be in heating mode while others could be in cooling mode
	Bidirectional HTF flow	**Not applicable as unidirectional energy flow forces a direction of the energy flow while bidirectional HTF flow forces bidirectional fluid flow** (Hangartner et al., 2018)	**Typical operational mode for 5GDHC (bidirectional network)** There are decentralized feed pumping stations Some users could be in heating mode while others could be in cooling mode

1.3.2 Energy sources

In 5GDHC networks, the main supply of heat can come from a variety of sources, e.g. waste water, ground based sources, lake water, solar-thermal collectors, and air-to-water heat exchangers. In principle, the integration of additional storage capacity only makes sense if the available sources are limited in terms of capacity or availability. This is the case for waste water treatment plants, different types of industrial or service waste heat, outside air or solar energy, which are described in the following sections. Lake water, as the most common source combined with low-temperature networks, does not have this limitation. Lakes themselves can be seen as a type of storage and their available power is mainly limited by the diameters of the pipes/barrels and the available pumps. Geothermal energy from boreholes cannot be seen as an energy source in the context of low temperature networks. As not only single probes but large borehole fields are needed, they act themselves as storage and need other energy source to be regenerated.

Solar energy

Our institute has conducted intensive studies into so-called "solar-ice" systems, which provide heating demands by integrating solar collectors, an ice storage, and a heat pump (Arenas-Larrañaga et al., 2024, Carbonell et al., 2018, 2016a,c, 2015, Philippen et al., 2012). Solar-ice systems are typically seen as an alternative to air and ground-source heat pump systems and have the potential to be more efficient with respect to the use of electricity. As opposed to ground-source systems, solar-ice systems do not need space for boreholes drilled around or below the building. This is an advantage when fossil fuel-based heating systems are replaced in existing buildings in urban areas and might be important for the reduction of CO_2-emissions, especially for refurbished buildings. Solar-ice systems, unlike air and ground source systems, are not affected by noise or ground water regulations. These arguments have been decisive for the growing deployment of solar-ice systems in Switzerland despite of their higher installation cost of the commissioned systems compared to air and ground source heat pump systems.

In comparison to ground source, solar-ice systems offer a solution with similar or higher energetic efficiency. Hence, one can think of a solar-ice systems as *full freely regenerated* ground source heat pump system where the borehole field is substituted by solar thermal collectors and an ice storage. This feature might become even more important if future regulations start to impose ground regeneration. Currently, solar-ice systems might be a bit more expensive than ground source systems without regeneration, but they are certainly cheaper if regeneration is necessary. Moreover, near future developments are expected to decrease the solar-ice installation cost by eliminating the need of heat exchangers in the ice storage (Gurruchaga et al., 2023).

There are numerous examples of larger buildings or entire building complexes being heated with ice storage tanks and solar thermal systems. Most of these systems use uncovered solar collectors to melt and heat the storages sometimes in combination with waste heat. These examples show that the combination of solar and ice can provide a viable source for heat pumps for the whole year. In this project, the "solar and ice" concept is scaled an combined with 5GDHC networks.

Waste water treatment plant

In the white paper published by the Swiss Thermal Grids Association (Sres and Nussbaumer, 2014), total potential of approx. 8 TWh/a was attributed heat recovery from Waste Water (WW). Only 1.9 TWh/a of that potential could be utilised in DH systems. Waste water, mainly from households, offers a relatively constant temperature with low fluctuations over seasons. Because Waste Water Treatment Plant (WWTP) collect WW from large catchment areas, the residual energy from WW can be extracted centrally and cost-effectively at these locations. Both the combination of many buildings and the thermal exchange with the waste water pipe network greatly equalise local fluctuations in output and temperature. Even if the temperature drops slightly in winter due to interaction with the pipe network and in the classifiers, it is usually above 10°C even in winter and is therefore a very attractive source for heat pumps. There are various examples of 5GDHC networks using WWTP as heat sources, e.g. the network of Jona used in this project is a typical representative example of this kind of networks.

Industrial processes

There are various other sources of waste energy from different processes, which can be used in 5GDHC. A typical examples is cooling energy from data centers or server farms, as it is the case for the FGZ "Anergy" also utilised in this project. Other network's examples are the waste heat from food cooling used in Gossau or the industrial waste heat in Visp-West. For industrial processes rather constant energy availability can be assumed through out the year.

Air-to-water heat exchangers

Air is mainly used as source for individual heat pumps providing a widely available and cost-effective technology. However, air-source heat pumps have lower efficiency during cold periods compared to other technologies such as ground-source heat pumps. When not combined with a heat pump, air can be used as renewable heat source via Air-to-Water Heat Exchanger (AWHX). In combination with other sources or storage technologies Air-to-Water Heat Exchanger (AWHX) can provide cheap energy to a DH network as long as the air's temperature is above the minimum required grid temperature. For example, in the "Suurstoffi anergy grid" or at the Dolder local heating system, Air-to-Water Heat Exchanger (AWHX) are used to regenerate borehole fields and a borehole thermal energy storage respectively. Therefore, also the combination of AWHXs and ice storage seems promising and thus considered in the present project.

1.4 Ice storages

The fundamental benefit of using ice storage concepts relies on reducing the need of the storage volume by making use of the high latent heat of fusion released when ice is formed. Icing a specific mass of water releases the same energy as cooling the same amount of water from 80 °C to 0 °C. Thus, although remaining always above the solidification temperature of water would lead to higher system performance using heat pumps, the required storage volume would be prohibitively large for applications in which the ice storage is used as source for heat pumps. Ice storages are a well proven technology for cooling applications where their main role consists in peak shaving of cooling loads at noon or in providing high cooling power for industrial processes. Ice storages have a very large variety of applications, from building cooling using both decentralized or centralized concepts with district cooling networks (Kozawa et al. (2005)) to industrial applications such as breweries and dairies as well as commercial refrigeration for food conservation (Kauffeld et al., 2010)). To the author's knowledge, ice storage has not been proposed as a storage technology for 5GDHC networks previously.

The different ice storage concepts on the market and under development can be split into four categories:

1. **Storage filled with heat exchangers (ice-on-hx)**. The most widespread ice storage technology has the storage tanks filled with evenly distributed heat exchangers, which can be coils, capillary mats or flat plates. An anti-freeze solution circulates in the inner part of the heat exchanger freezing the water from the outer part of the heat exchanger which is contained in the storage vessel. The water freezes and grows on the heat transfer surface between the heat exchanger and the storage vessel decreasing the heat exchanger efficiency due to the low thermal conductivity of ice and the growing thermal resistance in the ice generation process. For cylindrical heat transfer surfaces, e.g. coils and capillary mats, the increase of ice thickness is partially compensated by the increase in the heat exchanger area between the solid ice and the liquid water until the growth of ice is constrained (Carbonell et al., 2016c)[1]. Ice storage systems can be realised above the ground using containers or buried in the ground. In order to avoid damaging the storage vessel due to ice expansion when water is frozen, such systems cannot be frozen fully. Thus, a maximum mass ice fraction of 80 % is assumed. This technology is mature and reliable without moving parts. However, since the heat exchanger needs to be installed covering the whole storage volume, it adds a significant capital cost into the storage solution. Several manufacturers such as Viessmann, Fafco, Baltimore or Gefca offer ice storage systems using this technology in Europe.
2. **Storages with de-icing capabilities**. To prevent the increasing heat transfer resistance of the ice layer, heat exchangers with de-icing capabilities were developed for ice storage tanks. In the technology devel-

[1] Ice constrainment refers to the physical contact between ice layers from different heat transfer surfaces, e.g. parallel tubes or plates.

oped several years ago at our institute (Carbonell et al., 2016b,c, 2015, Philippen et al., 2012), flat heat exchangers are installed at the bottom of the ice storage tank. For de-icing, a periodic heat input melts a thin interface layer, whereupon the existing ice plate detaches from the heat exchanger and floats to the water's surface. This de-icing strategy requires a somewhat more complex hydraulic integration and control. The principle was developed at the SPF in co-operation with the Elektrizitätswerk Rapperswil/Jona (EWJR) and is marketed by Soltop energie. Other commercial systems used in industrial cooling processes use a heat exchanger above the storage vessel where de-icing is provided by waste heat. When de-iced, ice falls down into the ice storage vessel.

3. **Macro-encapsulated ice storages**. An alternative way to simplify the heat exchanger design is to use plastic containers filled with water and a nucleator to avoid supercooling. This allows to use kind-of a packed bed ice storage concept where the plastic capsules are placed inside the storage vessel, which is filled with an antifreeze heat transfer fluid. Encapsulation can be done using different geometries, e.g. spheres (Bédécarrats et al., 1996) commercialised by Cristopia, cylinders (MacPhee and Dincer, 2009) or rectangular shapes produced e.g. by Phase Change Material Products Limited in the UK. Although this storage technology is very simply to use, the thermal efficiency is rather low for large capsules. Moreover, it needs to use an antifreeze solution in the whole storage volume not occupied by the capsules with the associated increase of cost for large volumes. Moreover, little experience is available for large scale applications.

4. **Ice surry storages**. In order to decouple power needs from the energy storage capacity, ice slurry concepts can be used. These systems separate the ice generation and storage processes allowing to eliminate the formation of ice on the heat transfer surface as well as the need of in-vessel heat exchangers. Commercial ice slurry systems use mechanically scraped-surface heat exchangers, where ice is formed on a cold surface and is then removed continuously by a rotating mechanical arm that scrapes ice from a cylindrical heat transfer surface. To be able to detach the ice from the heat transfer surface easily, water is usually mixed with an anti-freeze solution forcing the evaporator to operate at low temperatures. This, together with the fact that the rotating mechanical scraper needs electricity to operate, decrease the energetic efficiency of the device. Moreover, due to mechanical loads, the rotating auger is not easily to scale-up to high power needs and demands for high capital and maintenance cost. Thus, at our institute, we have been developing an alternative passive slurry concept based on the supercooling method and a flow-based crystallizer (Carbonell et al., 2017b, 2020, 2022) that has no moving parts. This technology is still under development and is not yet available on a large scale. Nevertheless, a significant cost reduction is expected compared to the other ice storage technologies explained above. Higher cost reduction are expected for large systems thanks to be possibility to use large earth storage tanks (without heat exchangers) benefiting from similar scaling effect as conventional large scale water storage tanks, e.g. pit storages.

In this project, we chose to use commercially available ice storage systems with capillary mat heat exchangers, such as those offered by Fafco and Gefca, for the following reasons:

- Ice slurry storage systems using the supercooling method are not yet ready for the market and those using ice scraper technology are too expensive for our application.
- Available data sources for de-icing and encapsulation in large scale applications is insufficient for our purposes. Further more, de-icing cannot be guaranteed in a decentralised network because of the lack of a central heat pump.
- In the project Ice-Ex financed by the Swiss Federal Office of Energy (SFOE) (Carbonell et al., 2017a) we found that capillary mats was the most efficient and cost-economic heat exchanger option compared to coils and flat plates.

2 Methods

2.1 Pytrnsys framework

State-of-the-art methods use transient (also called dynamic) simulations to predict the behaviour of thermal energy systems. In these, the temperatures of all relevant components are simulated over time. This is in contrast to more "static" approaches where the evolution of the temperatures is less resolved - e.g., monthly (assumed) averages - and the focus is more on the energy fluxes based on these aggregated temperatures. The efficiency of many renewable energy systems are usually very sensitive to temperatures levels. Moreover, renewable thermal energy systems exhibit variations not only on the demand side but also on the supply side. Thus, supply and demand are not guaranteed to, and often will not, match at all times in renewable systems. This mismatch is the reason for the need for energy storage in renewable systems. The storages can act as additional supply or demand, depending on the need at the moment. For renewable systems, it is therefore not sufficient to consider aggregate values, because we must ensure that supply (including storages) matches demand at all times - not just in aggregate terms. In fossil-fuel based systems this is easily done as the supply can simply be increased by burning more fuel when the demand increases and the efficiency of a fuel based system is less sensitive to temperature compared to a heat pump or a solar thermal collector, e.g. Therefore, dynamic calculations considering the transient evolution of components is necessary to properly characterise thermal renewable systems.

TRNSYS[2] ("TRaNsient SYstem Simulation Program") is a commercial simulation program often used for simulating (renewable) energy systems in academia and industry. It comes with many ready-to-use component models like heat pumps, thermal energy storages, solar thermal collectors, etc. Additional libraries of simulation models for *TRNSYS* can be purchased from a company called *TESS*[3]. Simulation models from *TESS* are provided with their implementation in the *FORTRAN* programming language and so can be modified and extended if needed. In this project, the buried twin pipe model from *TESS* was used and extended to allow flow in arbitrary directions.

In the current project we use TRNSYS in combination with *pytrnsys*. *Pytrnsys* is a framework created at our institute with the vision of providing researchers with a flexible tool to simplify the workflow of employing *TRNSYS* allowing to use most of the functionality of the python package without having to know python in detail. For that we use configuration files with some scripting functionality that is described in the documentation[4]. *Pytrnsys* is not intended to substitute skills in *TRNSYS*, but will certainly make the *TRNSYS* user's workflow easier. We are aiming at reducing the time needed to get into *TRNSYS* and to set up a system, but also at improving the quality and reliability of the outcome. The latter is facilitated by the many control options, e.g., the automatic generation of an energetic system balance to be assessed on a yearly and monthly basis by default and on a daily or hourly basis if desired. Moreover, it can be used in education thanks to the visualization of the results on the GUI and the existence of examples that can be executed and processed with one click. Still, *pytrnsys* is not meant to use a GUI for everything, but it is rather a flexible framework using a hybrid approach. This means the GUI is only used where necessary, i.e., to create a hydraulic system, build a *.dck file and visualize the temperatures and mass flow rates. For the rest, *pytrnsys* relies on text input from the user. Each component is implemented in a text file with the extension *.ddck, which is a modular part of the complete *.dck. The *pytrnsys* approach is to have each model implemented in a *.ddck-file allowing the users to store and share the models on GIT. *Pytrnsys* takes care of stacking all *.ddck-files together to generate a complete *.dck-file that can be executed by *TRNSYS*. Note that *pytrnsys* does not deal with *TYPE* development or anything related to modelling in general. Thus, it is not foreseen to use *pytrnsys* to develop a python *TYPE*. An overview of the different *pytrnsys* or *TRNSYS* specific terms is given in table 2.

Deck file In *TRNSYS* a system is defined by a so-called *deck* or *dck* file. This is a human-readable text file specifying all the simulation models (also called "components") and their parameterizations - e.g., for a pipe,

[2] `https://trnsys.org/`
[3] `https://www.trnsys.com/tess-libraries/index.html`
[4] `https://pytrnsys.readthedocs.io`

Term	Description
*.dck	Suffix of a TRNSYS deck file: A master text file which includes parameter definitions and what subroutines are used.
*.ddck	Suffix to describe a modular part of a *.dck file with a well defined interface. Multiple *.ddck files are combined via the *.config file to generate the *.dck file.
*.config	Suffix to describe a configuration file. There are two different *.config files within *pytrnsys*, one is used to setup a simulation run, the other one is used to set up the processing of a simulation.
TYPE	A component that is normally written in *Fortran* which represents a specific part of a system that should be simulated, such as a solar collector or a heat pump.

Table 2: Overview of *pytrnsys* or *TRNSYS* specific terms.

the length, fluid heat capacity and thermal transmittance, etc - which comprise the simulated system. Equally important, the deck file specifies how components are connected to each other, i.e. how one component's output becomes an other component's input.

In summary, a *deck* file lists all the simulation models of a system and their interconnections. The *deck* file can then be passed to *TRNSYS* for it to run a transient simulation of the whole system.

Customizing *TRNSYS* The simulations that were run for this project were untypically large (tens of sinks including heat pumps, many buried twin-pipes, etc.) for TRNSYS. For that reason, we had to modify parts of *TRNSYS* to enable it to simulate such large systems.

In this work, we look to answer questions such as "how does the Seasonal Performance Factor (SPF) change as we vary the relative collector size?". Answering such questions entails running a series of simulations (one for each relative collector size of interest) and comparing the results of the different simulations.

Variation For a set of parameters which we want to vary, we call a set of specific values for those parameters a "variation". Assuming we are varying the relative collector area, $A_{\mathrm{col,rel}}$, and the relative storage size $V_{\mathrm{store,\ rel}}$ at the same time, then one particular variation of interest might be ($V_{\mathrm{store,\ rel}}$=2 m^2 MWh^{-1}, $A_{\mathrm{col,rel}}$=20 m^3 GWh^{-1})

For each variation, a *TRNSYS deck file* has to be compiled - each containing a different set of values for the parameters being varied - and the *TRNSYS* application run on that *deck* file. Once the simulations have completed, the data of interest has to be extracted from each of the simulations' results and then plotted. Results can also be aggregated across different variations to compare variations against each other.

pytrnsys To simplify the tasks of preparing variations, running them, and post-processing results, an open-source software package written in Python called *pytrnsys*[5] has been developed at SPF Institute for Solar Technology.

pytrnsys also provides the ability to assemble larger systems from subsystems. Subsystems - like components above - can be parameterised. Being able to build larger systems from subsystems encourages re-usability and modularity and simplifies defining large systems.

Subsystems are defined in so called d*deck files*. Their format is based on that used by *deck* files, but with some additional extensions.

ddck files add a mechanism for passing hydraulic properties such as mass flow rate, fluid temperature, density and heat capacity between hydraulically connected subsystems. Variables can be defined as "private" within a *ddck* file. Private variables can only be seen from within the *ddck* file within which they are defined but not

[5] `https://github.com/SPF-OST/pytrnsys_gui`

from other *ddck* files. This is needed to prevent variable name clashes if a subsystem is reused multiple times within the overall system[6] (i.e. two heat pumps in the complete system).

pytrnsys takes care of rewriting all the subsystems' *ddck* files to connect them hydraulically and avoid variable name clashes and assemble them into a *deck* file that it can then hand off to *TRNSYS* for simulation.

GUI *pytrnsys* includes a GUI which can be used to draw the hydraulic setup of a system and then to automatically export a *ddck* file (the "hydraulic *ddck* file") containing all of the system's "simple" hydraulic components:

1. Pipes
2. Tee pieces
3. Valves
4. Pumps
5. Hot water taps
6. Cold water mains

Writing such a *hydraulic ddck file* by hand would be a laborious, error-prone and un-intuitive processes.

After exporting the *hydraulic ddck file*[7], the parameterised simulation runs and post-processing can be run by "plain" *pytrnsys* without any further need for the GUI.

Once a simulation has completed, the pytrnsys GUI can be used to visualise simulation results directly in the hydraulic scheme, showing temperatures and mass flow rates at any given time exactly where they occur in the system.

TRNSYS *Studio* vs. pytrnsys GUI A different GUI for graphically assembling deck files, which is part of the official *TRNSYS* distribution, exists. It is called *TRNSYS Studio*. Unlike the *pytrnsys GUI* it should be thought of more as a "graphical deck builder" than a GUI for creating and exporting hydraulic schemes: when building systems in *Studio*, each of a component's inputs needs to be connected to another component's output graphically, i.e. a lot more visual information is contained in a *Studio* scheme. By restricting itself exclusively to the hydraulic side of a system - e.g. control signals are not shown in the *pytrnsys GUI* - *pytrnsys GUI*'s hydraulic schemes are much more focused.

In addition, because the *pytrnsys GUI* is only concerned with hydraulic connections and not with the more general problem of connecting any two *TRNSYS* components - which might not even be hydraulic in nature - it can offer domain-informed features such as automatically connecting the hydraulic ports of two components without the user having to specify that output number, for instance, output seven of component one is its output temperature and that temperature should be passed to, e.g., input three of component two. Another consequence of restricting itself to hydraulic connections is that the *pytrnsys GUI* can know about "hydraulic loops". By hydraulic loop we mean all pipes, tee pieces, valves, and heat exchangers which are hydraulically connected and for which a fluid and its properties such as specific heat capacity and density can be defined. Then, any component which forms part of that loop will automatically retrieve fluid properties from the loop to which it is connected. This avoids typical errors in plain TRNSYS, e.g. using different values of specific heat for hydraulically connected components.

Post-processing of simulation results *pytrnsys* simplifies data analysis and plotting of both individual simulations and across simulations. *pytrnsys* includes the following features for post-processing results:

- Access to the values of constant expressions in the *deck* file and the ability to use these values in arbitrary algebraic expressions

[6] In which case the *ddck* file will be included multiple times in the final deck file, hence a way to prevent variable name clashes is needed.

[7] And, possibly, some other, additional, *ddck* files that the pytrnsys GUI can automatically export for the user.

- Simple statistics (min, max, average, total) on time series.
- Data selection (e.g. one particular year from a multi-year simulation)
- Integrating time series (hourly to daily series, monthly to yearly series).
- Cumulative values of time series
- Save data produced in the post-processing to file.
- Plot raw and processed data

pytrnsys supports different plot types, including histograms, bar charts, scatter plots, and interactive time series plots. Two commonly used plots in energy systems supported by *pytrsnsys* are the comfort plot and the Q-vs-T plot. The comfort plot will show whether temperature and relative humidity values fall within prescribed ranges (mandated for, e.g., residential buildings). The Q-vs-T plot shows at which temperatures heat is released or consumed in different parts of the system.

Another important plot type is the comparative plot. It can be used to plot one parameter of a variation against up to three others (by varying the colour and line style) in a single plot.

pytrnsys can also automatically generate a report which includes:

- General information like the time the simulation was run, how long it took, etc.
- The monthly heat balance in tabular and graphical form
- The monthly electricity balance
- The monthly SPF of the system

2.2 Extensions to *pytrnsys* developed during this project

To simulate a district heating network the pipes of the network are key components. In a 5$^{\text{th}}$ Generation of District Heating and Cooling (5GDHC) network, heat losses to the ground from the network can be expected to be lower than in a high-temperature network, but gains from the ground - particularly in winter, when the network temperature is low - can be assumed to be higher. In addition, when cooling demand in the network dominates and the network temperature is high, the ground is likely re-generated. For these reasons, the pipe-ground system is of interest also in low temperature networks.

Double pipe In this project, the pipe modelling is based on *TESS' Type 951 (Buried Noded Twin Pipe) Model*. In the course of this project, the type was extended to allow flow in both directions and parameterised for uninsulated pipes.It models a double pipe as two parallel cylindrical pipes insulated against each other. Each double pipe also models a cylindrical section of ground around the pipes. For the interactions with the surrounding ground, the two single pipes are lumped together and insulated jointly against the ground. The modelled section of ground ends at the so-called "far-field" which is modelled as an infinite heat reservoir at a temperature that only varies with the day in the year. The temperature of the far field is modelled as a simple sine wave over the year. Only the ground and the fluid in the pipes have a heat capacity.

The parameters used for the double pipes are summarised in Table 3.

2.2.1 Added GUI elements

In order to design the hydraulic scheme of the system the *pytrnsys* GUI had to be extended with hydraulic components for double pipes including:

1. Double reversible pipe
2. Double tee piece
3. Single double pipe connector

Description	Symbol	Value	Unit
Inner pipe diameter	$d_{p,inner}$	0.4028	m
Outer pipe diameter	$d_{p,outer}$	0.429	m
Thermal conductivity of pipe material	k_p	175	kJ /(h m K)
Centre-to-centre spacing of pipes	l_{c2c}	0.55	m
Diameter including casing	d_{casing}	2	m
Thermal conductivity of casing	k_{casing}	7	kJ /(h m K)
Thickness of pipe insulation	-	0 (i.e. not insulated)	m
Buried depth	l_{depth}	1.8	m
Thermal conductivity of soil	k_{soil}	8.64	kJ /(h m K)
Heat capacity of soil	-	1.0	kJ /(kg K)
Density of ground	-	1800	kg /m^3
Fluid	-	Water	-

Table 3: Parameters used for double pipes

4. Double double pipe connector

The graphical representation of these components in the GUI is shown in Figure 4. The double pipe to double

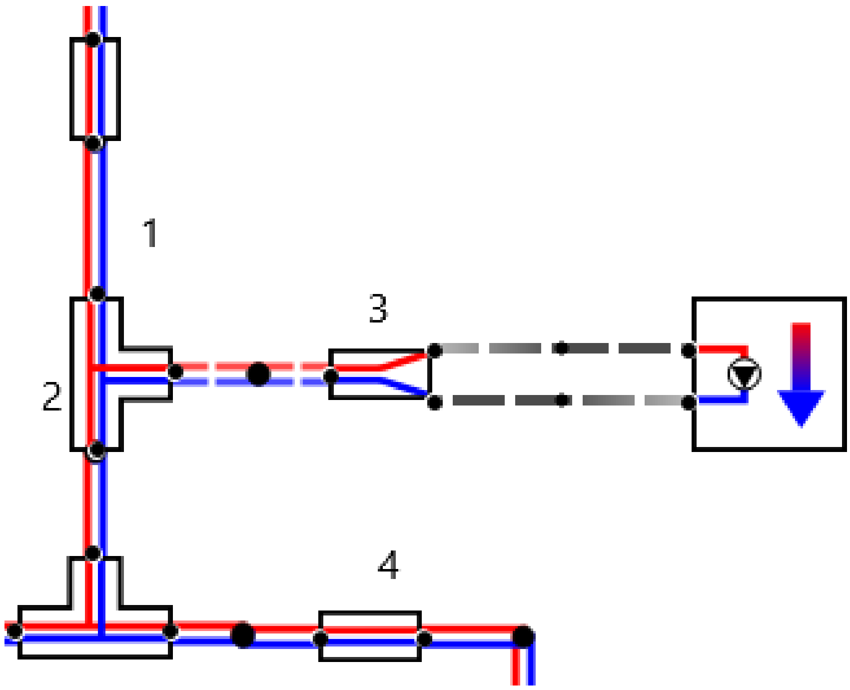

Figure 4: Hydraulic double pipe components available in the *pytrnsys* GUI
1 - double pipe, 2 - double tee piece, 3 - single double pipe connector, 4 - double double pipe connector

pipe connector is needed when a double pipe's parameters such as diameter or insulation properties change along the way. In addition, generic components where included to add and/or remove heat into or from the system (Fig.5). Additionally, the possibility of marking certain single or double pipes as "dummies" was added to the GUI, which are represented visually in the GUI using dashed lines, as can be seen in Figure 4. Dummy pipes don't have neither thermal capacity nor heat losses. They can be used for "non-physical" pipes which only exist to be able to complete the hydraulic diagram, to "disable" a part of a system (e.g. a leg in a district heating network which isn't yet in operation), or to represent parts of the system which it is felt can be neglected or which the user isn't interested in. Using dummy pipes can considerably speed up the simulation

Figure 5: Icons for generic heat source, sink, and flexible source/sink from left to right.

time as dummy pipes' underlying computational models are very simple unlike the ones of proper pipes.

2.2.2 Flow solver

The controller in a *pytrnsys* simulation acts on the system by controlling the mass flow rates of the pumps and/or the valve positions. Given mass-flow rates on the pumps and the valve positions are used as inputs for the mass flow solver TYPE to compute the resulting mass flow rates at each point (pipe, tee piece, component port, etc.) in the network. The mass flow solver is a *TRNSYS* component like any other and was implemented in *FORTRAN* at our institute. Because the mass flow rates are solved globally within one type, conservation of mass across the system is guaranteed at all times.

Solving the mass flow rates in such a centralised manner also allows the user to verify mass flow rates - e.g. for different operating modes in the development phase of the simulation - without having to simulate any components other than those which the mass flow solver is concerned about (the "hydraulic components"; pipes, tee pieces, valves). These hydraulic components connections and the TYPES definitions used for each of them, are exported automatically by pytrnsys without additional user inputs.

When solving for the mass flow rates only, all the non-hydraulic components (like, e.g., the ice storage in Fig. 6) are conceptually replaced by dummy pipes. Therefore, the mass flow rates in the system can be computed without having to specify the behaviour of the non-hydraulic components.

In the course of this project, the flow solver had to be extended to accept all the new double pipe elements. Further more, relative and absolute error tolerances for mass flow rates had to be introduced. This was necessary because the previously used, fixed values were sensible defaults in the context of simulating building-level energy systems, but did not transfer to the much larger mass flow rates that occur in DH networks.

2.2.3 Re-usability of modular components

In this project we needed to simulate systems which include multiple heat sinks. Each sink is modelled as a heat pump, a one-node SH storage/building, a one-node DHW storage and control logic deciding at what power to run the heat pump and whether to provide SH or DHW demands.

Every sink is represented by the same *ddck* file. This means that we needed to implement and maintain the behaviour of a heat sink only once. At the start of this project *pytrnsys* did not have the ability to use a *ddck* file multiple times. The reason were variable name clashes: by including a *ddck* file twice any variable defined in it would be defined twice. Therefore, "private" variables were introduced. A variable marked as private in a *ddck* file will not clash with itself when that *ddck* file is used twice. Instead, a new, unique variable will be created for the private "parent" variable each time the *ddck* file is used. This enabled us to use the heat sink *ddck* file multiple times within our simulation.

To ensure that the sinks don't all behave exactly the same and to more accurately capture the situation in a real network, where the amounts of heat and times at which they are required differ from source to source, a mechanism to change the demand profiles for heating and domestic hot water for each sink was added to *pytrnsys*. Thus, each sink is represented by the same *ddck* file, but each sink's underlying heating and domestic hot water profiles are different.

Different demand profiles ask for different heat pump capacities and storage sizes. To change these parameters from sink to sink, it is necessary to change the unique variable generated from a private variable upon inclusion of a *ddck* file.

This can be accomplished by the general ability within *pytrnsys* to change the value of any variable in the final, generated *deck* file to any value. This feature has long been part of *pytrnsys* and did not need to be added specifically for this project.

2.2.4 Automating the running and post-processing of simulations

As part of this project a great number of simulations were run. Managing that many simulations is a challenge.

The software (applications and libraries) and their versions used for performing these simulations must be the same to ensure that different results are not due to differences in the software.

Changes to a system's model need to be tracked and the results produced from a system model's particular version need to be tied to that version to be able to, given two sets of simulation results, tell exactly what the differences were in the models used which gave rise to the differences in the results.

Changes between system models (e.g. between a system with a solar collector field as a source and an air-water heat-exchanger as a source) should be tracked or be readily generated for inspection in order to check whether the differences in the systems are exactly the ones distinguishing the systems but no others. Only then can a sound comparison between the two systems be made.

git[8] is the most widely used distributed version control system (DVCS). A version control system tracks changes to a set of text files. Using a version control system, one can, if one wants to, track the changes (including addition and deletion) of each line of text within a project (i.e. set of files; in *git* parlance a project is called a "repository") back to the very beginning of the project. Furthermore, each change (also called "commit") to a line is given a unique ID and attributed to a person. It is also linked to a so-called "commit message". The commit message states the reason for why the changed was made. It is provided by the person who makes the commit. Finally the version control system keeps track of the time each commit was made.

Version control systems have long been in use in software development. The *pytrnsys* source code, e.g., is under version control and hosted publicly on *GitHub* since 2019.

GitHub is a web interface to the *git* DVCS. It is the largest public repository of computer programming source code in existence. The vast majority of open-source projects is hosted on *GitHub*.

GitHub boasts numerous other features in addition to being a user-friendly web interface to *git*. It can, for instance, be configured to perform various different actions whenever a commit is made to a project. Within *pytrnsys* this functionality is used to run our internal production quality tests to ensure that the latest changes to the *pytrnsys* source code didn't introduce any programming errors which break existing functionality.

The same infrastructure can be used to run simulations. This project's repository was configured in such a way that a simulation is run and its results post-processed automatically on a machine dedicated to running simulations each time a change is committed. This way, all the simulations are guaranteed to run on the same machine, using the exact same software. Furthermore, each simulation run is tied to a commit, i.e. has a unique identifier, a commit message giving the reason for the change, an author and a time stamp. Finally, the simulation results are automatically archived under the commit's unique ID and the author of the change to the source code is informed that the simulation associated with their change has finished and where they can find the archived results.

Many changes can be submitted in short succession and *GitHub* will take care of scheduling simulation runs: it will wait for one change's simulation run to finish before starting with the next change's simulation. In that way, the authors could submit multiple changes for simulation, have *GitHub* schedule the simulation runs through the night, and find the archived results the next day to analyse them.

To summarise, this project leveraged *git* and *GitHub* to:

[8] https://git-scm.com/

1. Track changes to system models during the whole lifetime of the project
2. Enable the line-by-line comparison of any two versions of any two systems
3. Ensure that simulations are always run within the same environment (hardware, operating system, software, etc.)
4. Automate the scheduling, running and post-processing of simulations
5. Tie simulation results to the model versions that produced them
6. Make it easy to re-visit and re-run specific system model versions

2.3 Simulation of 5GDHN with *TRNSYS/pytrnsys*

2.3.1 Modelling the EZL district heating network

The 5GDHC from EZL in Jona, Switzerland, was modelled in *pytrnsys* using the new features described above. The network served as the starting point for the investigations in this study. Fig. 6 shows the topology of the DH network.

The network consists of 22 users with a total demand of 7.6 GWh. The users are mainly multi family houses of different sizes. A simple scaling of all connected users is used for demand variations (see Section 2.4). The network itself consists of uninsulated plastic pipes, with a diameter of DN 450 in the main pipe which tapers in the arms down to DN 200. The different branches sum up to a total length of the grid of 3.2 km.

2.3.2 Ice storage model and integration

As explained in section 1.4, for this project we focus on ice storage concepts using capillary mat heat exchangers. The numerical model for the ice storage as well as the validation process is described in detail in Carbonell et al. (2018). The FORTRAN source code is available on *GitHub*[9]. In our simulations, the HX tubes have an outer diameter of 8.5 mm and a distance of 10 cm between tubes. The number of tubes was scaled with the ice storage volume.

The following considerations were made when we chose to focus on direct ice storage integration into 5GDHC over using an indirect integration:

1. Direct integration requires grid temperatures below 0 °C and therefore grid operation with an anti-freeze heat transfer medium.
2. The combination of single-storage systems with water-operated grids would require a large central heat pump that raises the energy released by freezing in the ice storage to a temperature level above the freezing point. This means that the investment in heat pump capacity would have to be made twice. First, to lift the outflow temperature of the ice store to above the freezing point and then, in the decentralised heat pumps, to reach the temperature level required at the consumers. Because storage systems in grids are needed in particular to cover peak power, this is associated with high investment costs. Furthermore, achieving the same temperature lift (from slightly below zero in the ice storage to the user temperature level) in two steps induces more heat exchanges, each inducing exergetic losses, and is therefore not desirable for moderate temperature lifts also from an energetic point of view.

Due to the above mentioned disadvantages of an indirect integration and the fact that water-antifreeze mixtures have already established themselves as a heat transfer medium for 5GDHCs without ice storage, we only considered direct integration in combination with antifreeze-containing grids in this project. However, as the network temperature needs to be slightly below zero degrees for direct integration, this operation mode poses a danger of freezing in the heat exchangers of water based energy sources. For this reason, we investigated hydraulic concepts and bypass strategies to avoid temperatures below the freezing point at such sources despite grid return temperatures below 0 °C.

[9] `https://github.com/SPF-OST/TrnsysType861_IceStorage`

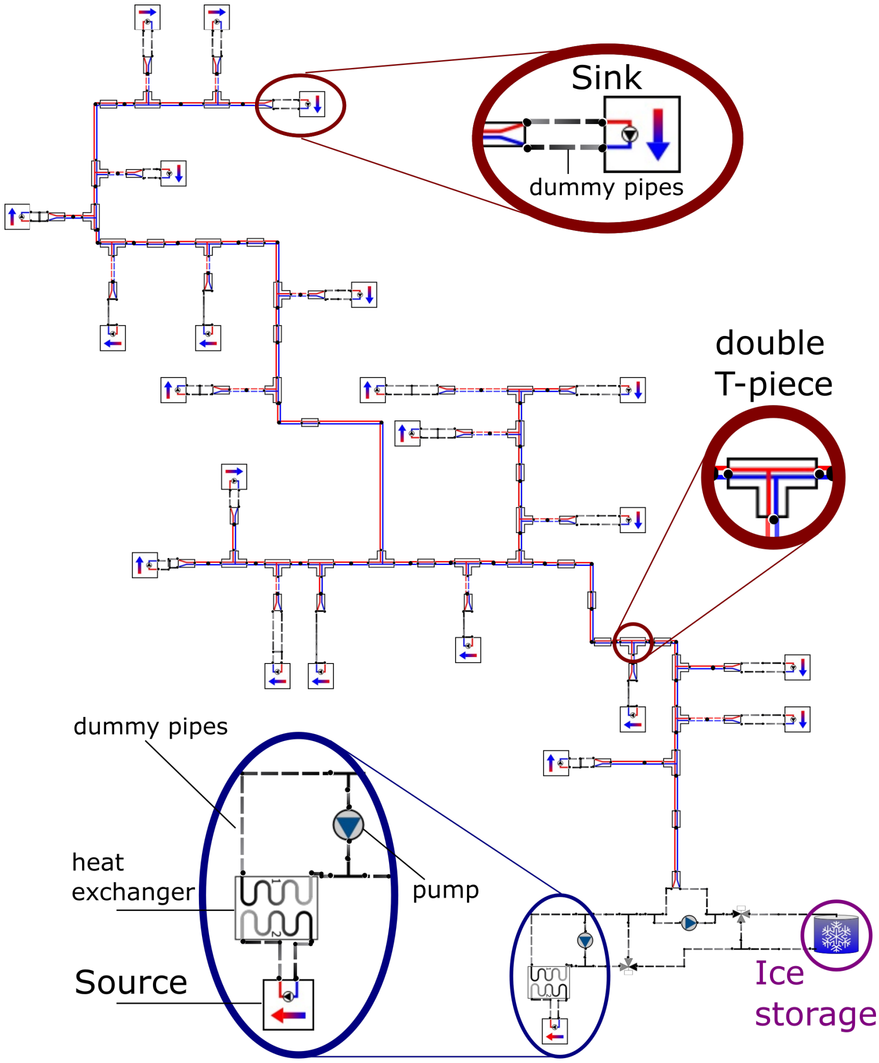

Figure 6: Topology of the modelled EZL district heating network in Jona. Indicated are: **Sinks:** Group multiple small consumers into a single heat sink with a single heat pump and sink specific demand profiles. **Double T-pieces:** Diverts hot and cold flow simultaneously. **Ice storage:** Stores sensible and latent heat to buffer demand. **Source:** A WWTP source provides the network's heat through a heat exchanger. The pump recirculates the carrier fluid (water/antifreeze mixture) to ensure the water on the WWTP side never drops below its freezing point. **Dummy pipes:** Pipes with dashed lines are "dummy pipes": they don't exhibit any thermal losses and don't have any heat capacity. See also the bottom of figure 7 for further details.

2.3.3 Control strategy for the source

In principle, the mass flow in a decentralised network is driven by the pumps in the connected buildings. However, additional pumps were used when integrating the WWTP source and ice storage to prevent either the ice storage from freezing completely or the WWTP heat exchanger from freezing. The return flow from the network is generally routed through the ice storage before it is returned to the source as can be observed in the lower left of Fig. 6.

When there is less demand in the network than the source is supplying, the ice store can be actively regenerated by imposing additional flow in the regeneration pump by-passing the network supply and return (Fig. 7). Active regeneration significantly lowers the ice storage volume needed to cover a given yearly demand. A comparison of active and passive regeneration strategies is given in Section 3.2. We use the diverting valve to by-pass the ice storage in case the maximum allowable mass ice fraction has been reached.

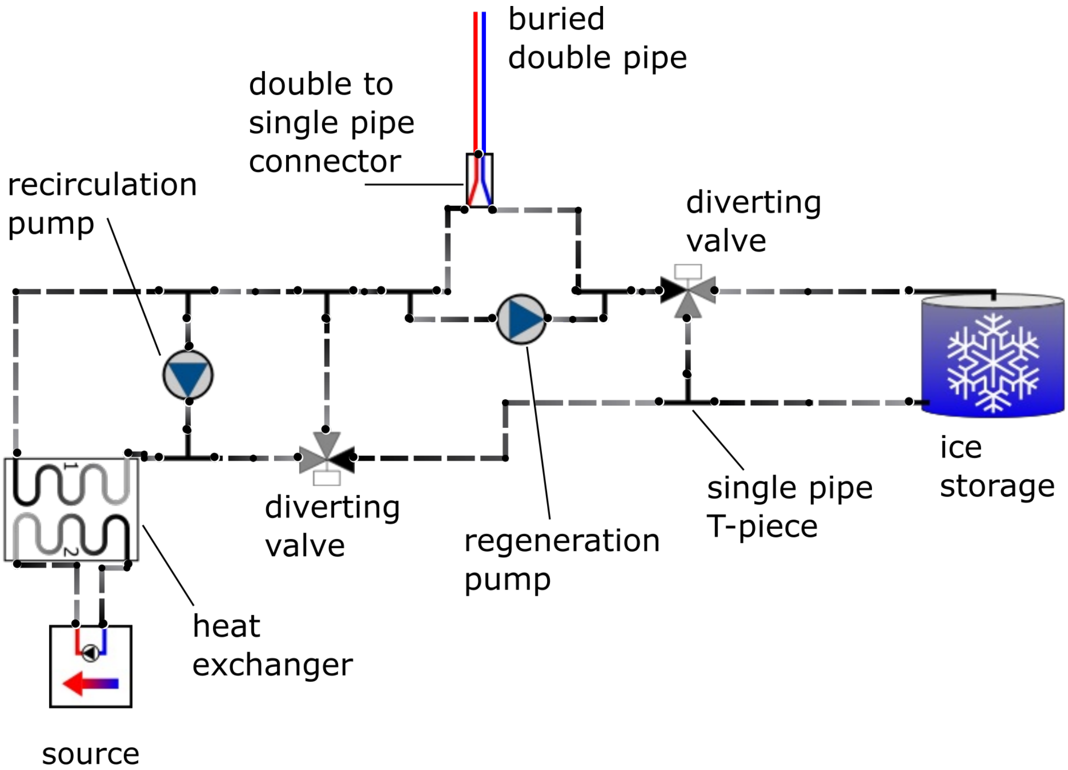

Figure 7: Central components at the source location of the modelled EZL district heating network in Jona. Besides the source and ice storage, these components are mainly needed for temperature control. See Section 2.3.3 for further explanation.

If the network temperature is too low, there is a danger of freezing the treated waste water in the Heat Exchanger (HX) with the WWTP. In that case, the re-circulation pump is activated (i.e. set to a constant positive mass flow) and the diverting valve just before the source HX is controlled to ensure the HX inlet temperature at the network side does not decrease below 2 °C. Freezing danger on the water bearing side of the HX (the side of the WWTP) is therefore avoided with some margin of security.

The valve before the HX can also be used to additionally control the return temperature of the source side of the HX, e.g. if we want to control for a fixed temperature difference over the source side, as would typically be the case for a Constant Temperature Source (CTS).

2.4 Demand profiles

Our simulations are simplified by grouping individual costumers along a network leg into so-called "sinks" (Fig. 6). Each of the sinks is defined by:

- a Heat Pump (HP) with a nominal power equal to the design needs of the network leg represented by the sink.
- demand profiles for DHW and SH.
- a storage tank each for hot water and for space heating.

We use a simple storage model for the "SH tank" corresponding to a one-node building to capture the thermal capacity of the buildings connected to the network leg. The internal storages are scaled according to the maximum yearly demand of the sink. The DHW is scaled to provide half an hour of the maximum demand, whereas the heat capacity of the buildings is set to two hours of maximum SH demand.

The design capacities of the network legs were provided by EZL. From these, the demand profiles were generated using a demand calculation tool developed at SPF (Ruesch and Haller, 2022). To generate a profile, the tool takes into account the following factors:

- weather data.
- HP capacity.
- total yearly heat demand.
- the fraction of the total demand needed for DHW and SH.
- the heating limit temperature, i.e. the temperature below which SH is necessary.

Fig. 8 shows example profiles for one of the sinks using two different ratio between DHW and SH demands (DHW/SH) ratios.

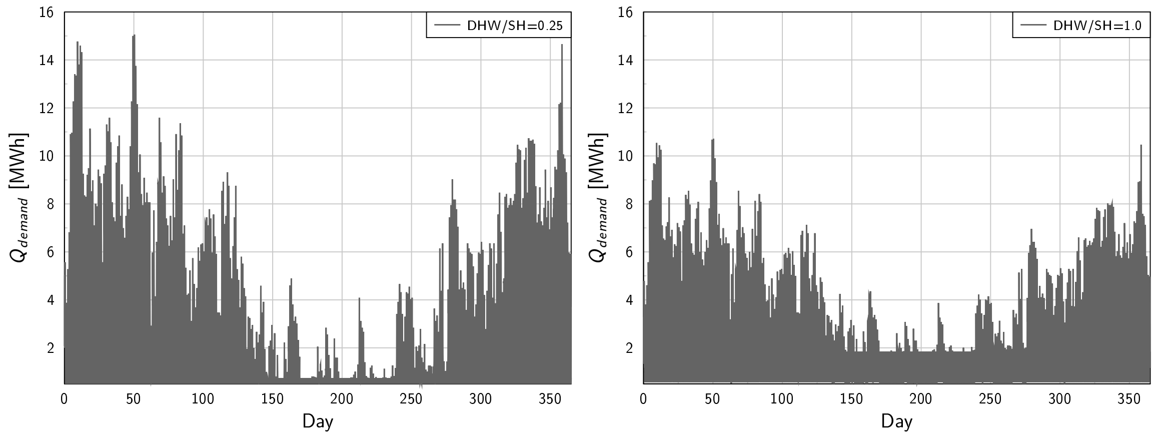

Figure 8: Example of hourly demand profiles for a full year for different ratios between DHW and SH.

The thermal storages for SH and DHW represent a part of the boundary of our simulation model: the demands are directly withdrawn from the storages, i.e. the heating distribution systems are not simulated. The HPs are controlled based on the storage temperatures by an on/off two-point controller with hysteresis. When a storage temperature drops below its minimum allowed temperature, the heat pump is turned on. The heat pump continues running until the storage temperature has reached a desired maximum temperature. At which stage, the heat pump turns off and remains off until the storage temperature falls below the minimum allowed temperature again. If both storages need charging, the DHW storage is prioritised over the SH/building storage.

The grid provides heat at the evaporator of the heat pump. The HPs lift that heat to the desired temperatures of the storages (SH: 37 °C, DHW: 60 °C). Due to their differing demand profiles, the sinks require different amounts of heat at different times. This, together with the thermal inertia of both storages, helps to smooth out the total heat demand in the system.

Different building standards are represented by differing demand profiles resulting from the heating limits used. They range from 13 °C for low energy buildings to 19 °C for poorly insulated buildings. However, for simplicity, the supply temperature is assumed to be the same. Heating demands for each network leg were provided by EZL and the insulation standards were chosen by the authors based on a visual impression from the buildings. Simulations were carried out for several ratios of DHW to SH demand.

Fig. 9 shows the energy delivered for heating to four different sinks as a function of the delivered temperature. In the results, most of the SH demand is provided between 39 °C to 40 °C regardless of the insulation standard.

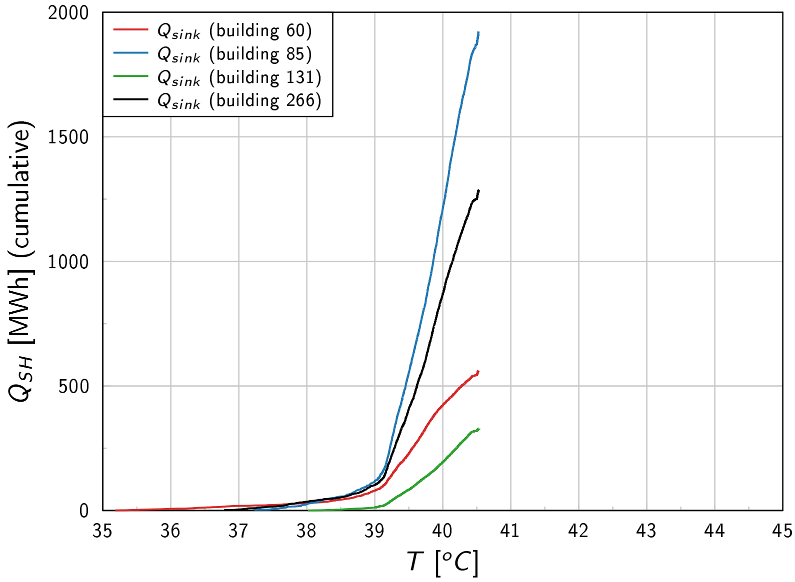

Figure 9: Cumulative space heating demand profiles as a function of delivered temperature for four different buildings and a DHW/SH ratio of 0.2.

Fig. 10 shows the demand profiles of the whole network for different DHW/SH ratios. In Fig. 10a the ratio between the cumulative energy demand and the peak demand (i.e. the cumulative full load hours) is shown for each day of the year. The latest value represents the yearly full load hours. The higher the DHW/SH ratio, the higher the full load hours.

The peak demand occurs in winter in the form of SH demand. By increasing the DHW portion, the overall demand profile becomes smoother, i.e. more linear in this plot, which means more constant over the year. This can be seen in Fig. 10b where the ratio between the (non-cumulative) hourly heat demands and the peak demand are plotted ordered from highest to lowest. In this plot, the number of days the relative demand was at a given value can directly be read out. A constant demand would show as a horizontal line at constant relative demand of 1. The plot shows that not much energy is delivered at peak power. What can be observed, too, is that at ratios of Q_{demand}/Q_{peak} below 0.2, the different DHW/SH ratios start to have a larger effect. The higher the DHW/SH ratio, the more horizontal the Q_{demand}/Q_{peak} becomes at low demands.

Lastly, we increased the overall heat demands of the grid by scaling all sinks by the same factor.

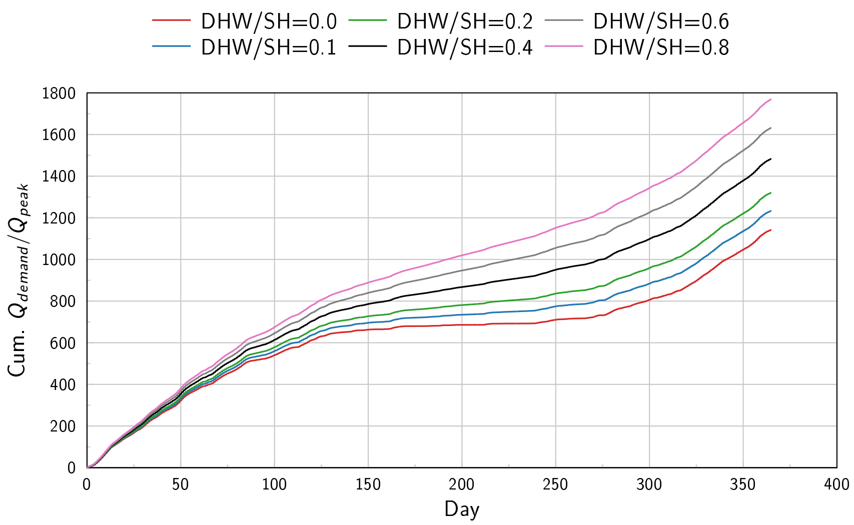

(a)

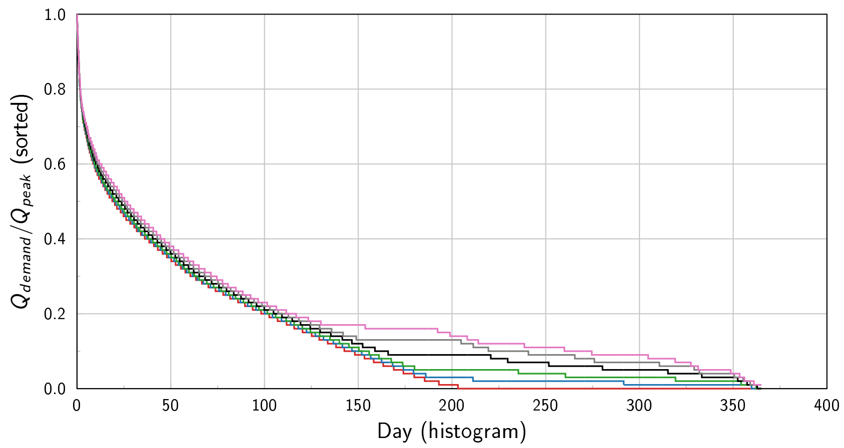

(b)

Figure 10: Demand profiles over a year for different DHW and SH ratios. **a)** Cumulative demand profiles divided by peak demand leading to cumulative full load hours. **b)** Heat demand divided by peak power and sorted from high to low ratios representing how many days the demand is at specific power.

2.5 Renewable heat sources

2.5.1 Waste Water Treatment Plant (WWTP)

The EZL District Heating Network is powered by a Waste Water Treatment Plant. Waste water from buildings has a nearly constant temperature throughout the year, but is cooled down in the piping and the basins, which result in lower source temperatures in winter. Inspired by the example network of EZL, we started our analysis with a WWTP source with a capacity of 6 MW [10] and coldest output temperature in February. We added a 3 MW source to be able to generalise the results. Based on typical temperatures of WWTPs, the outlet temperature of the WWTP source is modelled as a sine function over the year:

$$T_{src,out} = 17\,^{\circ}\mathrm{C} - 4\,^{\circ}\mathrm{C} \cdot \cos\left(\frac{t - 751}{8761} \cdot 2\pi\right), \tag{1}$$

where t is hour of the year. The source temperature thus oscillates between 13 °C and 21 °C to account for temperature differences over the seasons, with the minimum temperature occurring on February 1st. The heat is provided to the DH network via a heat exchanger. Fig. 11 shows the hourly temperature and the heat provided by the source over the year for two different source powers combined with ice storages of different sizes.

Figs. 12 and 13 show the cumulative heat provided by the source over the year for a nominal source power of 3 MW and 6 MW, respectively (solid lines), together with different levels of heat demands (dotted lines). The cumulative differences between source and demand for each case are shown in Figs. 12a and 13a. The difference between Q_{src} and Q_{demand} is always negative, which indicates that the source can never meet the full demand for these cases. Part of this missing demand is provided by each distributed heat pump by means of electrical power from the compressor. This is a common solution in 5GDHC networks. These HPs cannot provide enough additional energy to account for the strong dip between 50 and 150 days (Fig. 12a). This seasonal mismatch is met by the ice storage, which also meets some of the shorter timescale demands.

The cumulative profiles of the two source capacities look quite different (Figs. 12b and 13b). While the 6 MW case has a similar cumulative trend compared to the demand, the curves for the 3 MW case tend to collapse up till maximum 150 days (winter) for all demands. This indicates that the 3 MW source is used to its maximum power for each demand, as an increased demand does not lead to increased production by the source. This can also be observed by the hourly heat demand shown in Fig. 11a. Namely, the source is used constantly without much fluctuations, except for the overall increase in the heat delivered from 2.5 MW to 4 MW until day 150, corresponding to the increase in source temperature.

[10] Nominal powers/capacities for the WWTP sources are defined for a ΔT at the source of 13 K and mass flow rates of 430 210 kg/h for the 6 MW source and 215 105 kg/h for the 3 MW source, respectively.

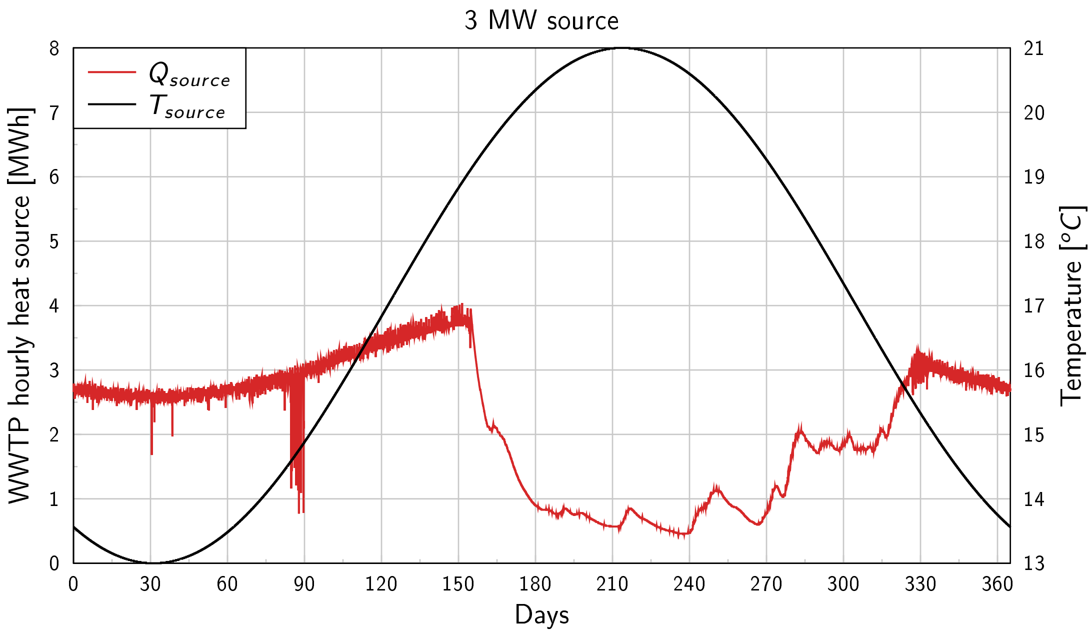

(a)

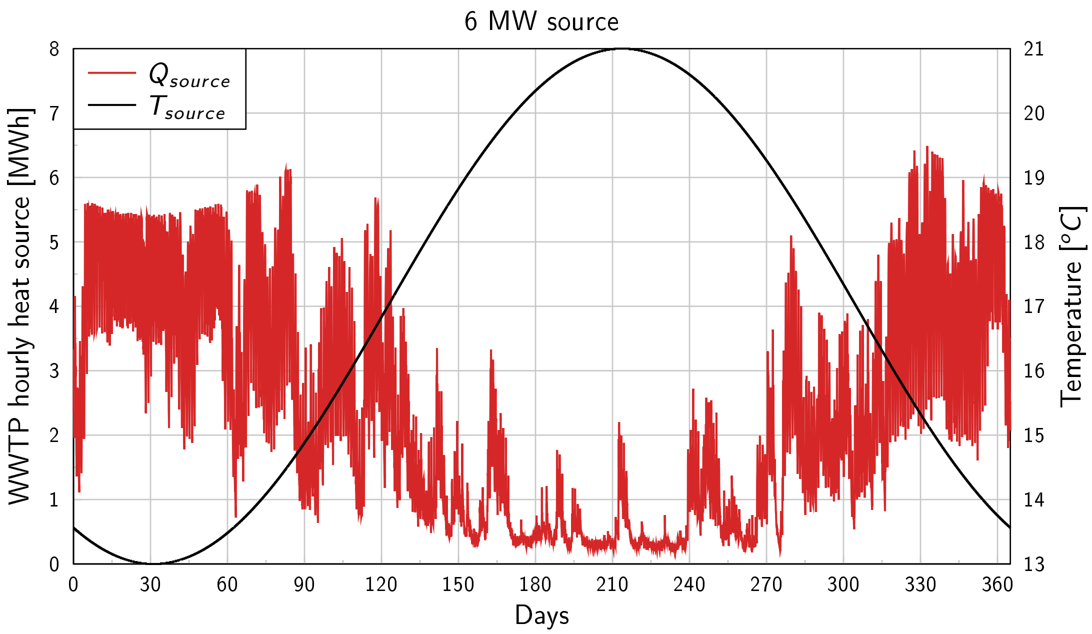

(b)

Figure 11: WWTP source and temperature profiles over a year for two source powers of **a)** 3 MW and **b)** 6 MW.

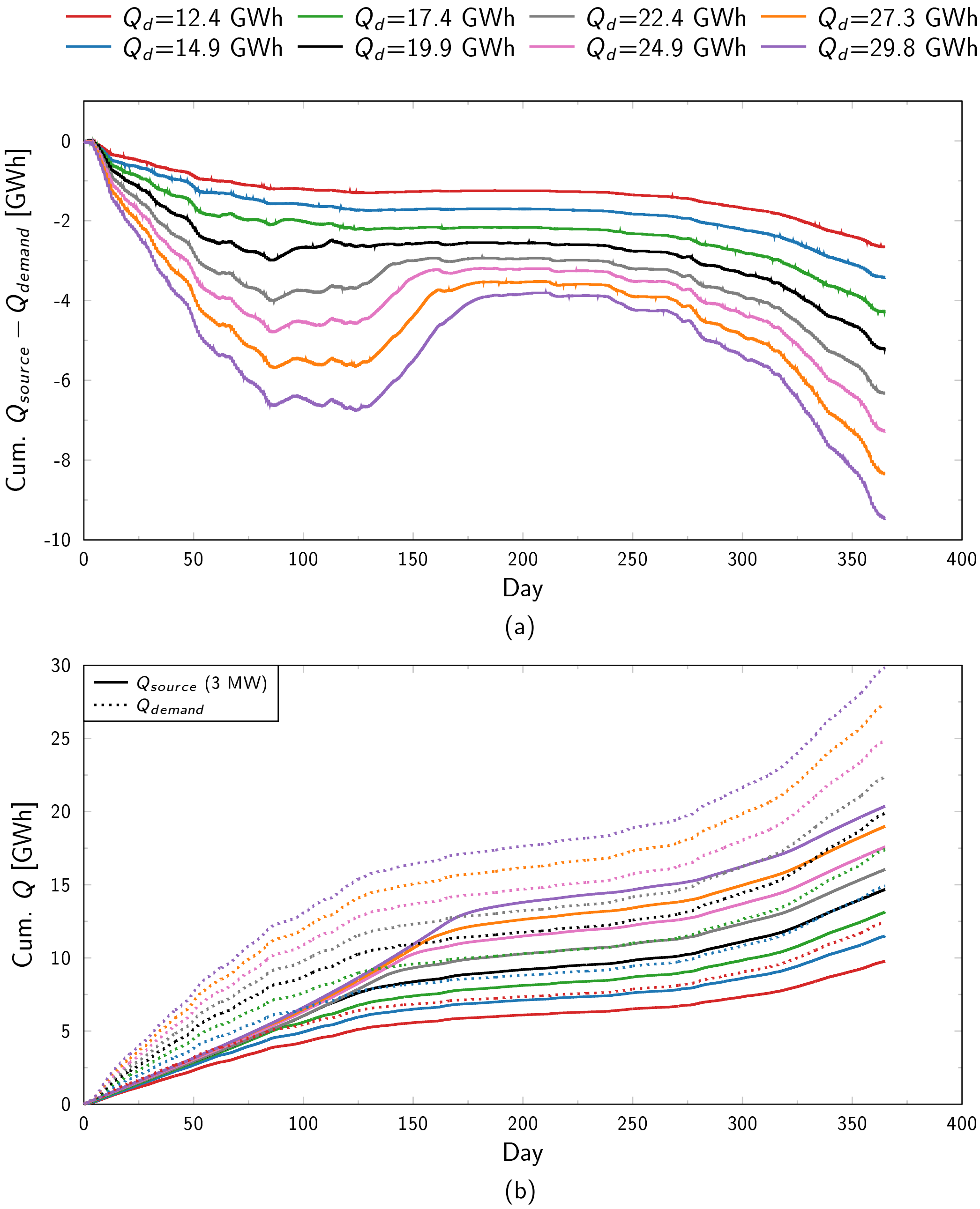

Figure 12: **a)** Cumulative difference between source and demand showcasing the need for storage and additional heat production. **b)** Corresponding source and demand profiles over a year. Cases using a 3 MW WWTP source for several heat demands using a DHW/SH ratio of 0.2.

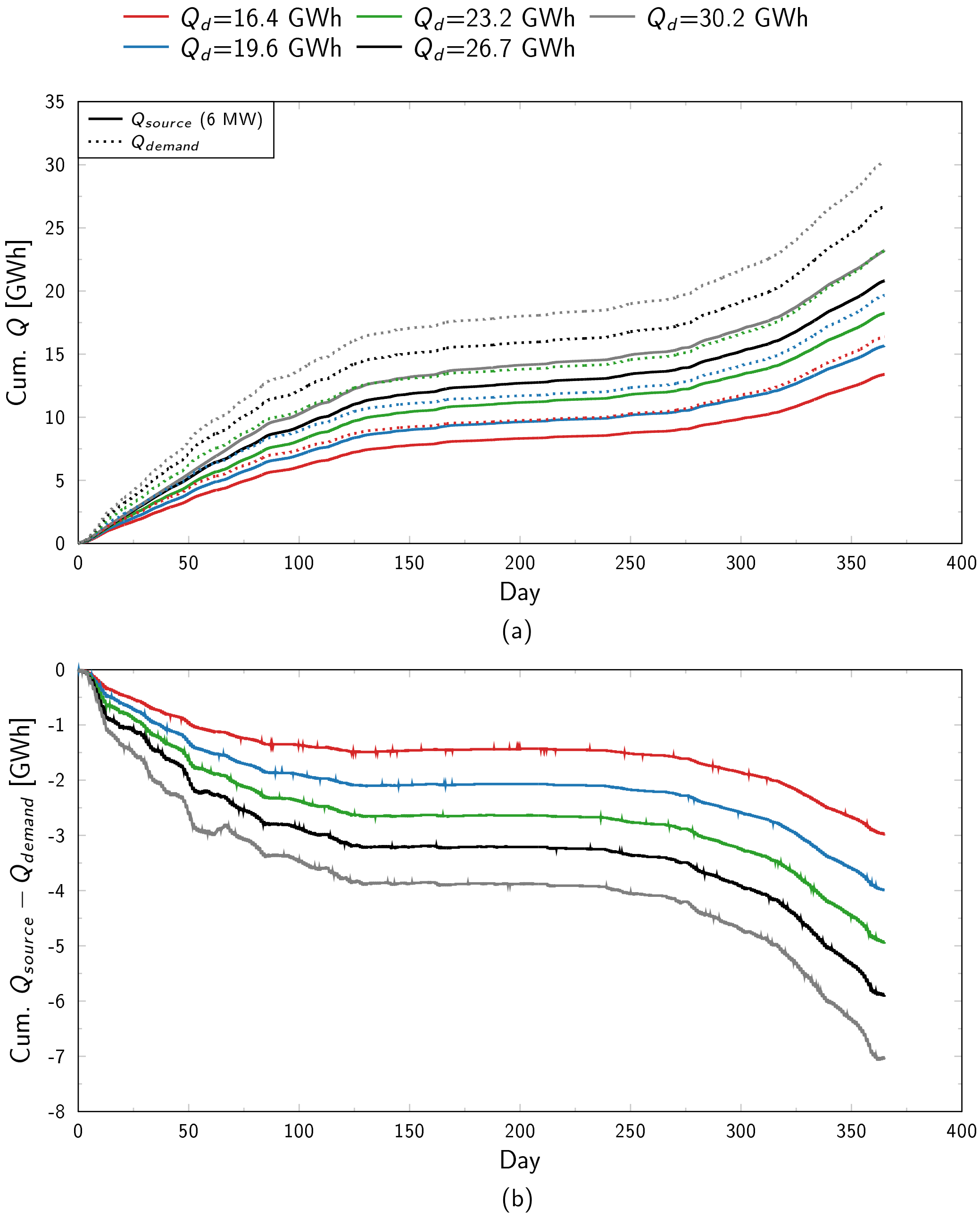

Figure 13: **a)** Cumulative difference between source and demand showcasing the need for storage and additional heat production. **b)** Corresponding source and demand profiles over a year. Cases using a 6 MW WWTP source for several heat demands using a DHW/SH ratio of 0.1.

2.5.2 Solar collectors

Solar-ice systems were systematically studied in our last SFOE funded project Big-Ice (Carbonell et al., 2021), which aimed to explore the potential of solar-ice systems for multi-family buildings. By means of dynamic system simulations with a large parameter variation analysis consisting of more than 3600 runs, the effects of different weather data, hydraulics on the primary (solar, ice and heat pump) loop, building demand profiles and sizes of key components such as collector field and ice storage, were analysed in detail. Scaling factors of ice storage and collector area were reported as m^3_{lat}/MWh and m^2/MWh respectively, based on the total heating demand. The term m^3_{lat}/MWh refers to the total volume of water that is frozen, i.e, the volume of the ice storage multiplied by the maximum ice fraction achieved during the simulation. In our calculations, the volume and mass ice fractions are equivalent, because we do not consider the expansion of ice in the simulations, as it is irrelevant in terms of energy.

Solar energy is provided using uncovered selective collectors. The solar source temperature and heat flows are shown in Fig. 14 for two collector fields of 1 m^2/MWh and 1.5 m^2/MWh. Comparing these results with the WWTP one can easily see the higher need for thermal energy storage for a highly fluctuating source such as solar. Fig. 14c and d show the hourly heat provided by solar and it might surprise the reader that the power provided does not increase in summer, but rather decrease. This is untypical for solar thermal collectors, since irradiation in summer is significantly higher. The main reason is that these simulations include an ice storage, which is regenerated by solar in winter at a very high efficiency since the operating temperature of the collectors is very low due to the sink at 0 °C from the ice storage.

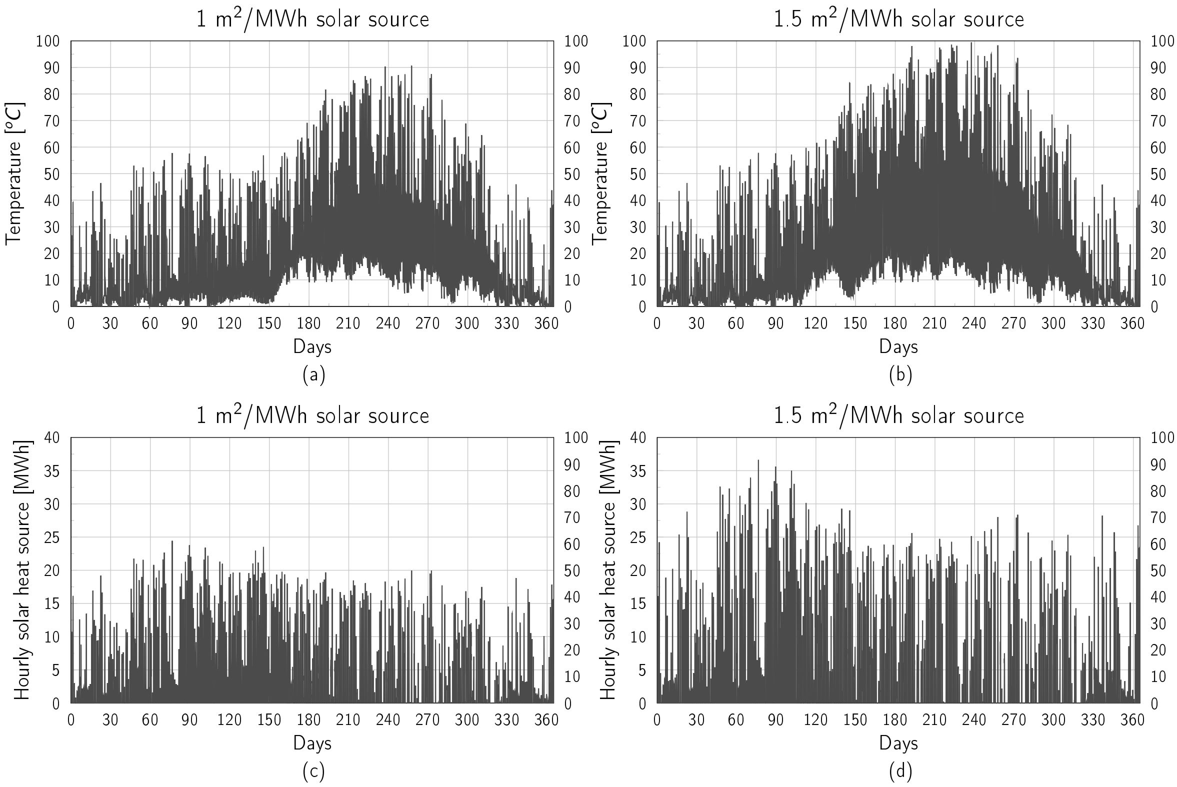

Figure 14: Hourly temperature **a)** and **b)** and solar heat production **c)** and **d)** for two collectors fields of 1 m^2/MWh and 1.5 m^2/MWh.

Fig. 15 shows an example of the cumulative solar heat provided as a function of the input (or output) temperatures of the collector field. The (non-cumulative) delivered heat as a function of temperature can be calculated using Eq. 2.

$$Q(\overline{T}) = \sum_{t \text{ where } T(t) = \overline{T}} Q(t), \tag{2}$$

where $\overline{T}$ corresponds to the temperature values on the x-axis in Fig. 15. Thus, any range of delivered energy (e.g. 0 GWh to 10 GWh) for the blue line does not correspond to the same time steps, nor the same temperature values as the same range for the red line.

Fig. 15 shows an important signal for ice storages which we will be pointing out many times. When there is ice in the storage, the temperature of the passing fluid will be suppressed until all ice is molten. Similarly, sub-zero temperatures are elevated by freezing the storage. The presence of ice in the storage thus dampens temperature fluctuations to near 0 °C. This phenomena corresponds to the almost vertical trend of the source-inlet temperature for the first ∼13 GWh (blue line in Fig. 15). In summary, when such a Q-vs-T plot shows a near vertical line near 0 °C, then this must mean that this cumulative energy is delivered while there is ice in the storage. It is incorrect to state that this energy is used to melt the storage, as this energy also corresponds to 1) times where the storage is freezing, 2) demand being met, and 3) energy lost in the network and the storages in the sinks.

The red line in Fig. 15 shows at which temperatures the collector field is providing energy. This curve is almost linear, with an inflection point occurring near 50 °C.

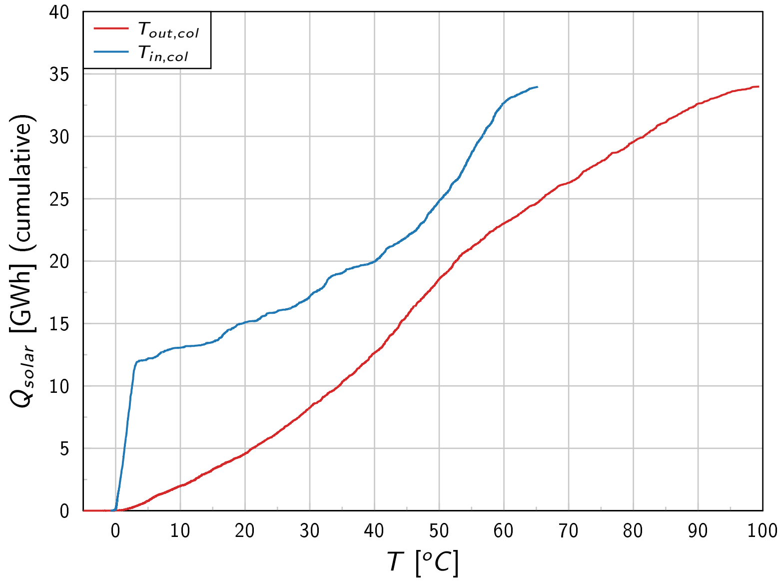

Figure 15: Cumulative solar heat provided as a function of the inlet and outlet temperatures of the collector for a case with 27.3 GWh yearly demand and a collector area of 1.5 m^2/MWh.

The cumulative heat provided by solar collectors over the year for 1 m^2/MWh is shown in Fig. 16a, c and e together with the heat demands for 1.0 m^2/MWh, 1.5 m^2/MWh and 2 m^2/MWh. The difference between source and demand are shown in Fig. 16b, d and f as cumulative values. From these plots it can be observed that a collector field of 1.0 m^2/MWh produces less energy than the the needed demand. The remaining difference is covered by the heat pump electricity. Larger collector areas induce higher temperatures in the system and therefore higher losses.A collector field of 1.5 m^2/MWh induces losses in the order of magnitude of the electricity input of the heat pumps, wherefore the demand and the solar inputs are similar. The difference between source and demand has a clear seasonal component with surplus production in summer and insufficient production in winter. Here is where the ice storage plays a clear seasonal role.

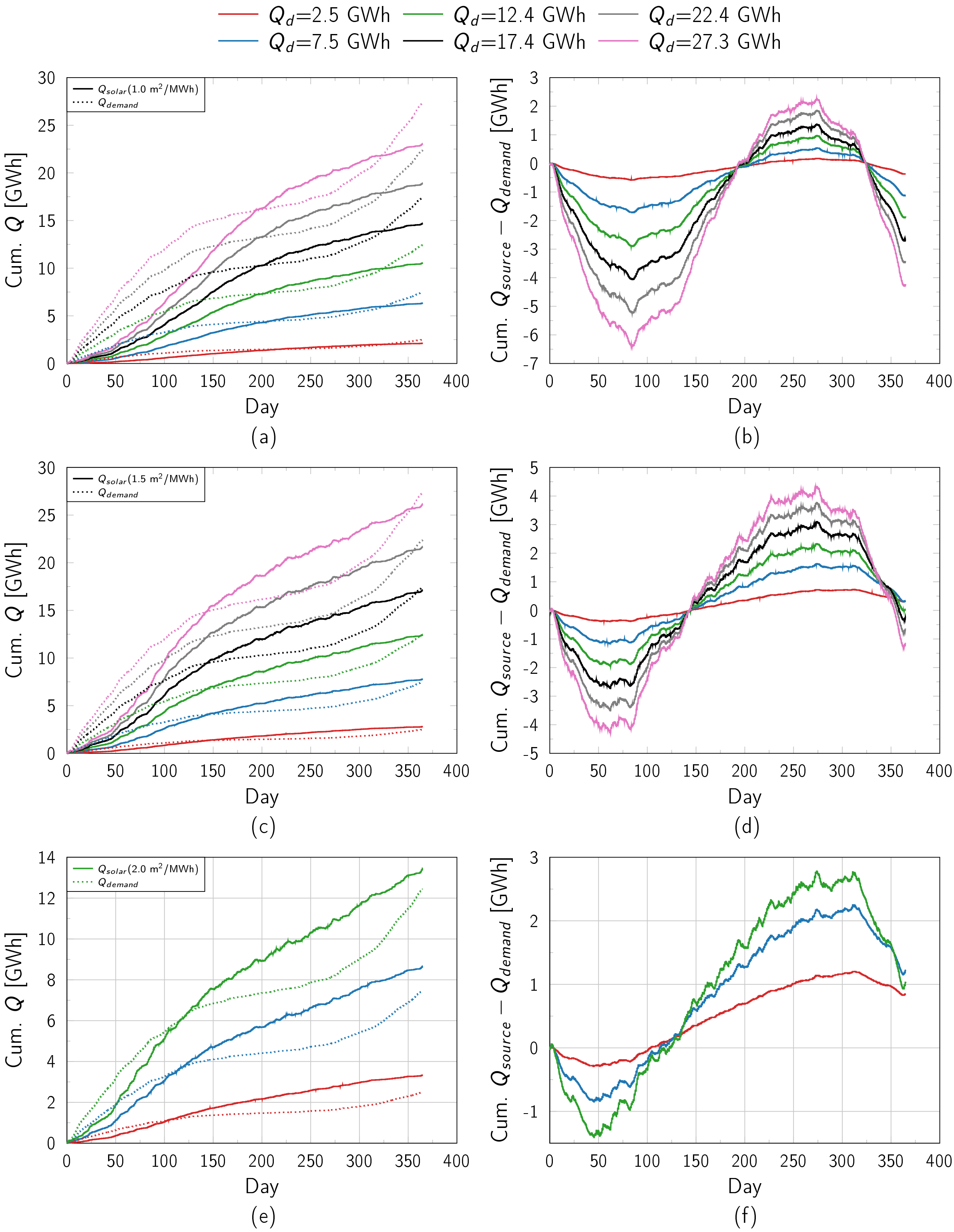

Figure 16: **a)**, **c)**, and **e)** source and demand profiles over a year. **b)**, **d)**, and **f)** cumulative difference between source and demand showcasing the need for storage and/or additional source(s). Cases using a collector field of 1.0 m^2/MWh, 1.5 m^2/MWh and 2 m^2/MWh source for several heat demands using a DHW/SH ratio of 0.2.

2.5.3 Ambient air

Ambient air is a vast thermal energy source that can be exploited using an Air-to-Water Heat Exchanger (AWHX). The size of an AWHX is defined by its nominal capacity at an average temperature difference between the source (outdoor air) and the sink (water or antifreeze). In the following, we always assume an average temperature difference of 5 K and vary the nominal capacity of the heat exchanger. Outside AWHX are easily scaled according to the expected demand. Thus, we use the concept of Full Load Hours (FLH) to vary the sizing of the heat exchangers, where the higher the FLH the lower the capacity (size) of the source. Sizing to a nominal output of 1 MW per GWh of demand therefore corresponds to 1000 FLH. The air source temperature and heat flows are shown in Fig. 17 for two heat exchanger sizes using 500 FLH and 2000 FLH. For this case, the temperature of the source is the same regardless of the capacity since the temperature of ambient air is not affected by heat exchanger sizes.

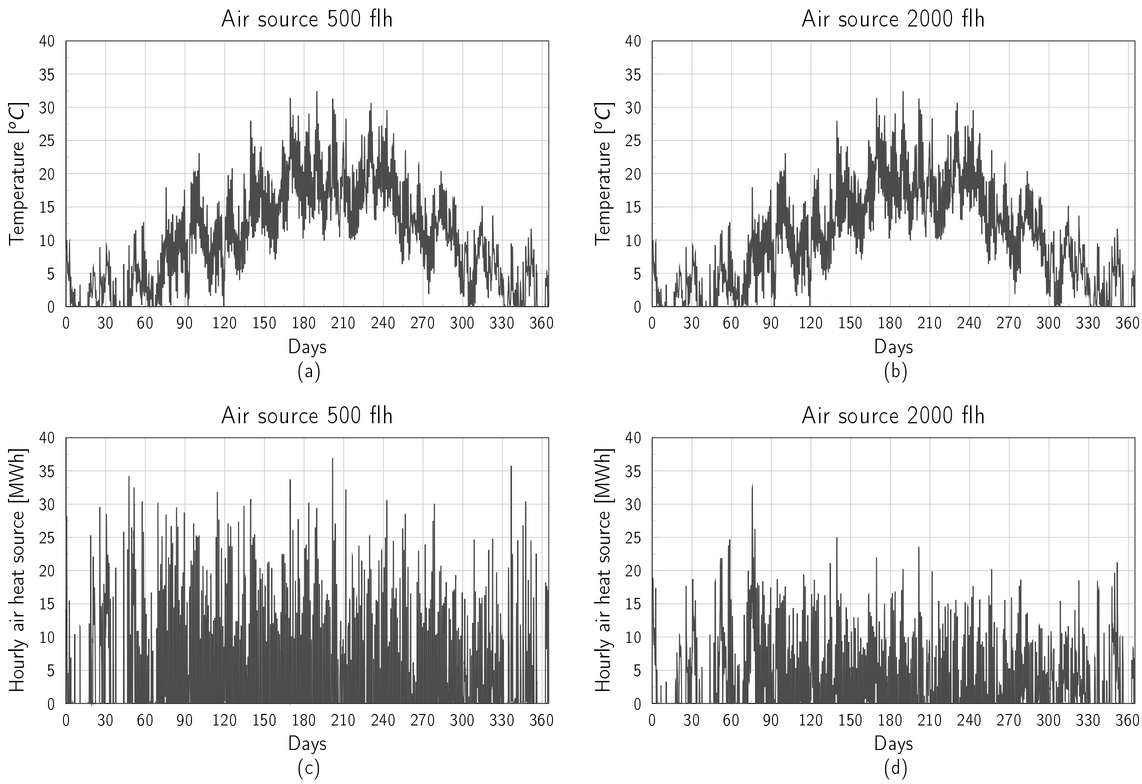

Figure 17: Hourly temperature **a)** and **b)** and air heat exchanger production **c)** and **d)** for two Air-to-Water Heat Exchanger (AWHX) with capacities of 500 flh and 2000 flh respectively. (Full Load Hours (FLH))

Fig. 18 shows an example of the cumulative heat extracted from the ambient air as a function of the inlet and outlet temperatures of the AWHX. Solid and dashed lines respectively display the energy extracted as a function of the inlet and outlet temperature on the air side of the Air-to-Water Heat Exchanger (AWHX). The smaller heat exchanger size of 2000 FLH shows a higher temperature difference between the inflowing and outflowing air and tends to produce the energy at a lower temperature. Here, the influence of ice in the storage is quite clear (see Section 2.5.2, whereas it is not visible for the 500 FLH case. Larger air heat exchangers (i.e. 500 FLH; red lines) are often operated below their nominal power, and therefore at also at lower temperature difference.

The cumulative heat provided by the AWHX over the year for 2000 FLH, 1000 FLH and 500 FLH are shown in Fig. 20a, c and d, respectively. The cumulative profiles follow the same trend after winter for all source capacities. These capacities, however, affect the cumulative source profiles for the first 60 to 90 days, and thus the differences to the demands displayed in Fig. 20b, d and f. This fact can be observed more clearly in

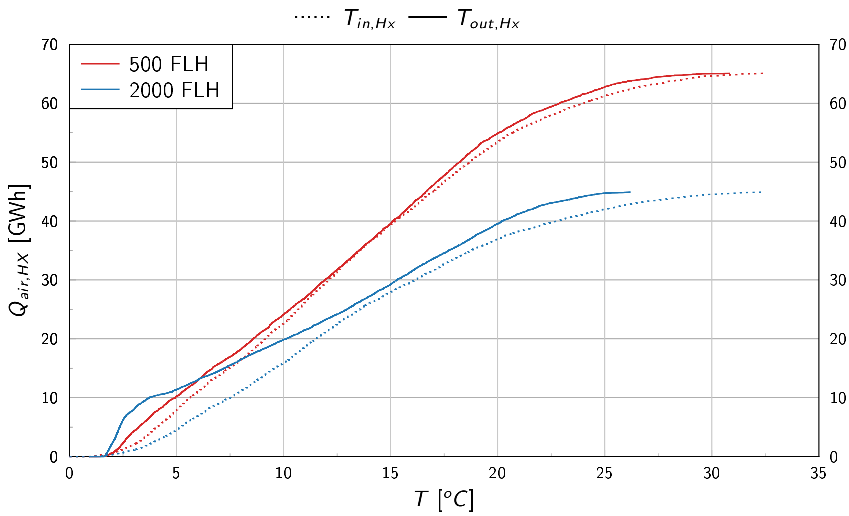

Figure 18: Cumulative ambient air heat provided as a function of the inlet and outlet temperature of the AWHX for a case with 500 and 2000 FLH sizing criteria for the AWHX. Temperatures refer to the source air side of the heat exchanger.

Fig. 19. Specially for large demands > 20 GWh, the smaller heat exchanger size (2000 FLH) shows a larger mismatch in winter between the demand and heat produced by the AWHX, which thus requires higher storage capacity.

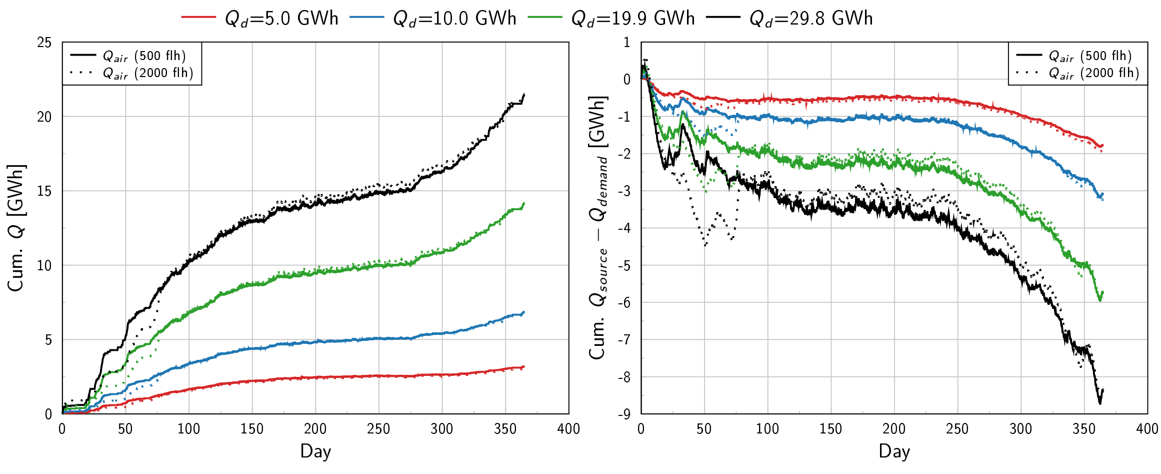

Figure 19: Comparison between source profiles using 500 and 2000 FLH as sizing criteria. **Left)** Source profiles over a year and **right)** cumulative difference between source and demand showcasing the need for storage and/or additional source(s). Cases for several heat demands using a DHW/SH ratio of 0.2.

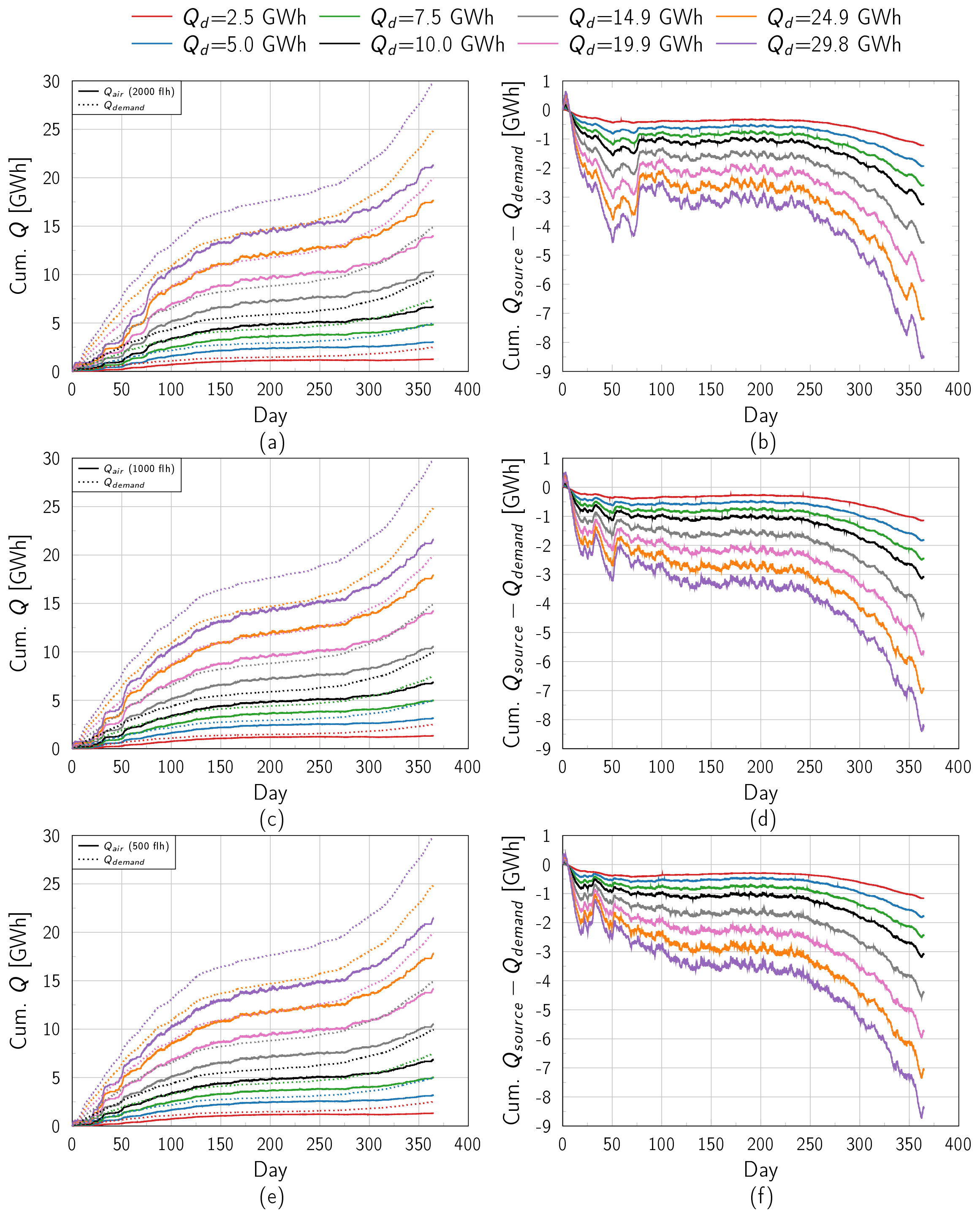

Figure 20: **a)**, **c)**, **d)** source and demand profiles over a year. **b)**, **d)**, and **f)** cumulative difference between source and demand showcasing the storage and additional source needs. Air heat exchanger cases with capacities calculated using 500 FLH, 1000 FLH and 2000 FLH for several heat demands using a DHW/SH ratio of 0.2.

2.5.4 Constant Temperature Source (CTS)

Examples of constant temperature source include waste heat from data centers, cooling, or food processes. We used a constant supply temperature of 15 °C to generalize these types of sources. Fig. 21 shows an example of the cumulative heat extracted from the CTS as a function of the temperatures flowing into (solid lines) and out of (dashed lines) the source. Since this is an ideal case with constant temperature supply, all energy is delivered at 15 °C at the source side of the heat exchanger with different energy exchanges as a function of the inlet temperature. The mass flow rate is assumed to be 1.5 Mt/h providing a nominal capacity of 6 MW.

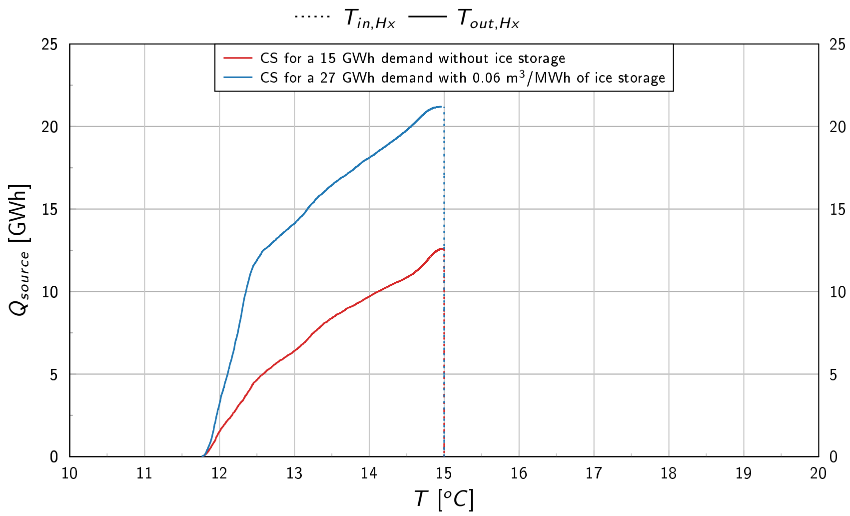

Figure 21: Cumulative heat provided by a CTS as a function of the temperatures flowing into and out of the source with an ideal constant supply of 15 °C and a capacity of 6 MW. Temperatures refer to the source water side of the heat exchanger.

Fig. 22 shows the CTS heat flows for a case with and without an ice storage. The minimum power extracted in winter when incorporating an ice storage is significantly higher compared to the case without an ice storage. The hourly heat provided using an ice storage never drops close to 0 MWh in winter time. The possibility to store energy from a 15 °C source in winter thus becomes very attractive, since a lot of energy can be stored to cover short term demands in an efficient latent thermal energy storage.

Fig. 23 shows the cumulative heat provided by the source over the year together with the heat demands (Fig. 23a), as well as the difference between heat supply and demand (Fig. 23b). Fig. 23b shows that insufficient source energy is available to cover yearly demands larger than 7.7 GWh. As stated before, the additional source energy is provided by each distributed heat pump by means of electrical power from the compressor and the ice storage will compensate the seasonal mismatch between source and demand. The source profiles and their differences with the demands look quite similar to the ones using a 6 MW WWTP since it is not constrained by the WWHX capacity as a difference to the 3 MW WWHX unit.

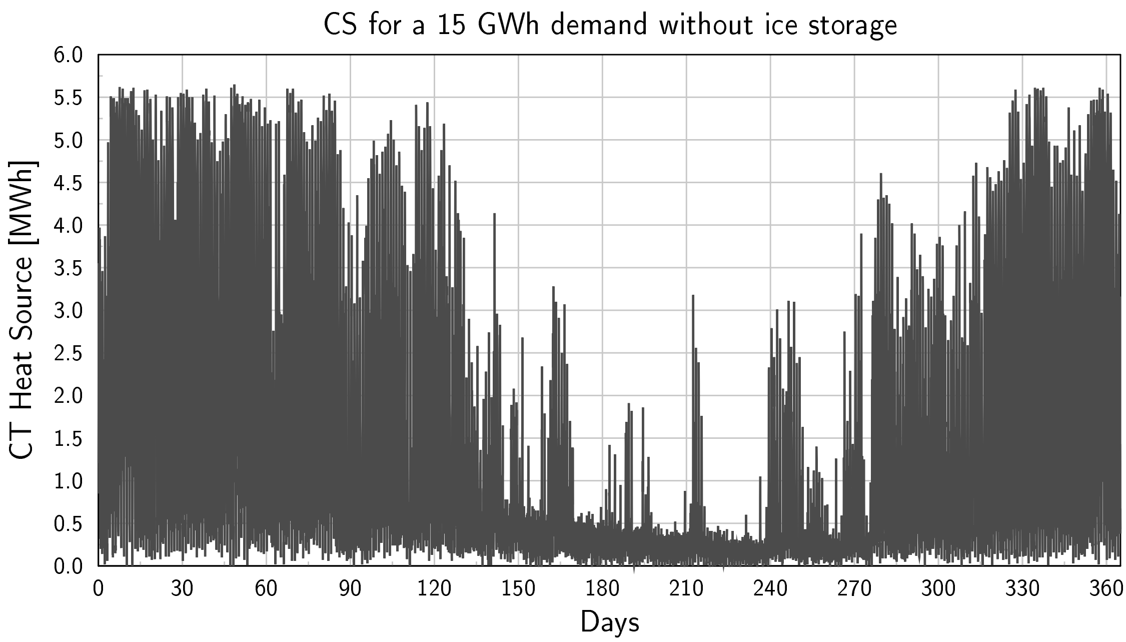

(a)

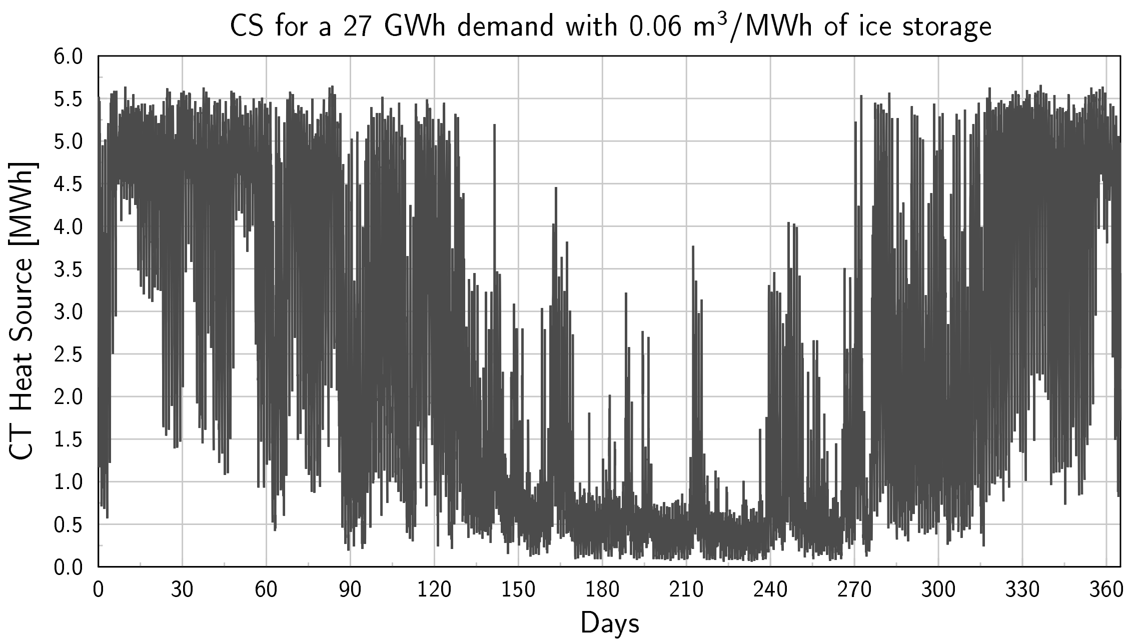

(b)

Figure 22: Hourly heat produced by the generic Constant Temperature Source (CTS) **a)** without and **b)** with an ice storage for CTS capacities of 500 FLH and 2000 FLH, respectively.

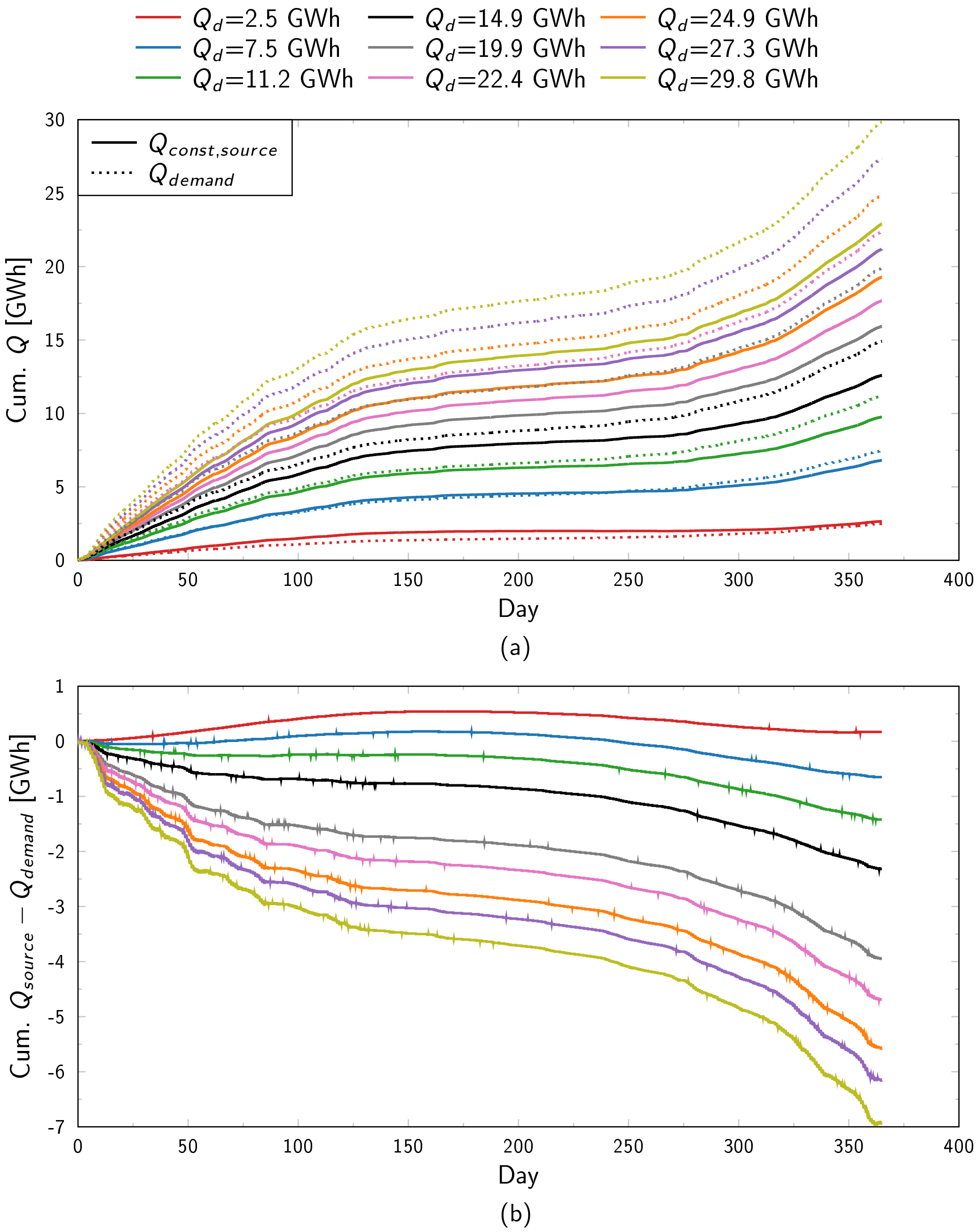

Figure 23: **a)** Source and demand profiles over a year and **b)** cumulative differences between source and demand showcasing the need for storage and/or additional source(s). Cases using a Constant Temperature Source (CTS) for several heat demands using a DHW/SH ratio of 0.2.

2.6 Key performance indicators

2.6.1 Energetic performance indicators

The main energetic performance indicator for the investigated systems is the System Performance Factor:

$$\text{SPF} = \frac{Q_{dhw} + Q_{sh}}{P_{el,T}} = \frac{Q_d}{P_{el,T}}, \tag{3}$$

where Q is the yearly heat demand and $P_{el,hp}$ the yearly electricity consumption of the distributed heat pumps. The subscripts dhw, sh and d stand for domestic hot water, space heating, and total heat demand respectively. None of the simulations in this report use a back-up system, i.e. neither an electric resistant nor a fuel boiler.

Where the ice storage is used to increase the Q_d, we define the additional demand Q_{add} using the maximum demand above which the ice storage is necessary, $Q^{max}_{without,ice}$. Specifically, we define $Q^{max}_{without,ice}$ as the demand required to reach a return temperature of 0 °C (see Section 2.7.1). The additional demand is thus defined as:

$$Q_{add} = Q_d - Q^{max}_{without,ice} \tag{4}$$

For the AWHX and solar thermal sources, $Q^{max}_{without} = 0$ since these sources can't cover the winter demands by themselves, even for very small demands.

The mass ice fraction M_{fice} is defined as the ratio between the mass of ice and the mass of ice and water as:

$$M_{fice} = \frac{M_{ice}}{M_{ice} + M_{water}} \tag{5}$$

We neglect the expansion of ice in our simulations and thus, the mass ice fraction equals the volumetric ice fraction, which is defined similar to Eq. 5, yet using volume instead of mass. The maximum mass ice fraction $M_{fice,max}$ allowed in the simulations is 0.8. Freezing above this value is usually avoided to reduce the risk of cracking the storage vessel due to ice expansion. Our simulations target a $M_{fice,max}$. However, it is not possible to exactly match the target of 0.8. Therefore, to aid comparison between simulations, we correct the volume of the storage considering only the latent part actually used in the simulation as:

$$V_{ice,lat} = V_{ice} \cdot M_{fice,max} \tag{6}$$

This strategy would also allow the comparison of other ice storage systems, where the $M_{fice,max}$ does not reach 0.8, e.g. ice slurry storages where the $M_{fice,max}$ is close to 0.5 (Arenas-Larrañaga et al., 2024) or the thermal de-icing concept developed at SPF (Carbonell et al., 2016c, 2015, Philippen et al., 2012) where the $M_{fice,max}$ might be in the range of 0.6 [11].

The number of cycles of the storage are calculated using both the latent and the sensible part of the storage. To calculate the number of cycles we use a reference nominal capacity as a base line using the latent heat that can be stored per m^3 of water assuming that 100 % of the water is iced as:

$$E_{cap,lat} = 92.36 \text{ in kWh/m}^3 \tag{7}$$

The sensible and latent number of cycles are calculated as the ratio between the delivered energy E_{del} and the reference latent capacity shown in Eq. 7.

$$E_{ncyle,lat} = E_{del} / E_{cap,lat} \tag{8}$$

[11] It was never really measured due to the ice floating on the surface. This makes the calculation of the ice fraction using water level monitoring inaccurate.

2.6.2 Economic performance indicators

For each system the heat costs are calculated using the annuity method. The electricity prices are taken from the price list of a regional Swiss utility and represent typical prices for medium customers. The cost of replacing components during the analysis period is added to the maintenance costs and ignored otherwise. This both greatly simplifies the calculation and avoids the difficult assumption of life time of each component and its residual value. However, one should keep in mind that ice storage casing is expected to last longer than any other components and thus the total cost would be reduced by accounting for that.

To calculate the present value of the total system PV_{sys} the present values of costs for electricity used by the decentral heat pumps (PV_{elec}) and maintenance (PV_{maint}) are added to the total investment costs (I):

$$PV_{sys} = I + PV_{elec} + PV_{maint} \tag{9}$$

The costs of electricity is calculated assuming a fixed yearly increase c of the energy price. The present value of electricity costs is:

for $r \neq c$:

$$PV_{elec} = E_0 \cdot \frac{1}{r-c} \cdot \left(1 - \left(\frac{1+c}{1+r}\right)^T\right) \tag{10}$$

for $r = c$:

$$PV_{elec} = E_0 \cdot \frac{T}{1+r} \tag{11}$$

where r is the rate of interest per annum; c the yearly price change rate of electricity; E_0 the electricity costs in year 1 and T the analysis period in years.

The yearly maintenance costs are derived from the investment costs I by a cost factor m. As a simplification it is assumed that part of the maintenance costs is allocated to replacement procurements for pumps, brine, etc. A relatively high maintenance factor m of 1 % is therefore chosen. The present value of maintenance costs is:

$$PV_{maint} = I \cdot m \cdot b \tag{12}$$

with:

$$b = \frac{(1+r)^T - 1}{(1+r)^T \cdot r} \tag{13}$$

where m is the yearly maintenance costs factor related to the total investment I.

The annuity of the heating system, i.e. the yearly payment of equal amount over the observation period T, is calculated by multiplying the present value with the annuity factor a:

$$\text{Annuity} = a \cdot PV_{sys} \tag{14}$$

with:

$$a = \frac{1}{b} \tag{15}$$

The heat generation costs are obtained by dividing annuity by the yearly amount of heat delivered by the heating system:

$$\text{Heat cost} = \frac{\text{Annuity}}{Q_d} \text{ in Rp./kWh or CHF/MWh} \tag{16}$$

2.7 Searching the parameter space

For each simulation conducted in this project, we need to target our maximum ice fraction assumed of 0.8. However, without sizing rules and with varying demands, it is very difficult to achieve the targeted ice fraction. Fig. 24 shows the parameter space used in the parametric studies conducted. This section describes how we minimized the number of required simulations while getting as much relevant information as possible. We therefore split this Section into the following parts: 1) cases without storage, 2) cases with storage.

In our simulations for the WWTP and the CPS, we increase the heating demand until the source capacity is first exhausted; as zero additional costs is the optimum when the existing infrastructure can meet the demand. The maximum demand where the ice storage is not necessary is defined as $Q^{max}_{without,ice}$ (see Eq. 4). Beyond the source capacity, the optimum storage size is the one that just reaches the maximum allowed mass ice fraction of 0.8 for a given demand.

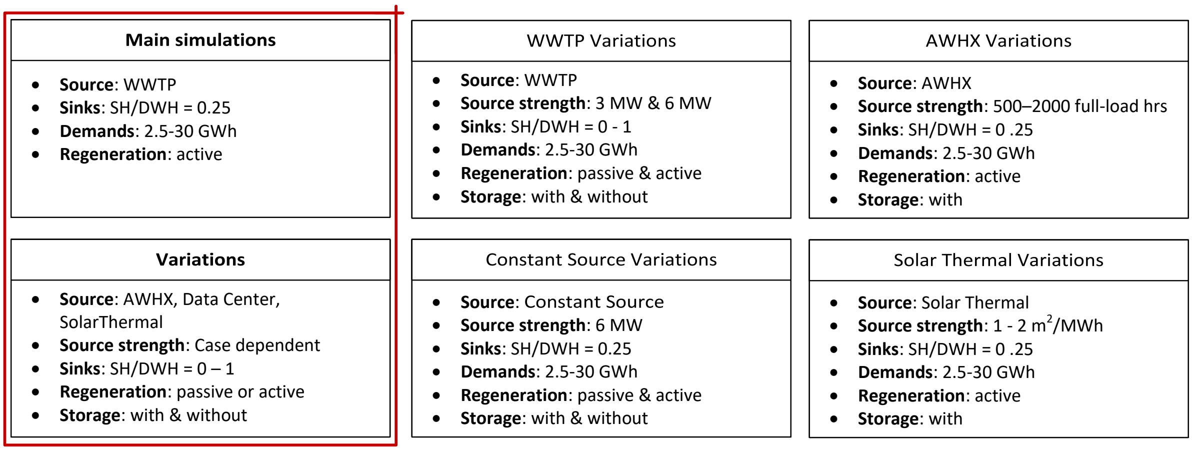

Figure 24: Description of parametric studies conducted in this project. The two containers in the red box respectively describe the main simulations and the variations around those. The other four containers focus on the variation done for each of the four source types. The AWHX and solar-thermal source do not have simulations without ice storage, as the demand in winter cannot be met without storage in our scenarios.

2.7.1 Cases without storage

For cases without an ice storage, simulations can be carried out easily without sizing rules. Thus, the issue of the parameter space is minimal. A grid search suffices, as long as the source can provide enough energy. This is never the case for the AWHX, nor for the solar-thermal source where an ice storage is ways necessary. As soon as the network's return temperature drops below the minimum temperature viable for the HPs, our simulations abort. This latter choice saves on computational cost, as the simulation aborts quite early in the year, i.e. in the coldest winter days.

The most interesting simulations for this category have the network's return temperature just below 0 °C. Although the simulation environment can handle these situations, they are critical in practice. Even with frost protection in the network, there is a risk of frost on the source side of the heat exchanger when operating below 0 °C. Ice storages become viable beyond this demand, as the latent energy can boost the network's return temperature up to 0 °C. The grid search thus has the aim of finding simulations where the network's return temperature drops just below 0 °C. This is easily found in two steps: a coarse grid search followed by a finer grid search near 0 °C.

Fig. 25 shows the network's return temperature as a function of demand for the WWTP variations (Fig. 24), and Fig. 26 shows $Q^{max}_{without}$ for the same. Here, $Q^{max}_{without,ice}$ increases linearly with the ratio of DHW to SH. Increasing the source capacity not only increases $Q^{max}_{without,ice}$; it also decreases the slope of $Q^{max}_{without,ice}$ as a function of the DHW/SH ratios.

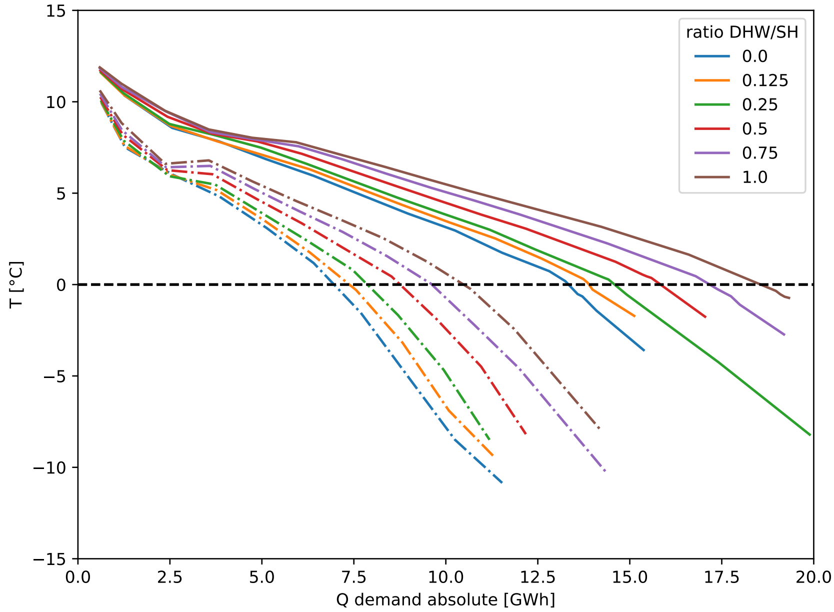

Figure 25: Network's return temperature as a function of demand for the WWTP variations without storage. Dashed lines indicate 3 MW source-capacity cases, whereas continuous lines indicate 6 MW capacity cases.

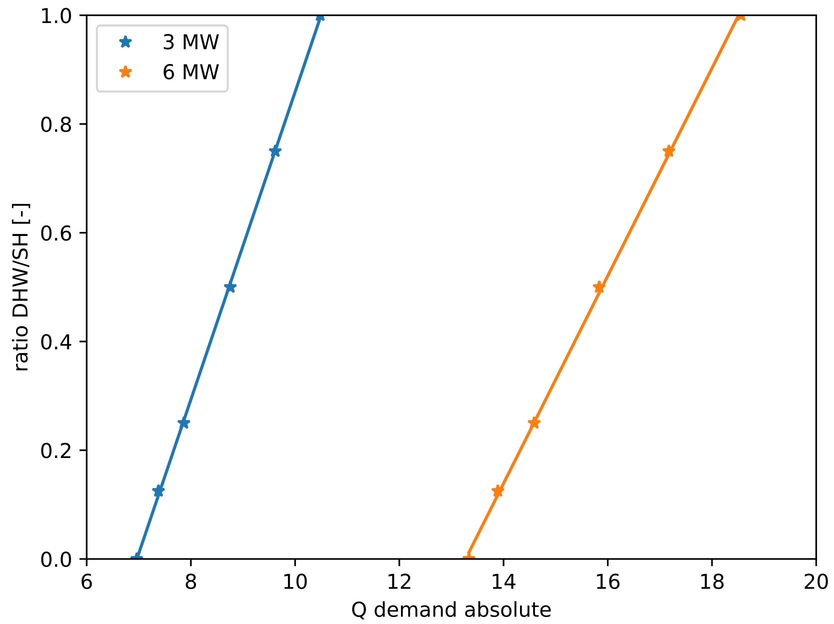

Figure 26: The maximum demand the source can provide without storage ($Q^{max}_{without,ice}$) as a function of demand for the WWTP variations without storage.

As the HPs provide more energy for DHW, thus reducing the energy needed from the source, increasing the DHW/SH ratio increases $Q^{max}_{without,ice}$. Simultaneously, increasing the DHW/SH ratio tends to create a more constant demand over the seasons and since the source is not strongly depending on the season, both demand and source are more aligned with a lower need to store energy.

2.7.2 Cases with storage

For cases with storage, the parameter space to cover the parametric studies considered in Fig. 24 is immense. The possible cases fall into three categories: 1) storage is insufficient, 2) storage is too large, and 3) storage is optimal. Similar to the cases without storage, most cases where storage is insufficient will lead our simulations to abort early in the year. After the storage reaches its maximum, it can no longer boost the return temperature of the network and the return temperature will rapidly plummet below the minimum required for the HPs.

There is only a small range of storage sizes that are optimal and a vast range of storage sizes that are too large. Too find the optimal sizes, we first performed a grid search for demands above $Q^{max}_{without,ice}$. Results without icing rules are shown in Fig. 27.

Fig. 27 shows the maximum ice ratio in a given simulation as a function of additional storage/additional demand. For each constant demand, the maximum ice fraction achieved in the simulation follow an exponential curve in this projection (Eq. 17). This is the case for each of the four sources we investigated.

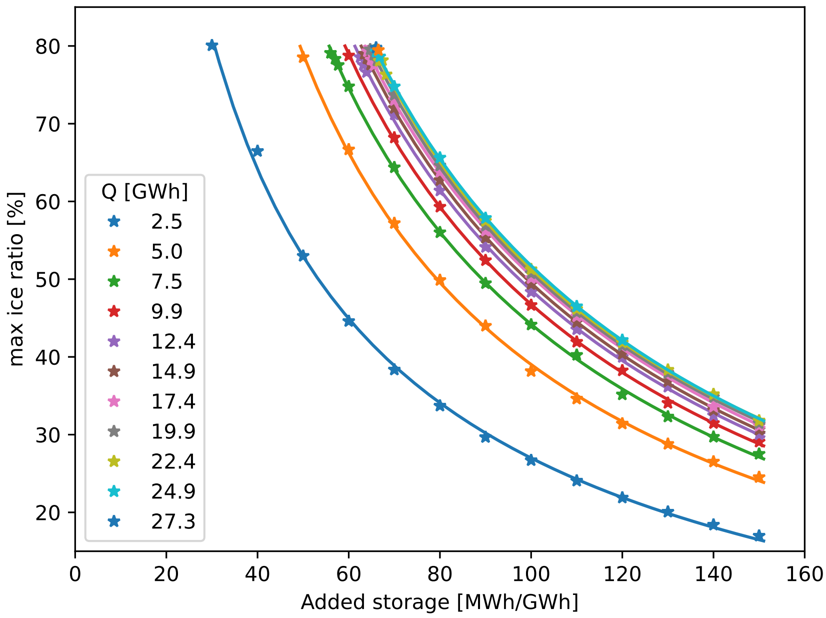

Figure 27: AWHX example: The maximum ice ratio in a given simulation as a function of additional storage/additional demand. Stars denote simulation results, whereas the lines are exponential fits. Each color corresponds to a constant demand.

$$\phi = a * (Q_{store})^b + c, \tag{17}$$

with ϕ the max ice fraction and Q_{store} the added storage per added demand. The coefficients a, b, and c are to be found through fitting.

Fitting these exponential curves allows a rapid prediction of the optimal storage size for a variation allowing thus to simulate each specific case targeting the maximum ice fraction close to 0.8. When discussing results in the following sections we mainly show configurations with well sized ice storage volumes reaching ice fractions close to the optimal 0.8 limit.

3 Results

We start this section with a validation of the reversible buried double pipe model by comparing it with measurement data from the FGZ network. This is followed by our investigation into active and passive regeneration. Based on these results, we will only show active regeneration cases when showing the results for optimal storage sizes. In such generalised results, we combine the example network Jona with different source types, while also varying the absolute demands and DHW to SH ratios. We have collected these main results according to the source type and present them in the following order: Solar-Thermal, WWTP, constant source, and AWHX.

3.1 Model validation

5GDHC networks usually feature uninsulated buried double pipes. These pipes interact significantly with both the ground and with each other, because of a lack of insulation. This Section presents our efforts to analyse such uninsulated and buried double pipes within an existing anergy network, to subsequently develop a numerical model and validate it with monitored data from an existing 5GDHC network.

Parts of the section below are reported as (Schubert et al., 2022).

3.1.1 Energetic analysis of an existing anergy network

This project requires insight in both the behaviour of insulated and buried double pipes by themselves, and as part of a district heating network. To gain such insights, we analyzed monitoring data from the 5GDHC network of Familienheim-Genossenschaft Zürich (FGZ) in Zurich. In its final stage of extension in 2050 this network will be serving the heating demands of approximately 5500 inhabitants occupying around 2200 dwellings. In 2020, which is the year analyzed below, the network included two data centers with a combined nominal cooling demand of 80 GWh/a, two ground probe fields with a combined 332 probes of 250 m length each, and six energy substations with a total installed power of 7.3 MW. The network nominally provided 35 GWh heat for space heating and domestic hot water. The energy reference area serviced was 185 000 m^2. The network length is 1500 m and untreated water is used as the heat transfer fluid.

The monthly energy balance of this network for the year 2020 is shown in Fig. 28. Network components that add heat to the system (sources) are on the positive side, while components that take heat from the system (sinks) are on the negative side. All values except for those labelled “pipes heat exchange” were extracted from monitoring data. Sources 1 and 2 are both data centers, with 1A and 1B representing two connections to the same data center. All sinks are substations serving various dwellings. Note that while energies for free cooling were recorded, their contribution is negligible and too small to be seen in the plot. The “pipes heat exchange” is defined as the difference between the sink and the source values, thus ensuring that a balance is achieved. We assume that these differences are entirely due to thermal losses and gains occurring in the network pipes and hence named them accordingly. It can clearly be seen that the heat losses through the pipes are higher in the warmer months from April to September than in the remaining colder ones. Since the ground is still relatively warm in November due to the warm summer months, there are small pipe heat gains during this month. The ground probe fields act as heat sinks from April to October and as heat sources for the remaining months.

There is a 580 m long section of the network between the two substations of "Source1" and "Groundsource2" without any substations in between. "Source1" is a node of source 1 and "Groundsource2" is a node of the ground probe field 2. This piece of double pipe is used for a deeper analysis of pipe losses and gains. Temperatures for said segment over the year 2020 are shown in Fig. 29.

The temperatures of the warm (solid line) and the cold (dashed line) pipes are shown at "Source1" (blue) and "GS2" (ground source 2; orange) in Fig. 29 a). The temperature level outside the heating period (April–October) is up to 27 °C in the warm pipe, while it stays just below 25 °C in the cold one. This is above the ground temperature even in the warm summer months and explains the pipe losses. From November to

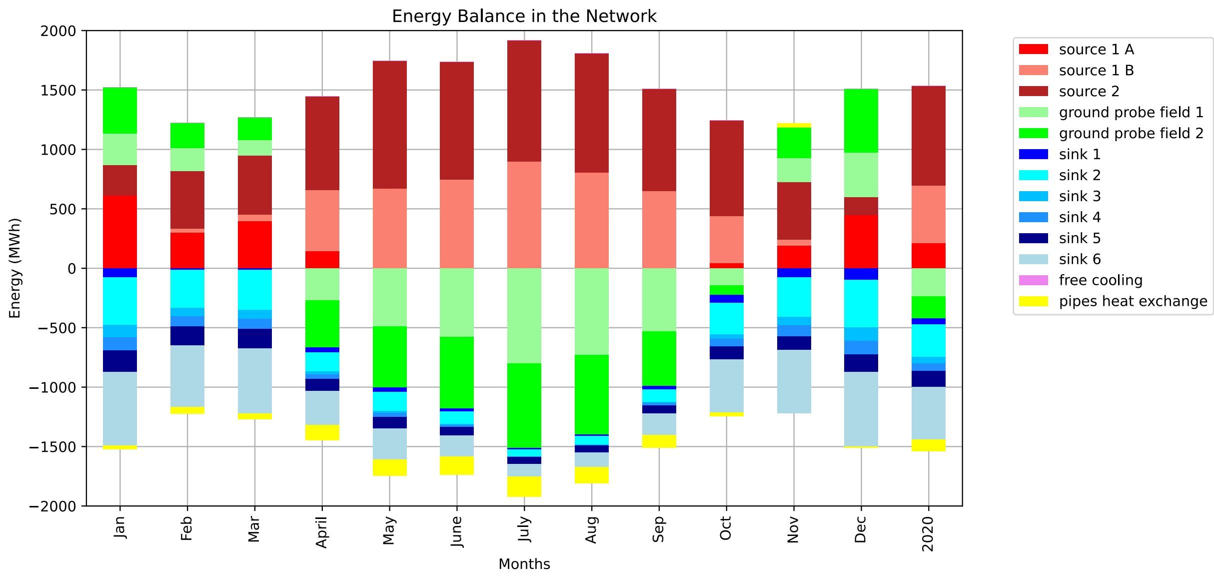

Figure 28: Monthly energy balance of the FGZ network. The bar labelled "2020" represents the yearly balance divided by 10 for comparability. Components on the positive side provided heat to the network, while those on the negative side extract heat.

March the temperature level of the network is around 15 °C in the warm pipe and around 11 °C in the cold pipe. The drop in temperature occurring in November marks the start of the heating season.

Fig. 29 b) shows the temperature differences for the warm pipe (red line) and the cold pipe (blue line) between the two substations "Source1" and "GS2". These temperature differences directly reflect the heat losses and gains for the two pipes over the examined section. The temperature difference is taken between the upstream and the downstream point in each pipe. This means that the difference is formed in an inverse fashion between the warm and the cold pipe, since the flow directions are opposite to one another. Consequently, heat losses are reflected by positive values and heat gains by negative values in the temperature difference. It should be noted that for the year 2020 there was a predominance of cooling over heating demand leading to relatively high network temperatures and hence to relatively large losses. These will be reduced when more heat sinks are connected to the network, as planned.

3.1.2 Validation of buried twin pipe model

In this project, the network pipes are simulated in TRNSYS using an extension of Type 951 from the TESS libraries[12] . Type 951 models a "buried twin pipe". This type was extended to allow changing flow directions in both pipes which is not possible with the original type.

While most parameters of the pipes, like, e.g., their diameter, are known from planning data, the thermal conductivities of both the pipe material and the soil are determined by fitting them to the monitoring data presented in the previous section.

In the buried double-pipe model, two identical pipes are symmetrically placed in a common casing with a fill material embedded by soil. The flow direction of the pipes is defined by the sign of the mass-flow rates which are model inputs. We only consider conductive heat transfer between the pipe, the filling material, and the soil. Thermal resistances between the pipes and between each pipe and the surrounding soil are calculated. Around the casing, a finite difference model of soil conduction is employed to calculate heat accumulation and dissipation. In real systems a rectangular cross section is dug out to lay the pipes and subsequently filled with

[12] `https://www.trnsys.com/tess-libraries`

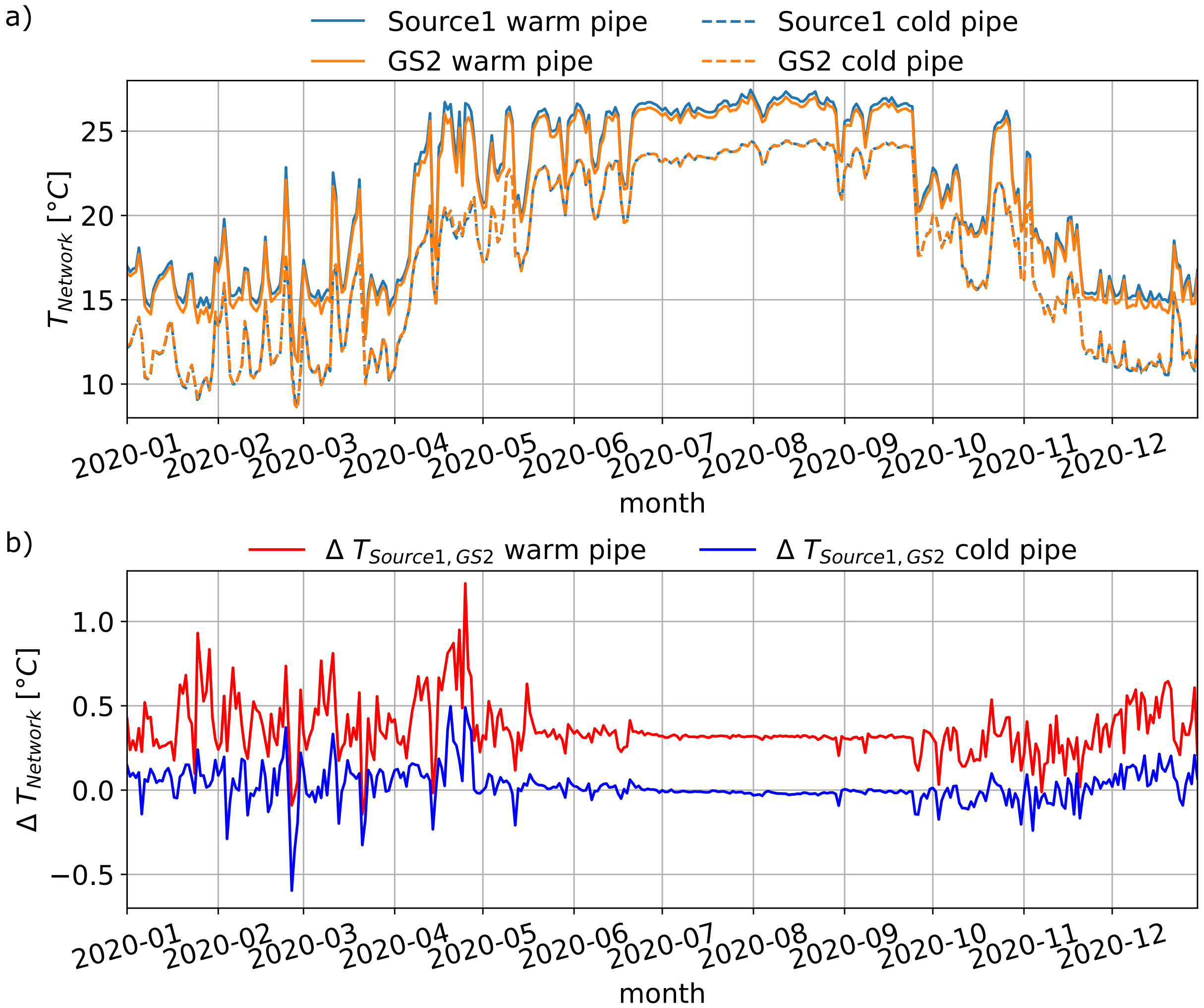

Figure 29: Pipe temperatures in the FGZ network at substations "Source1" and "Groundsource2": **a)**Absolute temperatures of the warm (solid lines) and cold (dashed lines) pipes. **b)** temperature difference ΔT between the two stations for the warm (red) and cold (blue) pipes.

filling material. In the model the geometry is concentric around the symmetry axis of the double pipe. Note that the radius around the symmetry axis for which interaction with soil can be considered is limited to the burying depth of the pipes. All geometric parameters are fixed to the physical values of the installed network. For the purpose of this validation, the pipes have an inner diameter of 42 cm, the distance between the centers of the pipes is around 75 cm, and the pipe depth is taken to be 2 m below the surface. The latter is close to the average pipe depth in the relevant part of the system.

In a first step, the effect of the meshing resolution was analyzed by varying the number of control volumes. The accuracy of the newly developed type did not increase when going beyond 5 radial and 4 circumferential soil nodes. Thus, the numbers of nodes were kept at these values. On the axial dimension, 20 nodes were used for the soil and 60 for the fluid. In a next step, we analyzed the effect of thermal properties (conductivity and capacity) of the filling material and surrounding soil. We mainly analysed the changes in the thermal conductivity of gravel and soil. For the pipe itself a typical heat conductivity value for plastic pipes was selected.

Thermal conductivities of ground and filling material vary over the year depending on the water saturation of the ground. Water saturated loam or gravel have much higher thermal conductivities than their dry counterparts.

A summary of thermal ground properties can be found in Santa et al. (2017). In the new model, the ground properties are assumed to be constant over time.

We used a simple simulation to calibrate both the thermal conductivities of the soil around and the gravel between the pipes. This simulation includes a section of double pipe representing the 580 m long section between "Source1" and "Groundsource2" analysed above. For this test simulation the inlet, temperatures and mass-flow rates of the two individual pipes were taken directly from the measured data. The simulation then yielded the respective outlet temperatures. The thermal conductivities were then varied to minimise the difference between annual losses measured in this part of the network and the annual losses determined through the simulation. Exploring different parameter variations, the best match between measurement data and model was found at a thermal conductivity of 3.00 W/(mK) for the filling material (gravel) and 2.35 W/(mK) for the soil. At these values the annual difference in thermal losses between the simulation and measured values is less than 6 %.

For the validation, we selected two periods of the simulated year that exhibit strong temperature dynamics. Fig. 30 shows the results for these two periods, where the solid lines are the model outlet temperatures, and the dashed lines are the measured inlet and outlet temperatures of the pipes. As mentioned above, the measured inlet temperatures are used as the model inlet temperatures. While there are some deviations, the model outlet temperatures (red and blue)follow their measured counterpart quite well within the small temperature difference with respect to the inlet temperature.

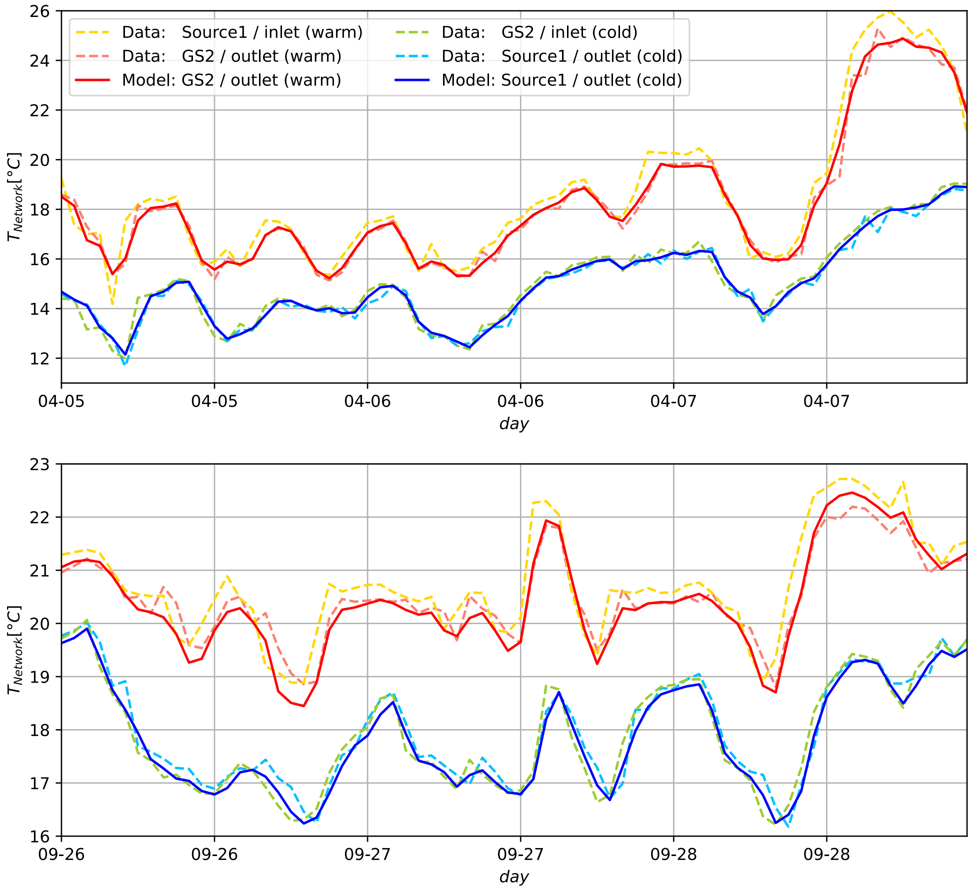

Figure 30: Comparison between the model outlet temperatures (solid lines) and the measured inlet and outlet temperatures (dashed lines) over two 3-day periods at the beginning of April and the end of September. These periods were chosen because of their pronounced temperature dynamics compared to other periods.

The adaptation and parameterisation of the double pipe model was validated with measurement data from the FGZ 5GDHC. The main purpose of this model, is to rapidly calculate temperature updates with sufficient accuracy, to allow us to run many yearly simulations with little computational cost. For this purpose, the simulated and measured data for the pipe section under consideration agreed very well with each other, especially considering the large uncertainties and the low temperature differences involved. The sensors used from the FGZ monitoring system were mainly installed for functional testing and not for scientific monitoring with temperature measurement uncertainties on the order of 0.5 K. This uncertainty is very high considering that 1) the temperature differences between flow and return is on the order of 4 K and 2) these differences are even lower between the inlet and outlet temperatures of the measured pipe section. Thus, the quantification of heat flows from measured temperature sensors and mass flow rates are also associated with high relative uncertainties. Moreover, temperature sensors were positioned in large pipes with diameters of DN 400 without ensuring they were installed in well mixed regions, which further increases the uncertainty. This means, that better data might have allowed for an even better validation, even for the simple model under consideration. Still, the main purpose of the model is to be accurate enough at minimal computational cost, which our validation has shown is the case. Despite the uncertainties, the numerical modelling of the double pipe system lead to the following conclusions.

The evaluation of the measurement data and the simulations show that the effect of the surrounding soil on the temperature of uninsulated pipes is small in the 5GDHC of FGZ. Due to the operating temperatures of the FGZ network above ground, measurements show that there are almost always heat losses to the ground ($\sim$7 % in July). The main exception is November, where there was a sudden drop in operating temperature due to the start of heating dominated operation, which explains the piping gains on the measurements. The difference in the overall balance between the gains and losses was only 6 % between the measured and simulated case. Though this should be taken into account when interpreting the results, the exchange with the far field is a negligible contribution to most of our simulations.

For those example network simulations that incorporated an ice storage, the operating temperatures in winter were below the temperature of the surrounding ground. As a result, the ground supplied heat to the pipes in winter, which accounts for approx. 5 % of a typical energy demand for the network analysed. Over the whole year, however, the losses that occur at higher operating temperatures in summer predominate for most sources. The shift towards more gains in winter with the ice storage integration corresponds to the expected effect of the lower operating temperatures.

3.2 Passive vs. active regeneration

In this Section, we will first discuss ice storage regeneration concepts. There are two ways of regenerating (melting) the ice storage, i.e. passively and actively.

In passive regeneration, we only use the volume flow generated by the decentralised pumps to regenerate the ice store. When demand is low, i.e. exactly when source capacity would be available for regeneration, only a small flow is required and the full capacity of the source is often not utilised. As described in the method section, we have therefore added an additional pump bypassing the grid to actively regenerate the ice store when demand is low. In this section we compare this active regeneration with passive regeneration and show why we only use the more efficient active regeneration for further analysis.

Here, we present two forms of results: 1) a direct comparison of the internal workings of the ice storage in active and passive mode, and 2) the impact the regeneration choice has on storage size and SPF values. For these comparisons, we will only present two CTS cases, as the results are qualitatively the same for WWTP cases.

Fig. 31 shows the ice storage temperature and the ice fraction for an active and a passive case.

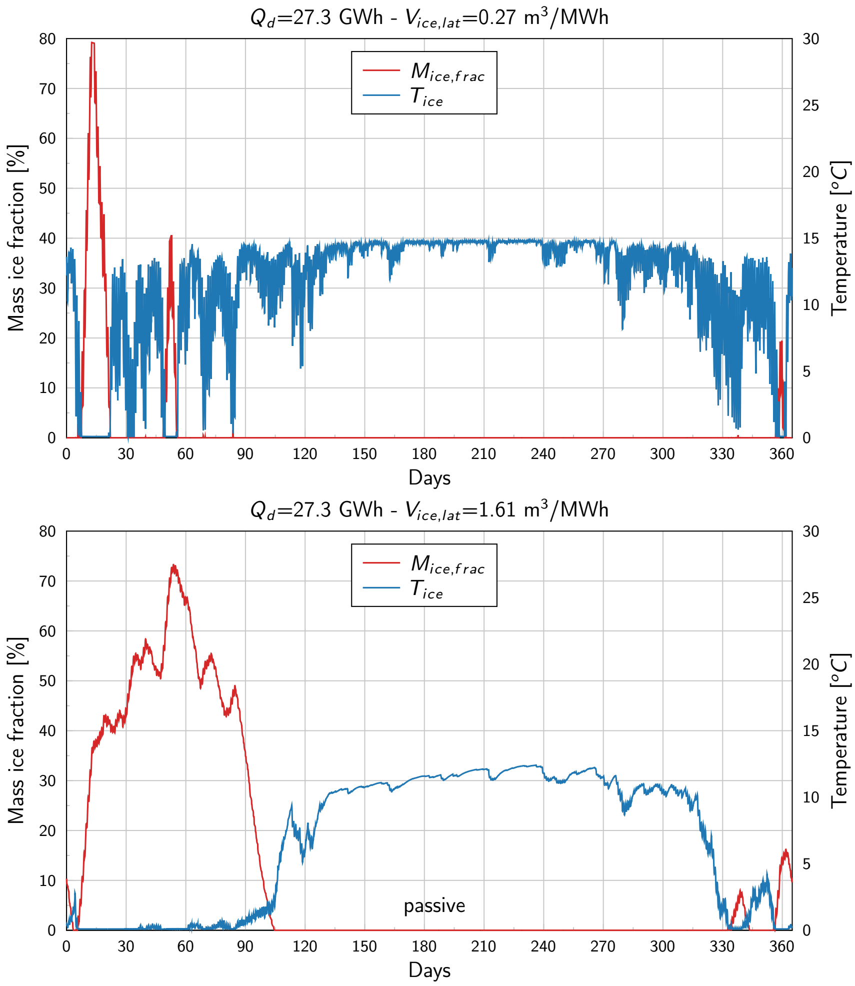

Figure 31: Comparison of passive (bottom) and active (top) regeneration results for the Constant Temperature Source (CTS) case, focusing on the mass ice fraction (red) and the average temperatures in the storage (blue). The passive case requires 1.61 m^3 per additional MWh of demand, whereas the active case only needs 0.25 m^3 per additional MWh of demand.

The active regeneration induces a quick melting of the ice in periods with low demand and therefore only shows two icing peaks between January and March. Furthermore, the rapid regeneration of the storage to 15 °C allows the usage of stored sensible heat, also in low demand periods in winter. On the other hand, the passive regeneration case cannot regenerate fully until mid-April.

The rapid regeneration in the active case not only allows an operation at higher temperatures in winter, but also the reduction of the storage size and associated cost.

Fig. 32 shows the impact of the regeneration choices on both storage size and SPF. Here, the SPF decreases non-linearly with increasing demand, even before the cross-over point ($Q_{add,d}$=0). For low added demands ($Q_{add,d}$=3 GWh), both active and passive regeneration have very similar SPF values. As $Q_{add,d}$ increases further, the SPF values of the active regeneration cases diverge non-linearly from the linear trend of the passive regeneration cases. Interestingly, the SPF values of the passive regeneration cases are independent of the storage size. In other words, there is no added benefit of having an over-sized storage from an SPF standpoint when using passive regeneration.

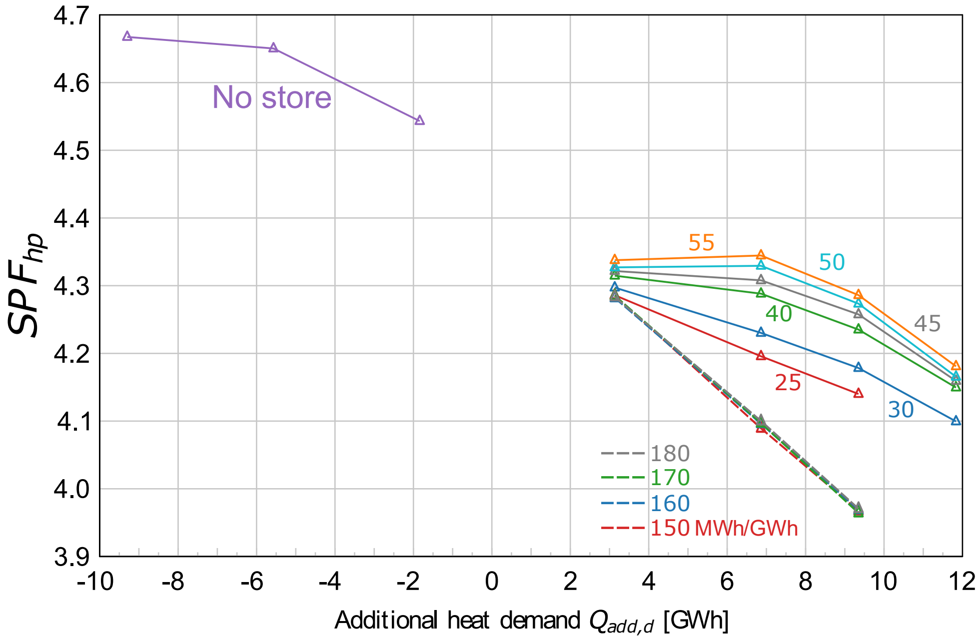

Figure 32: Seasonal Performance Factors (SPFs) as a function of additional heat demand ($Q_{add,d}$) for the active (solid lines) and passive (dashed lines) regeneration results for the Constant Temperature Source (CTS) case. Q_{add} is defined as the demand above the maximum demand, that the source can meet by itself. Colours show the relative size of the ice storage for each simulation.

For the active regeneration cases, Fig. 32 shows a stronger dependence of the SPF on the storage size. As the storage size increases, given the same demand, the SPF increases with it. These increased SPF values for the active regeneration cases are obtained using much smaller storage volumes. These results show, that passive integration (without an additional pump) of the ice storage tank is unfavourable and therefore the potential of an ice storage integration cannot be fully exploited. Active integration with an additional pump allows to meet the same demand with a smaller storage, decreasing the levelized cost of the storage. However, there is a need of additional pumping energy, which has not been analysed in detail.

In summary, an ice storage allows network operators to meet much more demand with the same source infrastructure. Active regeneration extends the maximum possible range beyond that of passive regeneration, while requiring less storages at the additional cost of pumping. Based on these results, we chose not to pursue passive regeneration further. Therefore, all subsequent results only include active regeneration.

3.3 WWTP source

We conducted the following variations for the WWTP cases: 1) DHW/SH ratios of 0, 0.1, 0.2, 0.4, 0.6, and 0.9, 2) heat demands up to 30 GWh, and 3) source-capacities of 3 MW and 6 MW. The corresponding results are presented in the following order: 1) Optimal storage sizes and SPF, 2) cumulative heat fluxes: 3 MW, and 3) cumulative heat fluxes and cumulative number of cycles: 6 MW.

3.3.1 Optimal storage sizes and SPF

Fig. 33 displays the optimal ice storage sizes using both m^3_{lat} per MWh and MWh_{lat} per GWh of overall heat demand as a function of that demand. The conversion factor between the two representations is 93 kWh_{lat}/m^3_{lat} obtained from the latent heat and the density of water.

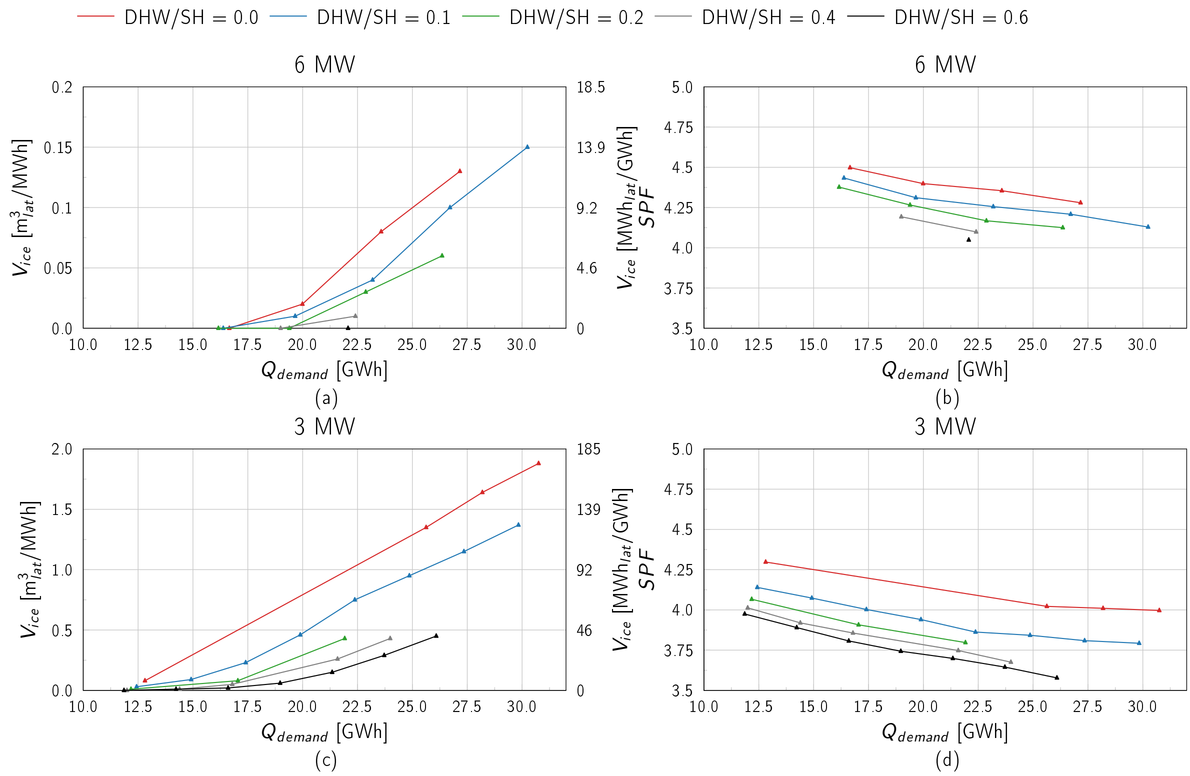

Figure 33: **a)** and **b)** optimal ice storage sizes and **c)** and **d)** SPF as function of the total heat demand for different DHW/SH ratios. Cases simulated with a WWTP source of 6 MW (top row) and 3 MW (bottom row).

These results show that an increase in the DHW/SH share lowers the required ice storage size. As shown in Fig. 10, increasing the DHW share produces a more constant hourly profile over the year (a more linear cumulative value), which decreases the need for a seasonal storage. This is expected since DHW is provided all year round while space heating has its peak in winter. Comparing the 3 MW case with the 6 MW case, the 3 MW case needs up to x10 larger ice storages. Roughly speaking, the ice storage starts to be necessary for heat demands > 12.5 GWh for the 3 MW source and > 17 GWh for the 6 MW source.

The SPF of the complete network ranges between 4 to 4.5 for the 6 MW source and between 3.6 and 4.3 for the 3 MW source decreasing with increasing demand and ice storage volumes. The larger the ice storage the more often the network is at low temperatures which results in a lower SPF. This effect is more significant for the 3 MW case due to the higher ice storage needs.

To compare optimal sizes using the 3 MW and the 6 MW WWTP sources, it is convenient to plot the results as a function of the full load hours (Fig. 34). The full load hours are calculated here using the typical expression, i.e. the ratio between the total heat demand in a year and the nominal source power (3 MW and 6 MW for WWTP sources). When plotting as a function of the FLH, the optimal sizes tend to be on the same order of magnitude for both sources. Here, the optimal sizes of the 3 MW source are about 10 times larger (Fig. 33c), compared to those from the 6 MW for the same heat demand (Fig. 33a).

Power units for most of the heating systems tend to be designed with FLHs in the order of 2000 h to 3000 h. If these heating systems are thus used within their design parameters, there is little to no need for an ice storage. For smaller sources (4000 flh to 5000 flh), when the demand increases to beyond the design parameters, WWTP sources need optimal ice storages sizes <0.15 m^3_{lat}/MWh for a DHW/SH ratio of 0.1 and <0.06 m^3_{lat}/MWh for a DHW/SH ratio ≥ 0.2 (Fig. 33).

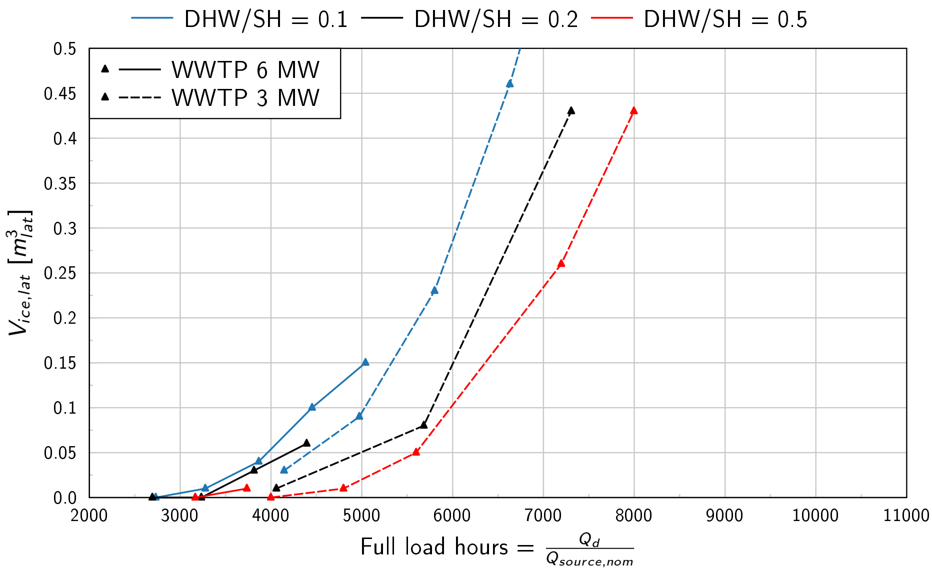

Figure 34: Optimal ice storage sizes as function of the full load hours for different DHW/SH ratios. Cases simulated with a WWTP source of 6 MW and 3 MW. Full load hours calculated as the ratio between the total heat demand and the nominal power source of 3 MW and 6 MW.

3.3.2 Cumulative heat fluxes: 3 MW

Fig. 35 shows the cumulative heat of the 3 MW WWTP source as a function of the temperature on the waste water side of the heat exchanger. The inlet temperature on the WW side represents the temperature of the source which varies between 13 °C to 21 °C (see also Fig. 11). The outlet temperature of the source at the WWTP side will be similar to the inlet temperature from the DH side. Four different scenarios are displayed in Fig. 35 including several demands and DHW/SH ratios. These results clearly show the operating limit of 2 °C on the source side, which we use to protect the source from freezing. The amount of energy provided close to 2 °C gives an indication of the times when the ice storage is partly frozen (see Section 2.5.2) and therefore the freezing protection bypass needs to be operated. This signal is especially strong for scenarios with a larger ice storage (1.35 m^3_{lat}/MWh; red solid line), where almost 14 GWh out of the total 18 GWh are provided when the return temperatures to the WWTP are below 3.5 °C.

To illustrate the role of the ice storage for the 3 MW source, we have displayed key cumulative energy flows over the year in Fig. 36 for four different scenarios including different demands and the need for ice storage (explained below). Fig. 37 shows the mass fraction of ice in the storage and the average temperature of the storage for the same scenarios as in Fig. 36.

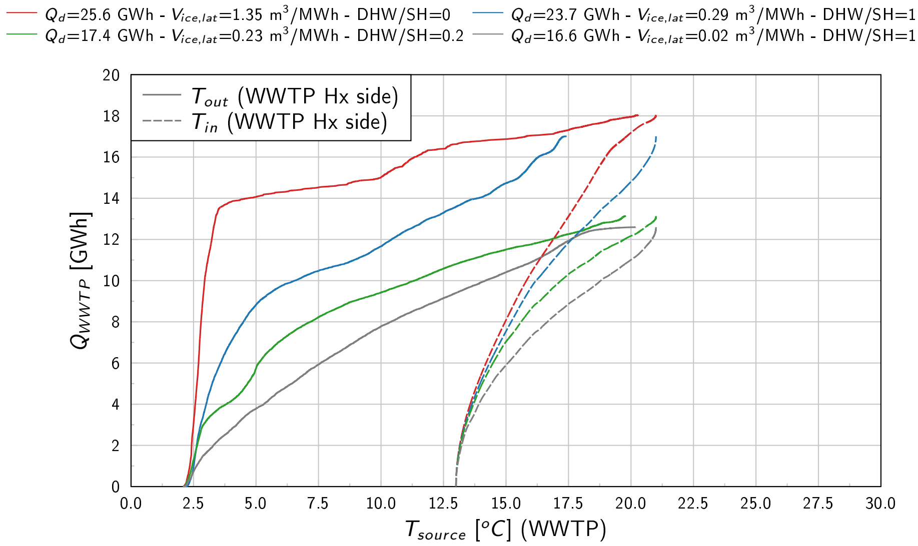

Figure 35: Cumulative heat provided by the 3 MW WWTP source as a function of the inlet and outlet temperature on the WWTP side of the heat exchanger for several demands and DHW/SH share scenarios.

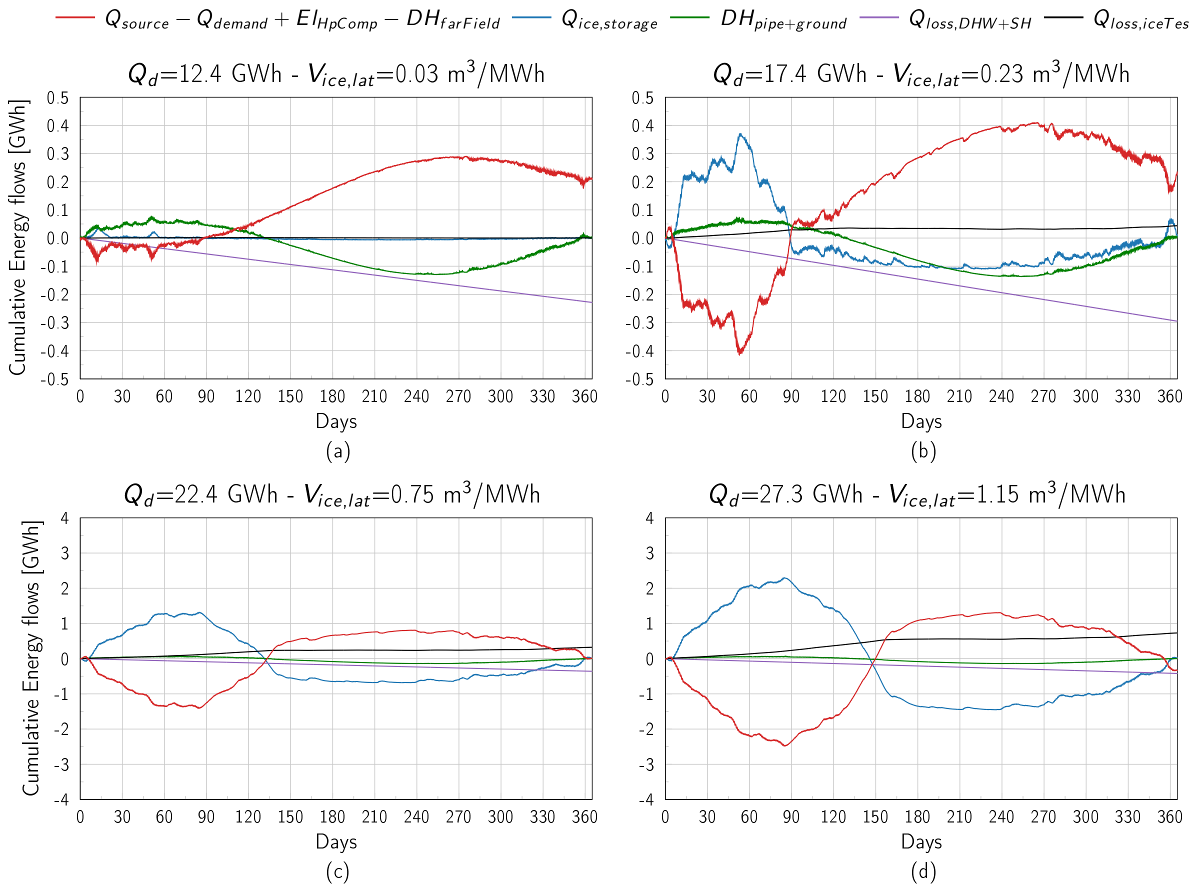

Figure 36: Cumulative energy flows over the year for different demand scenarios for the 3 MW source.

The red line (Fig. 36) shows the cumulative difference between the sources (WWTP and electricity from all the distributed heat pumps), the demand, and the losses to the far field from the buried pipes. The need for additional storage can thus be seen from this red line. The blue line shows the energy provided by the ice storage. The green line displays the energy moving into and out of the DH network piping (including the HTF and the surrounding ground of the piping network). The purple lines show the energy exchanged with the environment for SH and DHW storages and the black lines show the same for the ice storages.

The scenario shown in Fig. 36a is for a Q_d of 12.4 GWh that only needs a small ice storage of 0.03 m^3_{lat}/MWh. The red line (sources minus demands and far-field losses) shows the need for seasonal energy storage. It stays negative from day 1 to approximately day 90. However, this seasonality need, which is small compared to the overall demand (<0.1 GWh vs. 12.4 GWh), is mainly covered by gains from the ground around the DH piping. In this case, the ice storage only covers weekly peak loads.

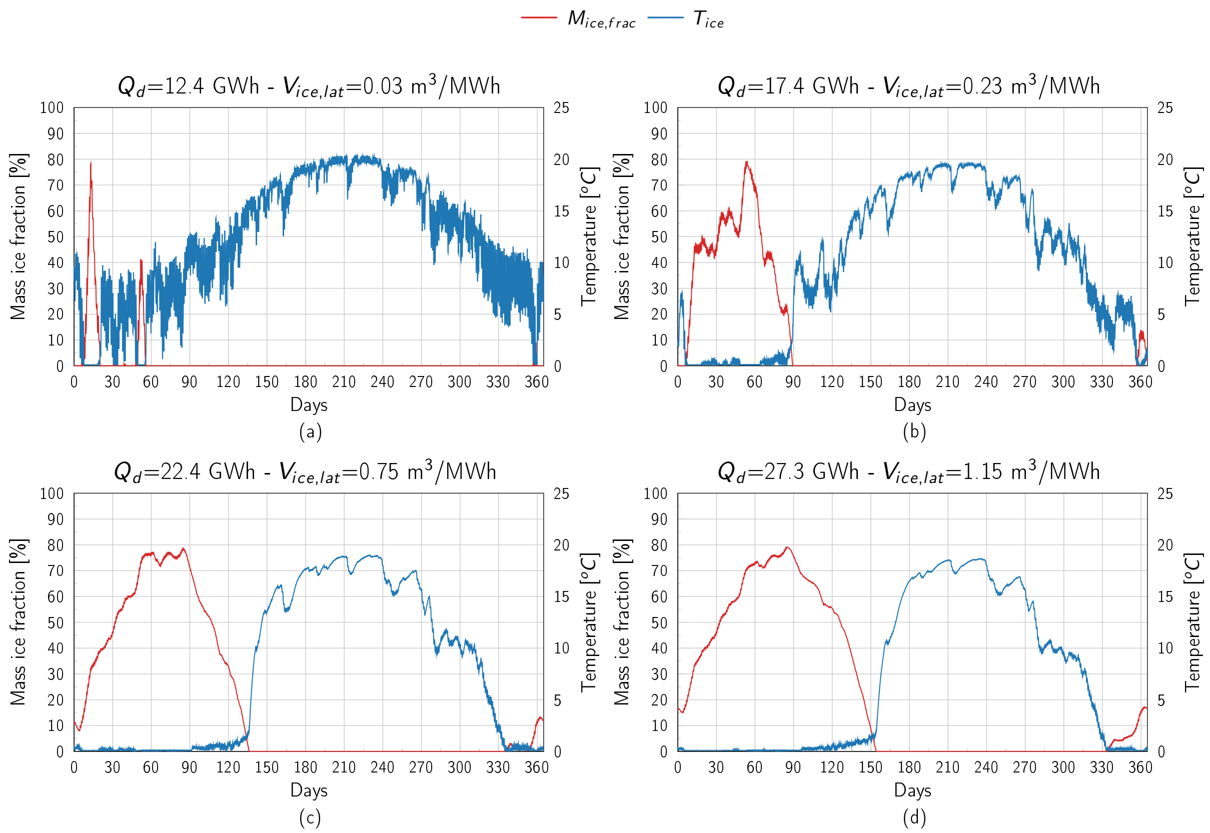

Figure 37: Mass ice fraction (left axis) and ice storage temperature (right axis) for different demand scenarios (same as Fig. 36) for the 3 MW source.

Details on the storage operation can be seen in Fig. 37a, which shows how the ice storage is being discharged from 10 °C to 0 °C and frozen to a mass fraction of 80 % in approximately two weeks and then recharged to about 8 °C in the same amount of time. Afterwards, it operates as a sensible storage for around a month, to then cover another short peak reaching an ice fraction of 40 % at around day 55.

A scenario with a higher demand of 17.4 GWh is shown in Figs. 36b and 37b. There is a pronounced need for energy storage in winter (red line in Fig. 36b), which cannot not be covered by the DH piping. Thus, a larger ice storage needs to cover the lack of source capacity in winter. Under these conditions, the ice storage is discharged (frozen) until roughly day 50 and recharged (melted) fully until approximately day 92. This can be seen even more clearly in Fig. 37b.

The scenarios with heat demands of 22.4 GWh and 27.3 GWh are respectively displayed in panels *c* and *d* of

Figs. 36 and 37. These results confirm the trend described above: the higher the demand and the required ice storage size, the larger the seasonality role of the ice storage. The ice storage contains ice for longer (melting at day 140 for 22.4 GWh demand and day 155 for 27.3 GWh demand).

Comparing all scenarios from Fig. 37 it is clear that the ice storage undergoes fewer state-of-charge fluctuations as the demand and ice storage size increase; it becomes ever more a seasonal storage with less cycles. In the sensible cycle, the ice storage is charged up to 20 °C (close to the maximum source temperature of 21 °C) in all cases. However, the maximum temperature reduces with increasing ice storage size.

3.3.3 Cumulative heat fluxes and cumulative number of cycles: 6 MW

Fig. 38 shows the cumulative energy flows over the year for the 6 MW source (panels a and b) for two different scenarios, as well as the corresponding ice fractions and storage temperatures (panels c and d).

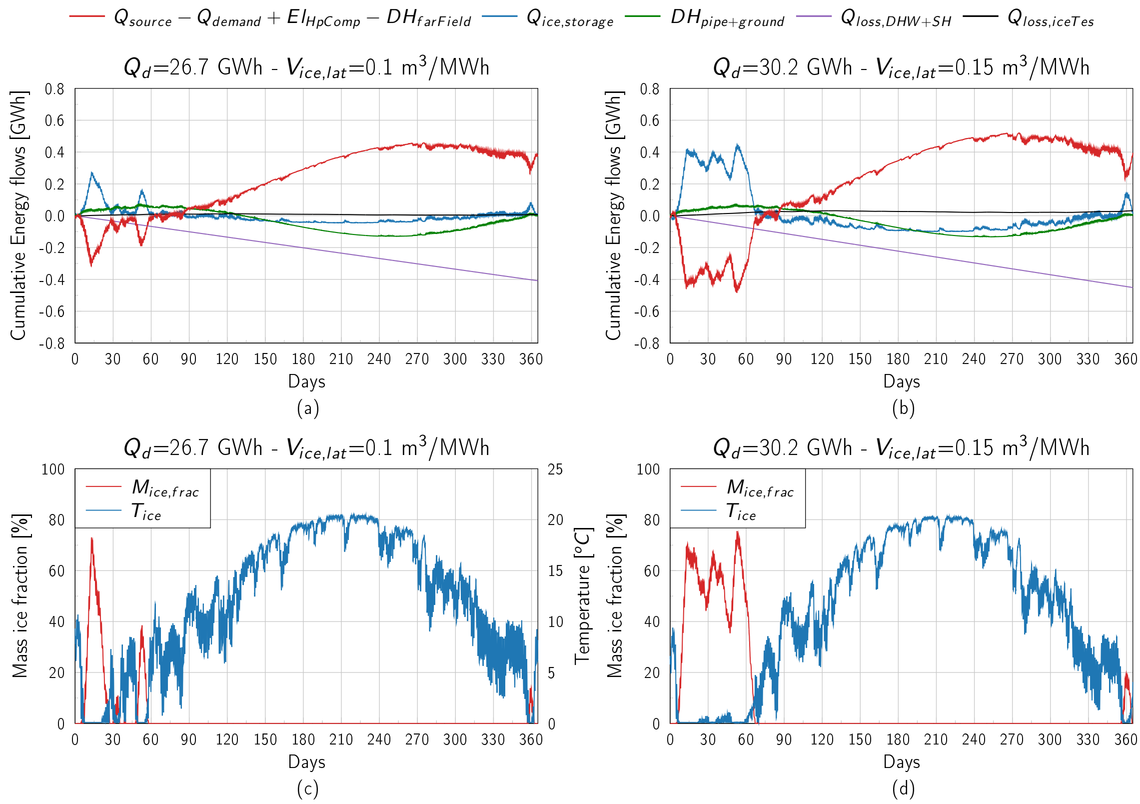

Figure 38: Cumulative energy flows over the year for the 6 MW source and a DHW/SH ration of 0.1 with **a)** 26.7 GWh demand and **b)** 30.2 GWh demand. **c)** and **d)** show the mass ice fraction (left y-axis) and average ice storage temperature (right y-axis) throughout the year for the same cases.

In these plots it can be seen that the ice storage is subject to more fluctuations in the latent state, compared to the 3 MW case. For a Q_d of 26.7 GWh the ice storage has two peaks in winter (Fig. 38c) and for a Q_d of 30.2 GWh the ice storage shows three peaks in winter (Fig. 38d). In the latter case, the storage is not completely melted between these peaks. For this large demand, the sensible heat stored in the ice storage (blue line) by being heated up to 20 °C in summer is of similar magnitude as the energy stored in the piping system (green line). At the end of the year, the energy lost from the warm storages of 0.4 GWh are of similar order of magnitude compared to the latent heat of the ice storage, since in these cases the ice storages are very small with sizes $<$ 0.15 m^3_{lat}/MWh.

Fig. 39 displays the ratio between the cumulative sensible and latent energy and the latent capacity of the storage, as well as the cumulative number of cycles of the ice storage.

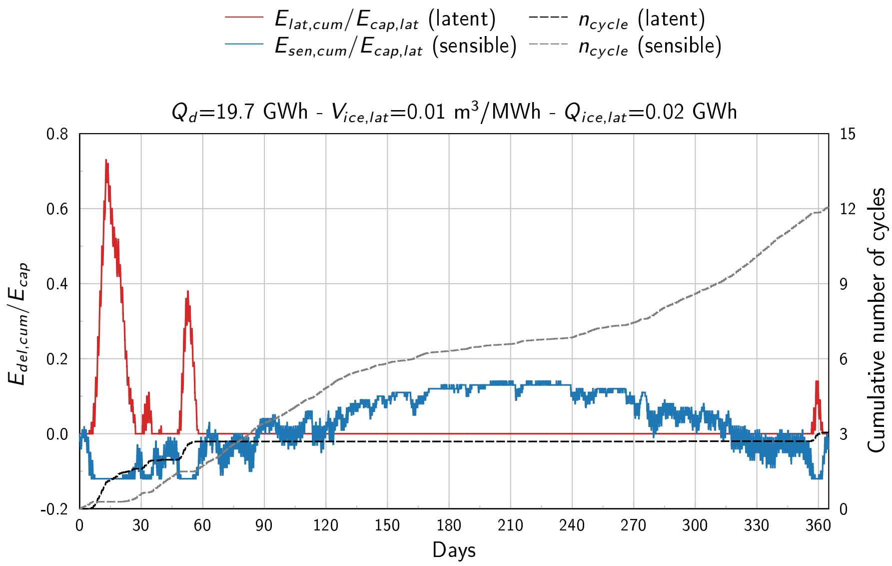

(a)

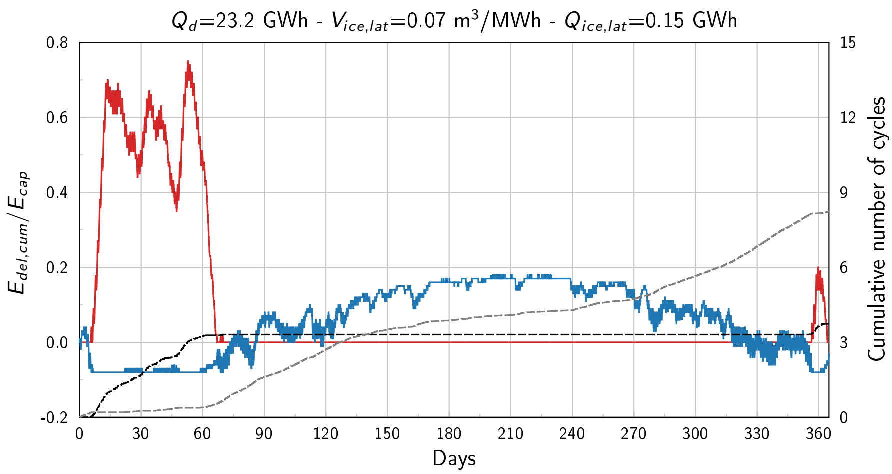

(b)

Figure 39: Comparison of storage cycles as well as energy ratios for two 6 MW cases. Cumulative ratio between energy delivered by the storage E_{cum} as latent (**red**), or sensible (**blue**), and the reference maximum latent capacity E_{cap}. Cumulative number of cycles for both the latent (**black**) and sensible (**grey**) parts.

As a reference, we use the maximum latent energy that can be extracted by icing 100 % of the ice storage, $E_{cap,lat}$. Thus, a ratio of $E_{lat,cum}/E_{cap,lat} = 0.8$ means that the ice storage is 80 % frozen. The remaining 20 % is left as fluid for security reasons, as the volume expansion of water while freezing could break (parts of) the storage vessel. Since the sensible part is also scaled to the latent reference capacity, a ratio of 1 would mean that the ice storage is heated up from 0 °C to 80 °C, which is the temperature difference for which the sensible specific energy of water equals its latent specific energy. Notice also that we are plotting cumulative values and thus the overall cumulative values depend on the initial State-Of-Charge (SOC) at day 0. Both cases shown in Fig. 39 for the 6 MW source indicate that the ice storage has three latent cycles and between 8 to 12 cycles sensible cycles over the year.

3.4 Solar source

We conducted the following variations for the solar-source cases: 1) heat demands up to 30 GWh, and 2) three collector fields with 1 m^2/MWh, 1.5 m^2/MWh and 2 m^2/MWh. The corresponding results are presented in the following order: 1) Optimal storage sizes and SPF, and 2) cumulative heat fluxes, and 3) cumulative number of cycles.

3.4.1 Optimal storage sizes and SPF

Fig. 40 shows both the optimal ice storage sizes and the corresponding SPF values as a function of the heat demand. The tendency is very similar for the three collector fields. For a large enough Q_d the m^3_{lat}/MWh remains relatively constant with values between 0.8 m^3/MWh to 2 m^3/MWh. The SPF values (Fig. 40b) are independent of Q_d (except for very low demands) and fall in the range of 4.1 to 4.6.

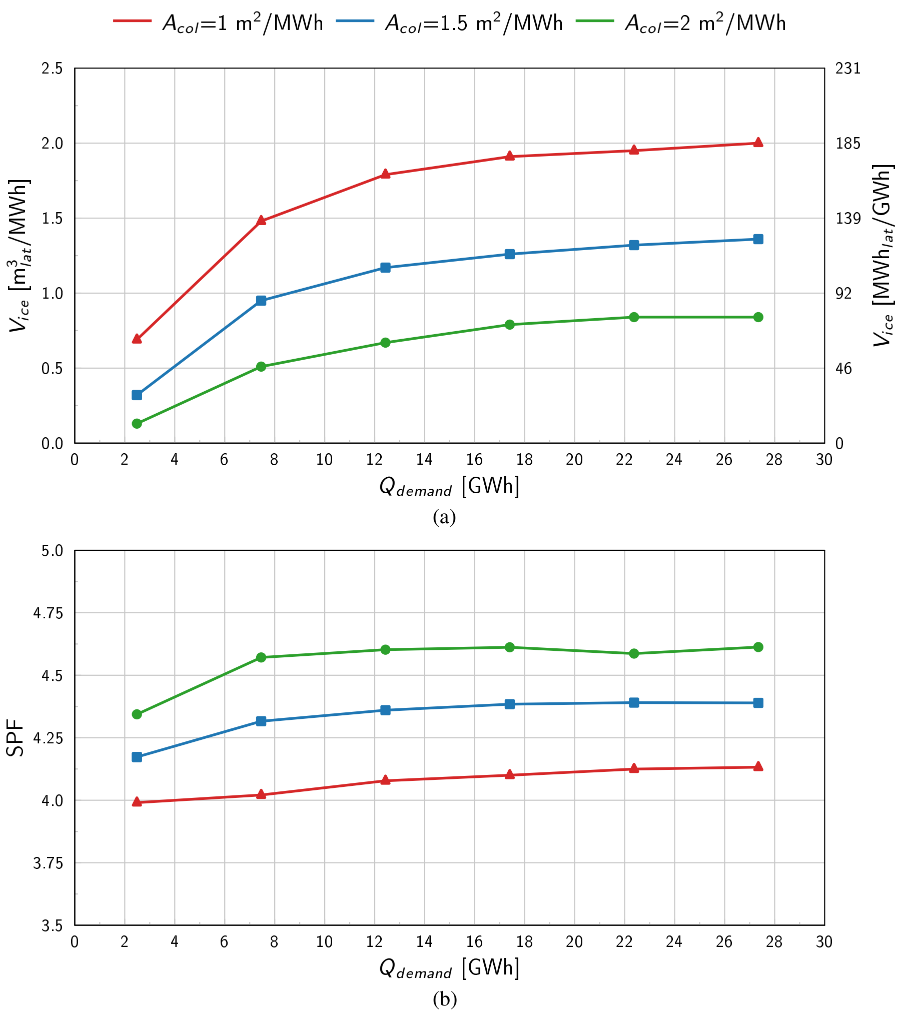

Figure 40: **a)** Optimal ice storage sizes and **b)** SPF as a function of heat demand for collector fields of 1 m^2/MWh, 1.5 m^2/MWh and 2 m^2/MWh.

3.4.2 Cumulative heat fluxes

Fig. 41 shows the main cumulative energy flows over the year for four different scenarios with differing demands and ice storage sizes.

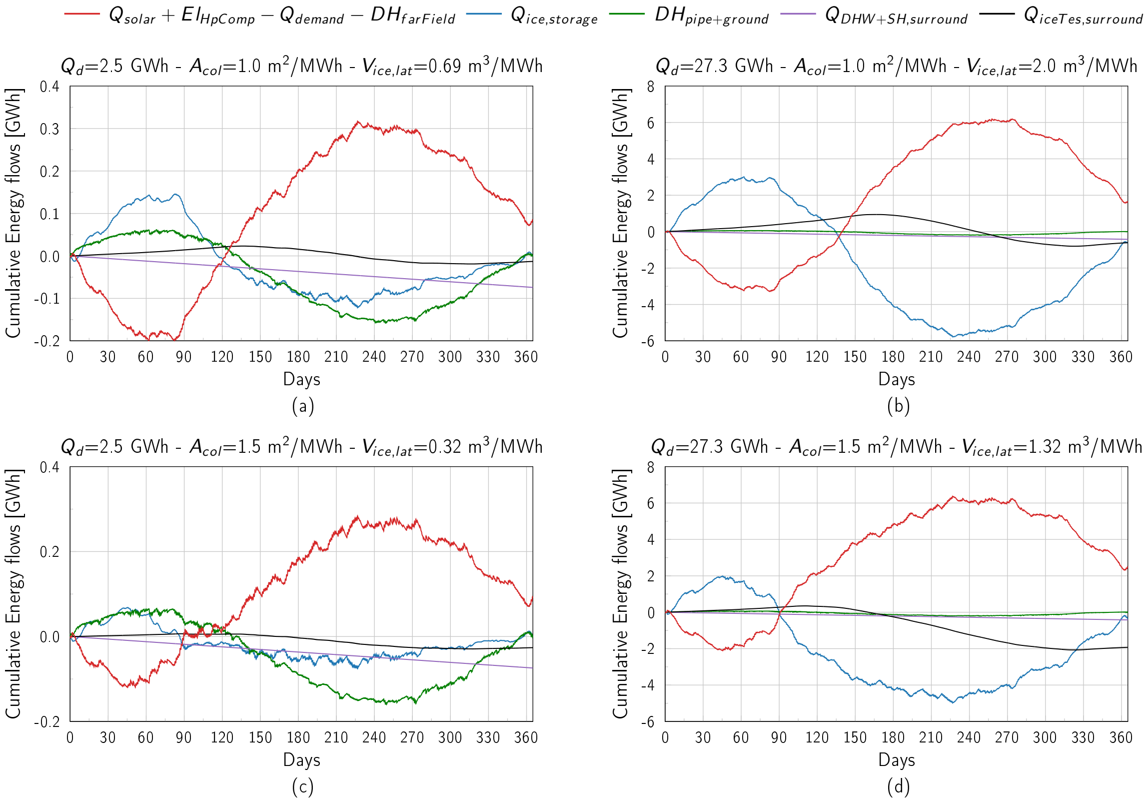

Figure 41: Cumulative energy flows over the year for different solar collector scenarios. **Top row)** results for a collector field of 1 m^2/MWh, **bottom row)** results for a collector field of 1.5 m^2/MWh, **left column)** 2.5 GWh demand, and **right column)** 27.3 GWh demand.

In all these cases, we can observe clear seasonality profiles. For the low demand of 2.5 GWh, the missing energy in winter is provided by both the ice storage and the DH piping with the surrounding ground. For the case of 1 m^2/MWh (Fig. 41a) the $DH_{pipe+ground}$, which can be considered as grid inertia, provides about half of what the ice storage delivers. For the 1.5 m^2/MWh (Fig. 41c) the ice storage and the DH pipe and ground deliver a similar magnitude of heat since the ice storage is almost halved due to the increased energy provided by the larger collector field. Both the ice storage and the DH pipe and ground balance over the year, i.e. they have similar charge and discharge magnitudes and thus will neither heat nor cool over the years. For this low demand of 2 GWh, the thermal losses of the SH and DHW storages become relevant in terms of absolute magnitude.

The scenarios with 27.3 GWh demand(Fig. 41b and d) have the ice storage as the only relevant piece balancing the energy mismatch between sources (solar and heat pump compressor) and sinks (demands and far field energy losses). Thus, for large demands both the thermal losses of the SH and DHW storages and the energy exchange between the ambient and the DH piping and surrounding ground become irrelevant. However, the heat exchanged between the ice storage and the ground is still very important, e.g., for the case of 1.5 m^2/MWh the ice storage is losing a significant amount of energy (-2 GWh). To asses the long-term impact of these exchanges, we extended the cases in the bottom row of Fig. 41 to 10 years (Fig. 42c and d).

In both cases the red line, displaying the sources minus the demand and far-field losses, increases over the years, which is compensated by the losses of both the ice (black line) and other storages (purple line) with the surroundings. For the low heat demand of 2.5 GWh the DH piping and ground surrounding it cycle every year providing a significant amount of energy in winter, which is of similar magnitude as the one from the ice storage. For the large demand of 27.3 GWh the effects of the cyclical behaviour of the DH piping and surrounding ground is irrelevant compared to the cycling effect of the ice storage. In this case, most of the excess energy provided by the sources is lost by the ice storage. Notice here that far field losses are already subtracted from the red line.

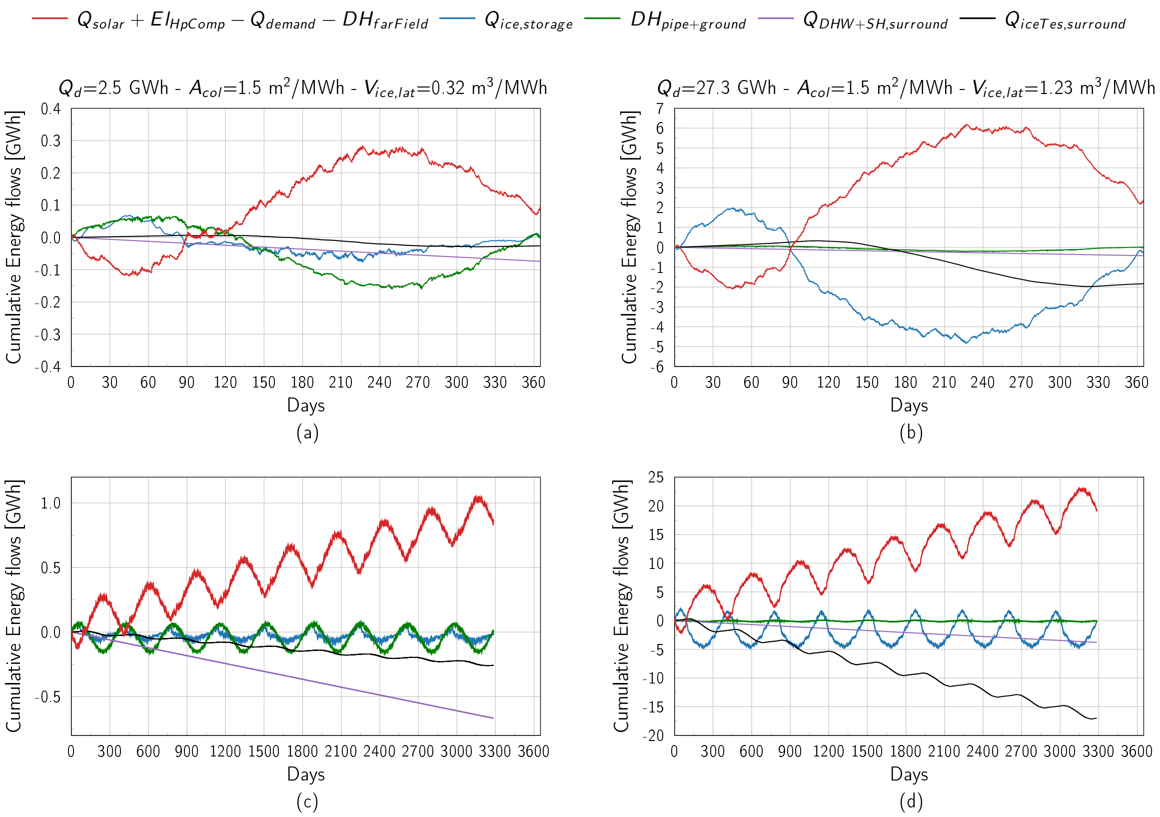

Figure 42: Cumulative energy flows of cases using a collector field of 1.5 m^2/MWh over one year (**top row**) and 9 years (**bottom row**), with 2.5 GWh **(left column)** demand and 27.3 GWh **(right column)** demand.

3.4.3 Cumulative number of cycles

Fig. 43 displays the ratio between the cumulative energy and the latent capacity of the storage separated into sensible and latent ratios, as well as the cumulative number of cycles of the ice storage for the scenarios shown in Fig. 41. In all cases, the latent part of the ice storage cycles between 1 to 1.5 times over the year (black line). The sensible part (gray line) cycles between 1.5 to 2.5 for the large demand, but the cycles of the sensible part increase up to 8.5 for the combination of small demand and large collector area (Fig. 43c).

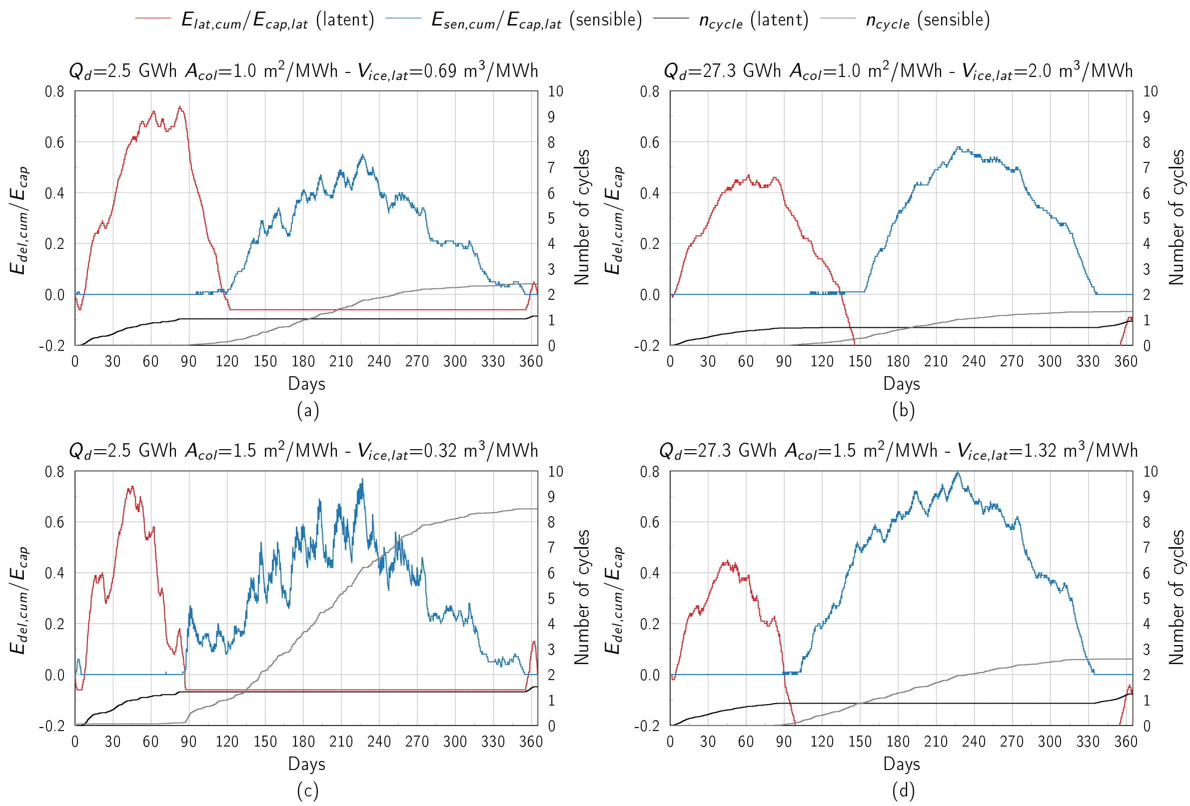

Figure 43: Comparison of storage cycles as well as energy ratios for the solar collector cases shown in Figs. 41. Cumulative ratio between energy delivered by the storage E_{cum} as latent (**red**), or sensible (**blue**), and the reference maximum latent capacity E_{cap}. Cumulative number of cycles for both the latent (**black**) and sensible (**grey**) parts.

3.5 Constant temperature source

For the constant-temperature-source cases we only varied the heat demands (up to 30 GWh). Each case has a DHW/SH ratio of 0.2 and a source capacity of 6 MW (nominal ΔT at source of 13 K and mass flow rate of 430 210 kg/h). The results are presented in the following order: 1) Optimal storage sizes and SPF, and 2) cumulative heat fluxes, and 3) cumulative number of cycles.

3.5.1 Optimal storage sizes and SPF

Fig. 44 shows the optimal ice storage sizes, as well as the corresponding SPF values. This source requires comparatively little storage. The maximum for this case lies below 0.1 m^3_{lat}/MWh for a Q_d of 30 GWh. Only demands above Q_d=20 GWh require a storage at all (see also Section 2.7.1).

3.5.2 Cumulative heat fluxes

Fig. 45 shows the cumulative energy flows over the year for four different scenarios. The corresponding mass ice fraction and the ice storage temperature of these scenarios are shown in Fig. 46.

As these cases have a very low need for an ice storage, the DH piping influence has the same order of magnitude (about 1% of the demand) even for large demand cases (Fig. 45). It can be seen from these plots that the DH network functions as a seasonal storage while the ice storage covers the winter peaks. The main difference

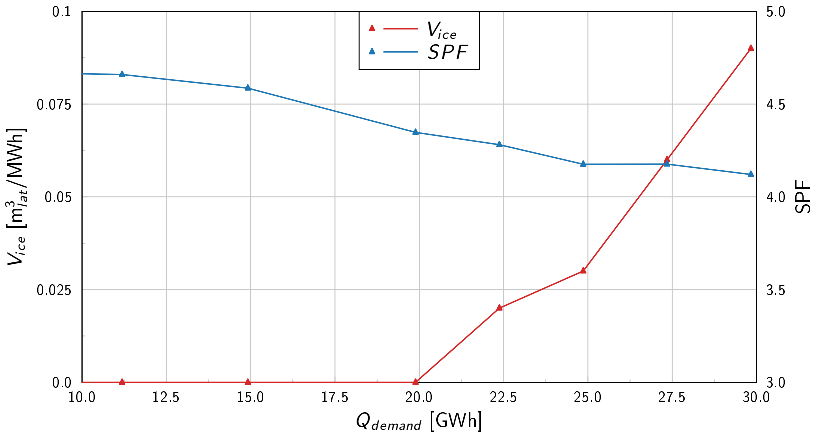

Figure 44: Optimal ice storage sizes (left y-axis) and SPF (right y-axis) as a function of heat demand for the constant temperature source with 6 MW capacity.

between these simulations is: The peak covered by the ice storage increases with the demand since the ice storage size increases with it.

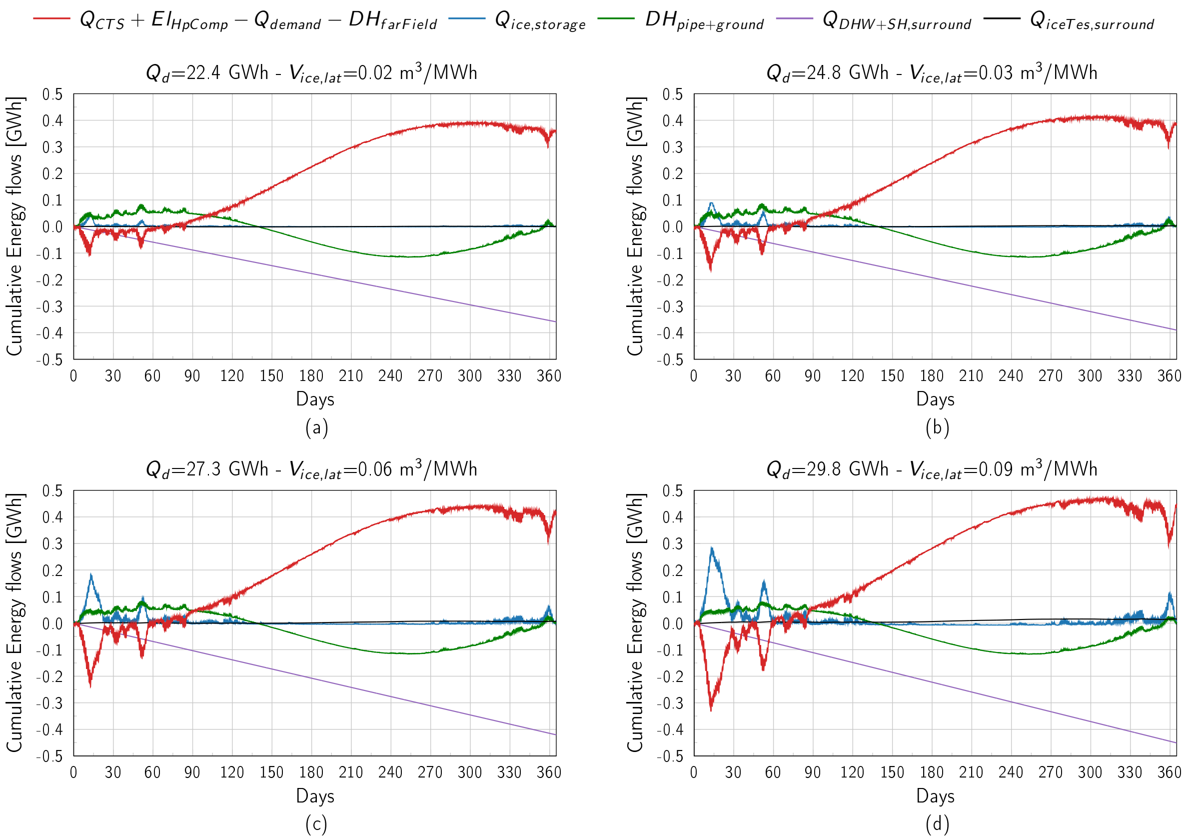

Figure 45: Cumulative energy flows over one year for four different scenarios with a heat demand of **a)** 22.4 GWh, **b)** 24.8 GWh, **c)** 27.3 GWh, and **d)** 29.8 GWh. Constant source cases with 6 MW capacity.

The results in Fig. 46 make it even more clear how the ice storage works as a peak storage. The source is large enough in winter to both melt the ice storage and even heat it close to the source temperature. It does this process twice for all demand cases. The larger the demand and the ice storage, the longer the ice storage is (partially) frozen.

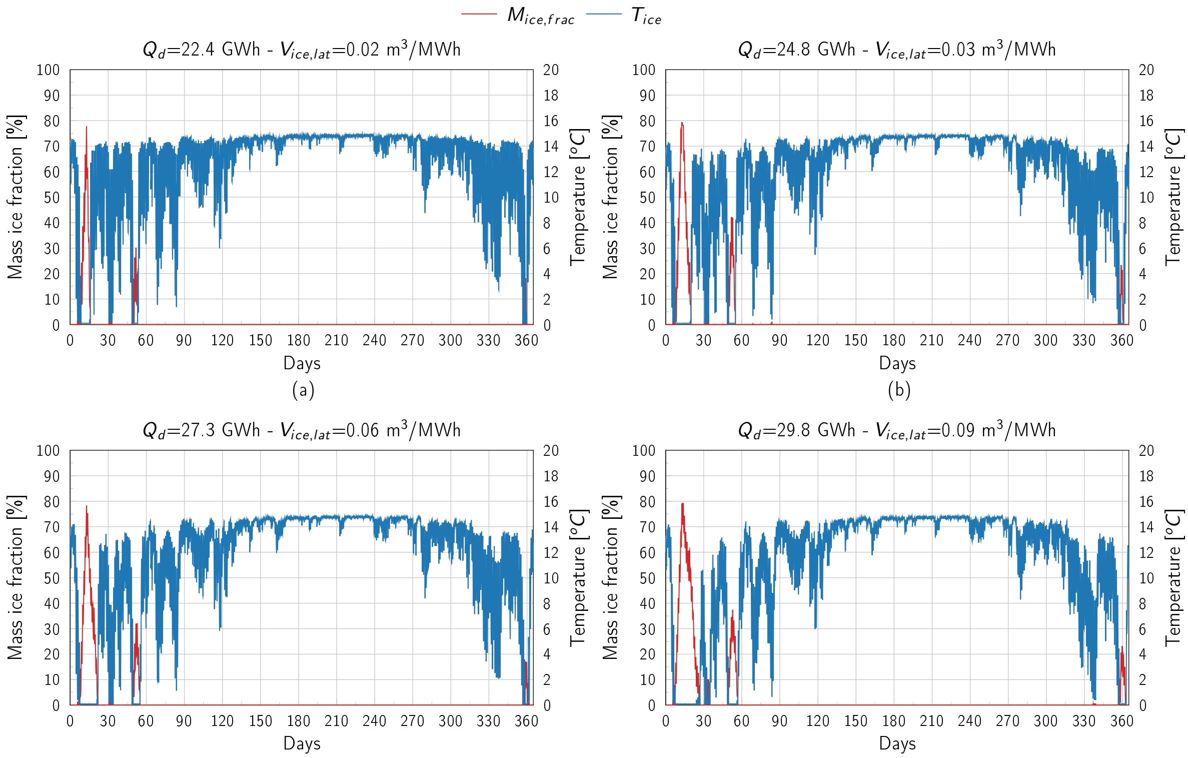

Figure 46: Mass ice fraction and ice storage temperature over one year for four different scenarios with a heat demand of **a)** 22.4 GWh, **b)** 24.8 GWh, **c)** 27.3 GWh, and **d)** 29.8 GWh. CTS with 6 MW capacity.

3.5.3 Cumulative number of cycles

The ratio between the hourly energy delivered by the ice storage and the latent capacity, as well as the cumulative number of cycles over a year is displayed in Fig. 47. In this case $E_{sen,cum}/E_{cap,lat}$ fluctuates below zero. This occurs, because the cumulative value starts on January 1st. On this date, the ice storage is fully charged at 14 °C for these cases. Thus, cumulative ratios can only decrease from that reference, or get back to zero when fully charged again. In all scenarios the ice storage cycles three to four times on its latent part. The number of cycles on the sensible part decreases with increasing ice storage size from 17 to 12 times for 22.4 GWh to 29.8 GWh, respectively.

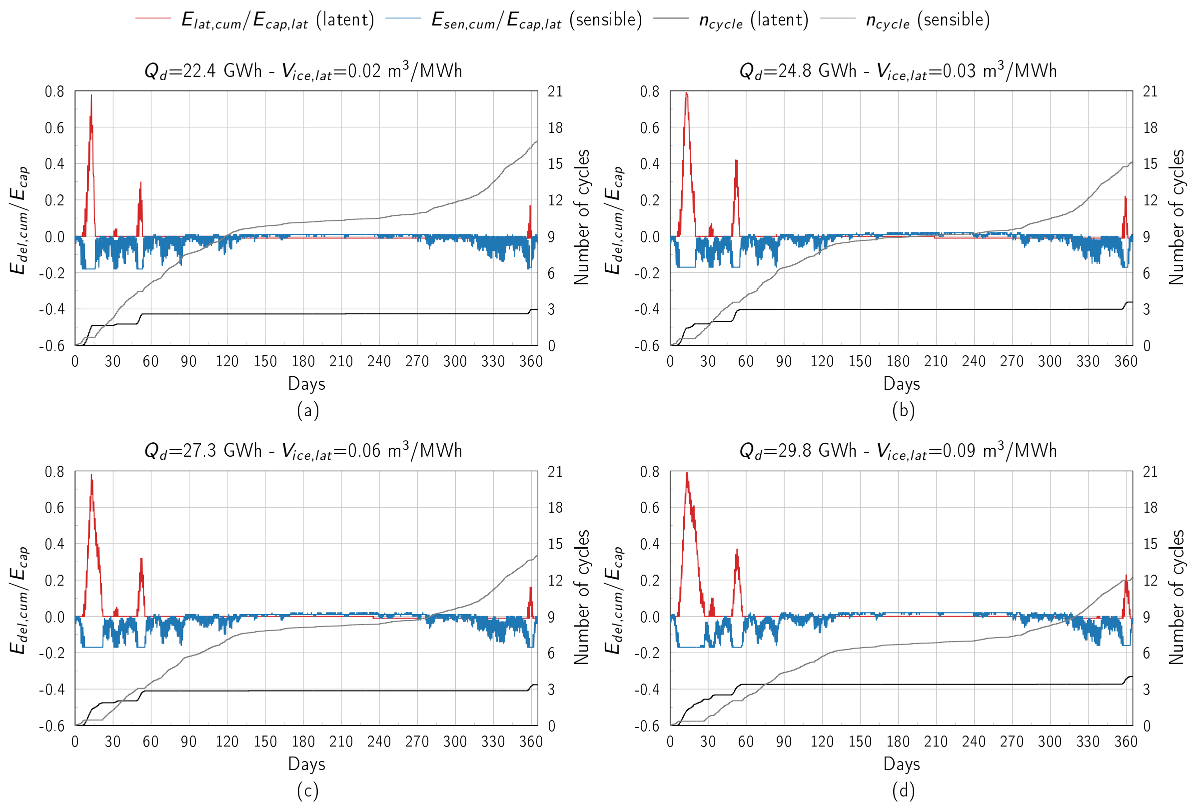

Figure 47: Cumulative ratio between energy delivered by the storage E_{cum} and the reference maximum latent capacity E_{cap} (left y-axis) and the cumulative number of cycles both for the latent and sensible part (right y-axis). Cases using four different scenarios with a heat demand of **a)** 22.4 GWh, **b)** 24.8 GWh, **c)** 27.3 GWh, and **d)** 29.8 GWh. CTS with 5.5 MWcapacity.

3.6 Air source

For the Air-to-Water Heat Exchanger (AWHX) cases we varied the source capacities as a function of the heat demands (up to 30 GWh) using the following full-load hour (FLH) values: 500, 1000, 1500 and 2000. All cases use DHW/SH = 0.2. The results are presented as follows: 1) Optimal storage sizes and SPF, and 2) cumulative heat fluxes, and 3) cumulative number of cycles.

3.6.1 Optimal storage sizes and SPF

As the FLHs increase, the heat exchanger size decreases and, correspondingly, the required ice storage size increases to compensate for the lower heat exchanger capacity (Fig. 48). Additionally, the SPF reduces with increasing FLHs. The required ice storage sizes are in the range of 0.6 m^3_{lat}/MWh for an AWHX with $<$ 1000 FLH. For all cases, the SPF lies between ~3.85 and 3.93.

Fig. 49 shows the resulting optimum storage sizes as a function of demand and FLHs from two points of view. The required storage increases linearly with increasing demand as the AWHX capacity increases (Fig. 49a), while the slope of the storage size increases with increasing full-load hours. The required storage sizes show a quadratic increase when decreasing the AWHX capacity and keeping the same demands (Fig. 49b).

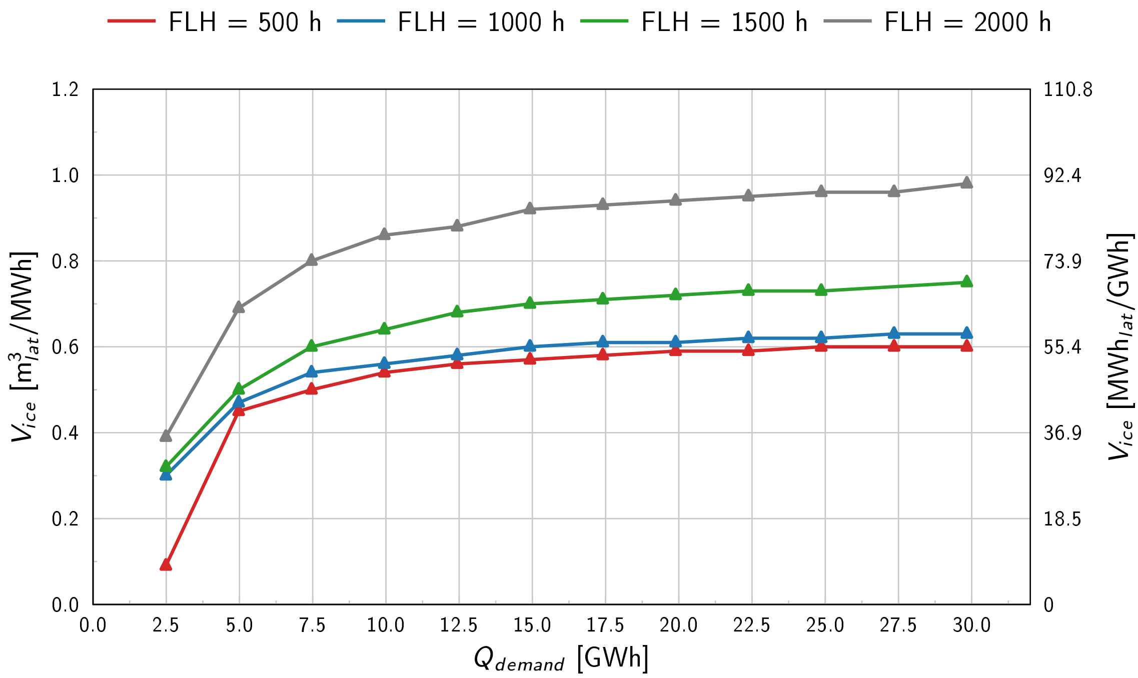

(a)

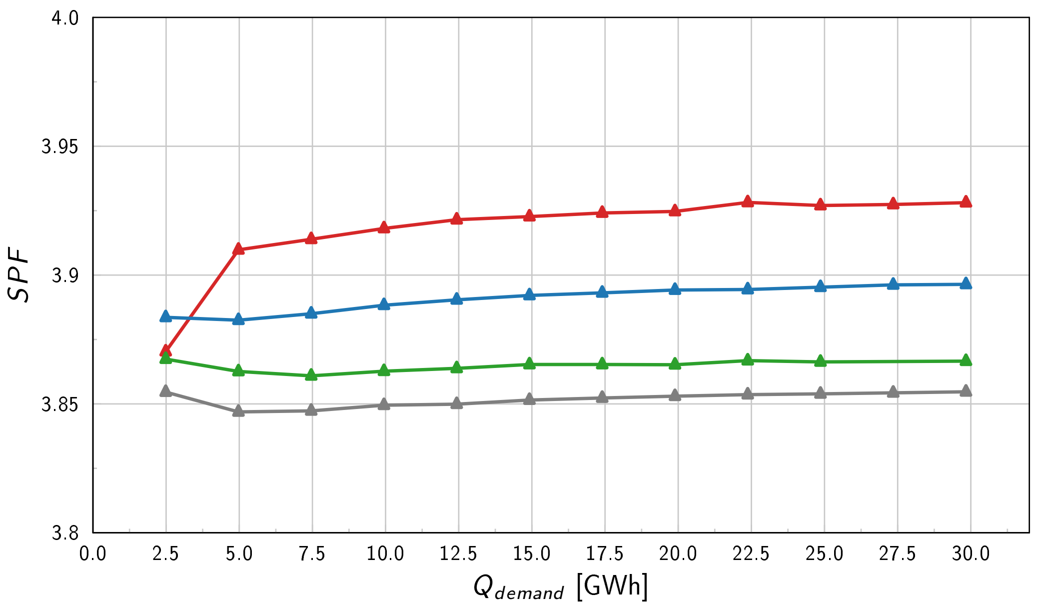

(b)

Figure 48: **a)** optimal ice storage sizes, and **b)** SPF, as a function of the overall heat demand. Cases simulated with an air source for different air heat exchanger capacities represented as full load hours (FLH).

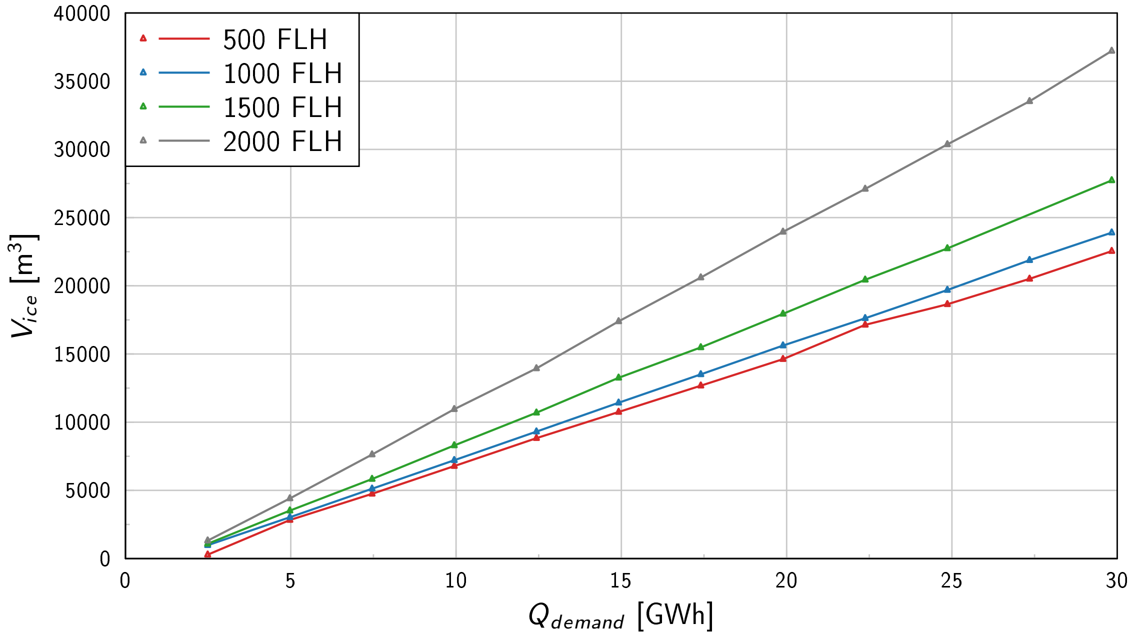

(a)

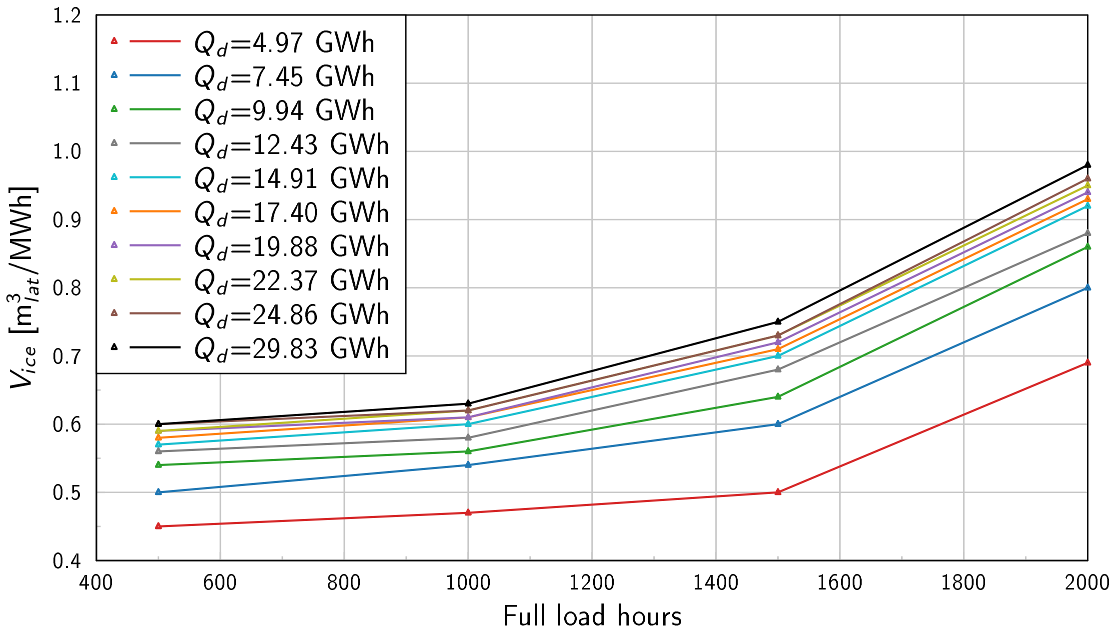

(b)

Figure 49: **Left)** absolute ice storage sizes as a function of the overall heat demand and **right)** impact of increasing the full-load hours on the required storage size at constant demands. Cases simulated with an air source for different air heat exchanger capacities represented as full load hours (FLH).

3.6.2 Cumulative heat fluxes

Fig. 50 shows the cumulative energy flows, mass ice fraction, and ice storage temperature for two cases. In both cases, the winter gap is mainly covered by the ice storage. The 500 FLH air source is large enough to completely melt all ice once. A second period of ice formation occurs approximately day 35 to 50. The 2000 FLH air source has the ice storage (partially) frozen until day 75 without being completely melted in between. In both cases the ice storage has the same seasonal role.

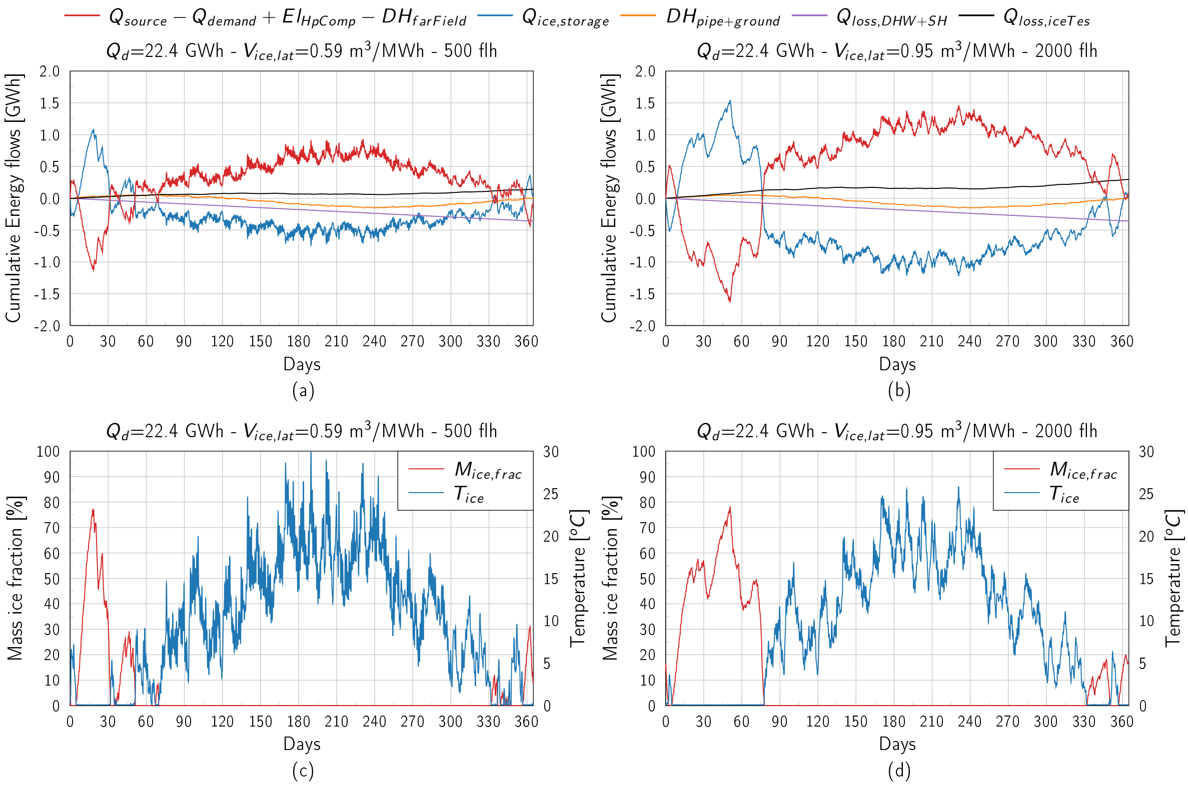

Figure 50: **Top row)** Cumulative energy flows over the year for a demand of 22.4 GWh. **Bottom row)** mass ice fraction (left y-axis) and ice storage temperature (right y-axis) over the yearly days. Cases using an AWHX with 500 flh (**left column**) and 2000 flh (**right column**).

3.6.3 Cumulative number of cycles

Fig. 51 shows the ratio between the hourly energy delivered by the ice storage and the latent capacity, as well as the cumulative number of cycles over a year. The ice storage cycles around two times in its latent form and between 5 to 13 on the sensible side.

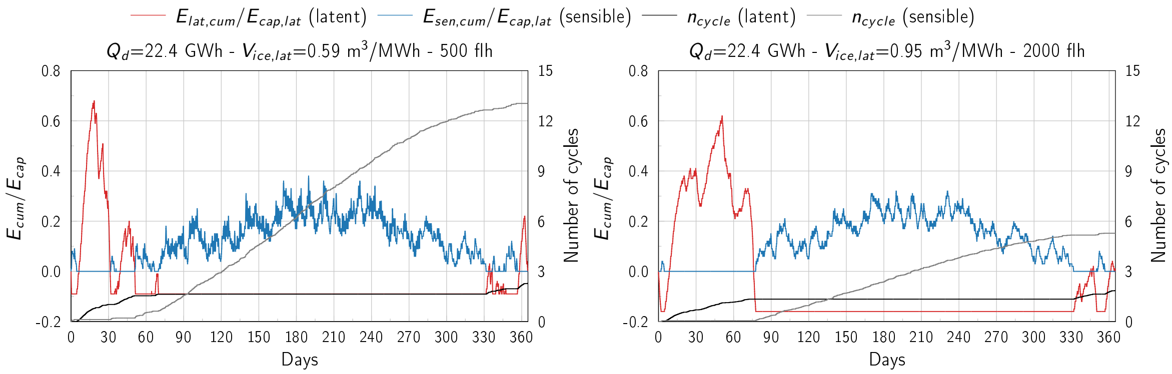

Figure 51: Cumulative ratio between energy delivered by the storage E_{cum} and the reference maximum latent capacity E_{cap} (left y-axis) and the cumulative number of cycles both for the latent and sensible part (right y-axis). Cases using two AWHX capacities of 500 FLH and 2000 FLH and one heat demand of 22.4 GWh.

4 Discussion

In this project, we adapted and extended some TRNSYS types and pytrnsys-specific components with the aim to model decentralised bidirectional district heating networks using pytrnsys and its GUI. For these type of simulations it was necessary to implement in pytrnsys what in TRNSYS is known as macros, i.e. pieces of the simulation that could be multiplied easily and automatically. In our case, this was necessary to minimize the work required to include many sinks. We also implemented underground bidirectional double pipes as connecting elements between DH legs. Due to the large mass flow rates involved, we also needed to adapt the mass flow solver. All these new features were tested in several scenarios using the example of the EZL network as a base case.

In this project, we analysed the sizing of ice storage systems in combination with 5GDHC networks and the following promising sources: 1) waste heat from WWTP (Section 3.3) 2) solar heat (Section 3.4), 3) a constant temperature source (Section 3.5), and 4) ambient air (Section 3.6). The sizing of the ice storage depends on many other parameters beyond the characteristics of the primary heat source.

Both solar cases make use of temperatures close to 0 °C since in this case the solar loop has no risk of freezing due to the use of an antifreeze solution (see Section 2.5.2). For the waste water cases (WWTP and CTS), the inlet temperature on the DH side has to be kept above 2 °C to avoid freezing the water from the other side of the heat exchanger. For the air source there is no need to control this temperature. However, ambient temperatures below 2 °C will clearly not allow the ice to melt and thus cannot be used to produce energy.

Fig. 52 shows the cumulative heat provided by each source as a function of either the inlet temperature (Fig. 52a) or the outlet temperature (Fig. 52b) of the Heat Transfer Fluid (HTF) from the DH side. As described in Section 2.5.2, a near vertical line near 0 °C in Fig. 52a corresponds to (partially) frozen conditions in the ice storage. All cases in Fig. 52a show this signal except for the CTS, the 6 MW WWTP, and the 500 FLH AWHX. When comparing these results to the mass-fraction of ice (e.g. Figs. 43 and 46), the presence and absence of this signal also correlates with a seasonal usage (or lack thereof) of the ice storage.

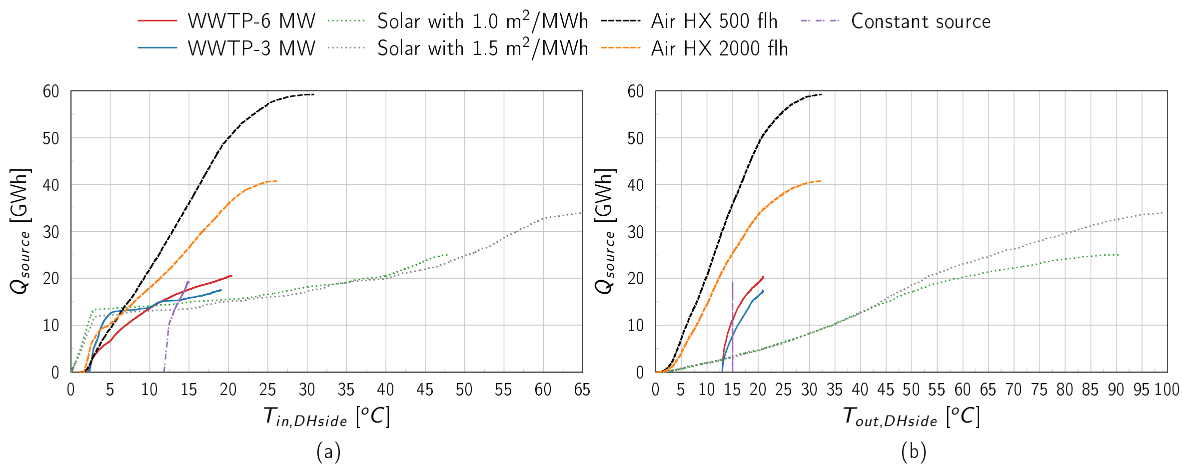

Figure 52: Cumulative heat provided by each source as a function of the **a)** inlet and **b)** outlet HTF temperature on the DH side of the heat exchanger. Results for different Q_d, i.e. 24.8 GWh for all air cases, CTS and WWTP-3MW, 26.3 GWh for WWTP-6MW and 27.3 GWh for all solar cases.

For the cumulative energy flows of the outlet temperature on the DH side (Fig. 52b), the solar cases reach very high temperatures (up to 90 °C to 100 °C). DH networks using solar collectors are commonly uninsulated. Therefore, circulating a HTF at such high temperatures will lead to high losses, which thus diminishes the effective use of this solar heat to directly provide DHW. These thermal losses also reduce the SPF, since the HP has to make up for these losses. The $T_{out,DHside}$ values (Fig. 52b) already give an indication of which sources will have higher heat pump efficiencies. As a simple rule, the higher these temperatures, the higher the efficiency of the distributed heat pumps. However, since the SPF of the heat pump ultimately depends on the delivered energy at a variety of temperatures, the SPF cannot easily be estimated using only this plot.

A normalized view of the energy delivered by the source provides a different point of view. Here, we normalize the delivered energy using the peak power of each yearly simulation, which we will refer to as peakload hours (as the definition is almost identical to full-load hours). Fig. 53a shows the cumulative peak-load hours for all sources. The largest number of peak-load hours need to be provided by the WWTPs and CTS, which we will now group into Waste Water Heat Sources (WWHSs). The main reason is better explained using Fig. 53b, where the ratio between the energy provided and the peak power is more homogeneously distributed along the x-axis for the WWHSs, which corresponds to less hours at high power and thus a better use of the source at large capacities. The simulated solar sources have peak hourly capacities ranging from 11 MW to 20 MW for 1 m^2/MWh and 2 m^2/MWh respectively. The AWHX cases have peak hourly capacities ranging from 14 MW to 41 MW for 2000 FLH and 500 FLH respectively. Thus, both solar and air have peak power capacities significantly larger than all the WWHS, which range from 3 MW to 6 MW.

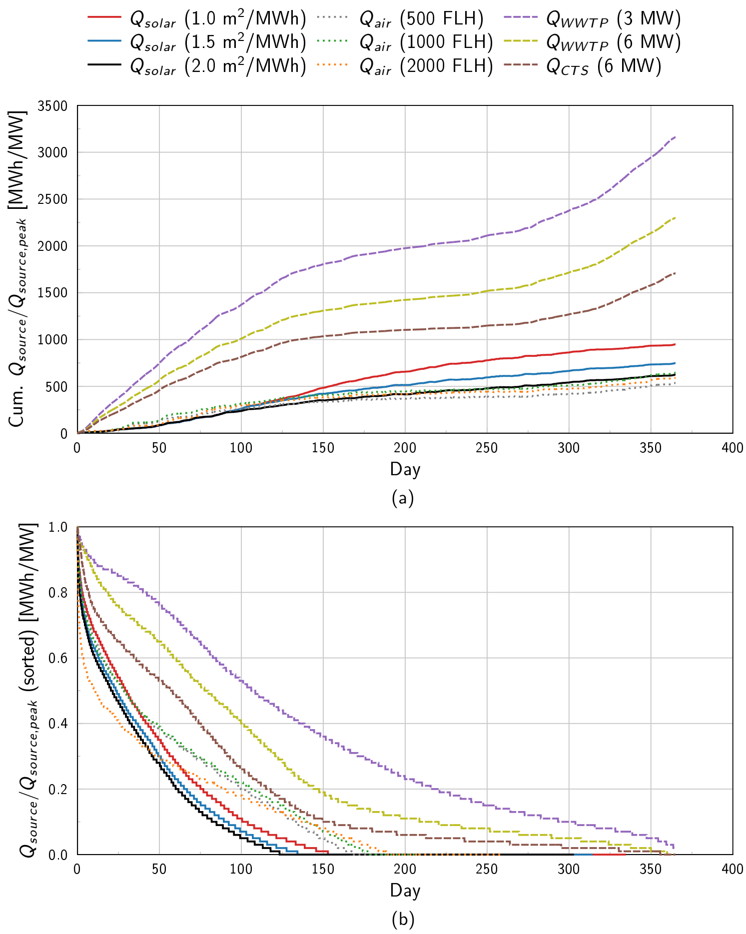

Figure 53: Source profiles over a year for different sources. **a)** Cumulative demand profiles divided by peak demand leading to *cumulative peak-load hours* and **b)** heat demand divided by peak power and sorted from high to low ratios representing how many days the demand is at specific power.

The cumulative energy delivered by all the sources on similar heat demands are displayed in Fig. 54a. Since the heat demands for each case are not exactly the same, we plotted them in Fig. 54b to support the appropriate interpretation. As a general trend, the solar source provides less energy in winter (e.g. from day 1 to day

60), which is the crucial period for heating. All the WWHSs are able to provide more energy in winter, which directly predicts a lower need for ice storage capacity. Comparing air to solar, these sources all perform poorly between day 1 to day 30. The AWHX performs better by the end of winter (from day 30 to day 60), especially as the amount of FLHs increases. After winter, solar becomes a better source, as it provides a better energetic efficiency. However, sizing depends on the critical winter times and therefore solar requires larger ice storages compared to air. Some of the solar cases produced more energy than there was demand (e.g. 2.0 m^2/MWh. Thus, a significant part of the solar energy is lost in the ground for these cases. The AWHX cases have a similar amount of energy delivered by the sources regardless of the heat exchanger sizing. The main difference is the energy extracted in winter times, which is larger for stronger heat exchangers, which reduces the need for ice storage capacity. Differences between an AWHX using 1000 FLH and 500 FLH are very small and therefore 1000 FLH seems a proper sizing for the analysed cases. Except for solar, all sources have a cumulative profile similar to that of the demand. As expected, the curvature of the solar-source result is the opposite of the curvature of the demand, with less energy delivered in winter and way more energy provided in summer. This is the main reason why we need an ice storage with a seasonal role in this case.

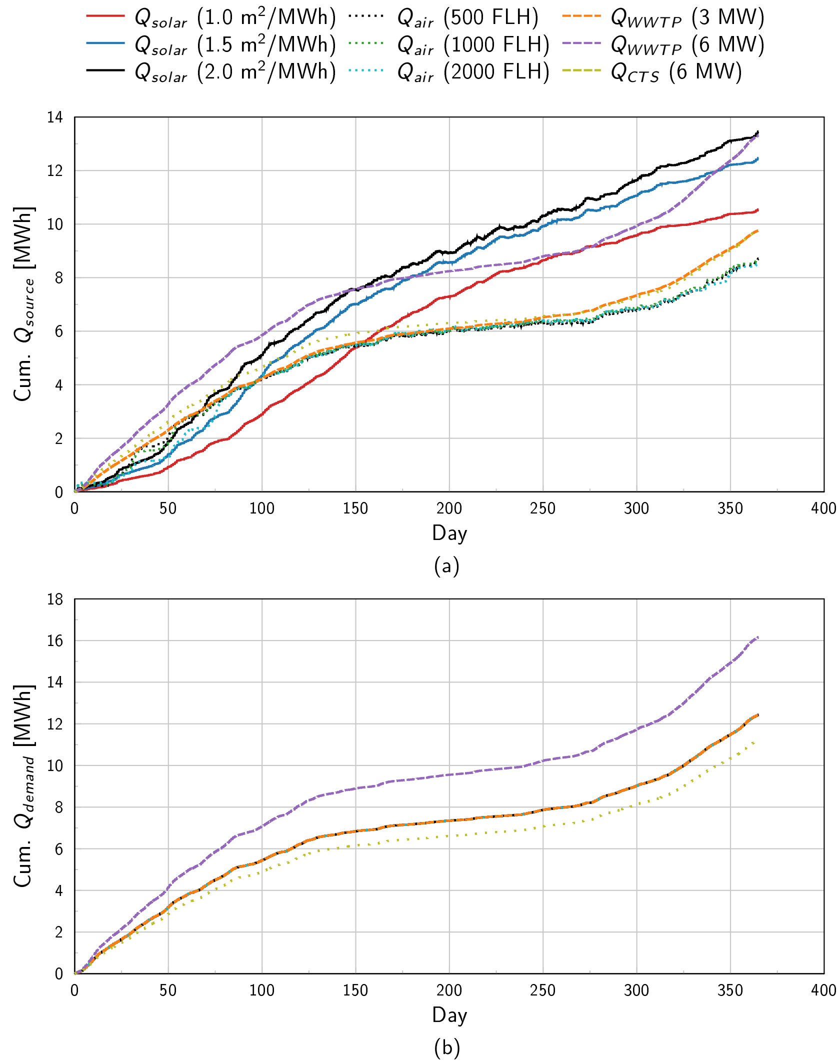

Figure 54: **a)** Cumulative energy over the days provided by all sources and **b)** cumulative energy demand.

4.1 Sizing of ice storages in 5GDHC

Fig. 55 shows optimal ice storage sizes as a function of the heat demand for all sources.

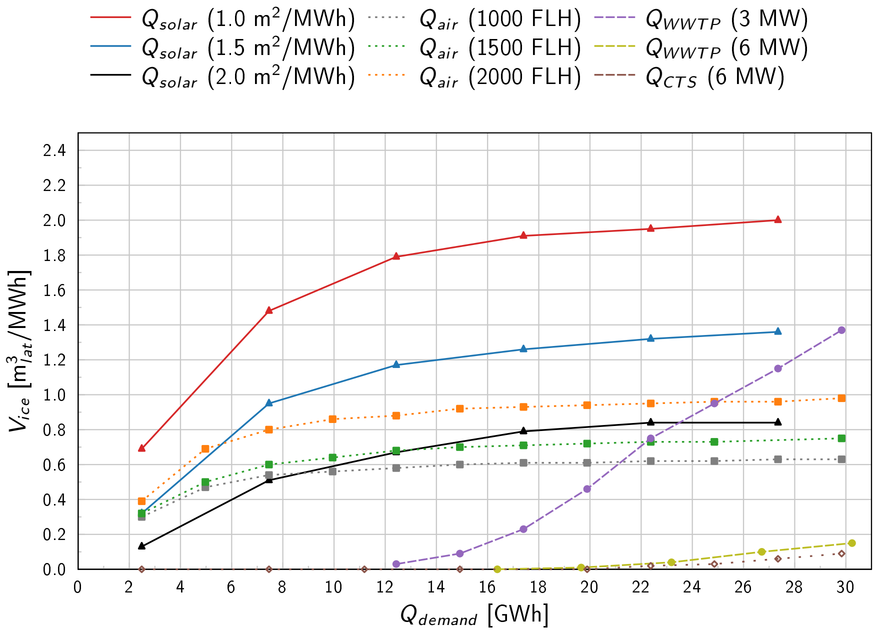

Figure 55: Optimal ice storage sizes as a function of the overall network heat demand. Cases simulated with all sources.

The starting point for sizing ice storage is different when considering waste heat sources with a limited capacity than when considering engineered sources such as solar or ambient air. The size or capacity of technical sources can be designed to meet certain demand, and their designed sizes will increased as demand increases. That's why we didn't look at one specific size (for example of the collector field) together With variable demands, but at several specific sizes relative to the demand. On the other hand, for the Waste Water Heat Source (WWHS) cases, we focused on extending the network with an ice storage to meet additional demand exceeding the limits of the source. Here the source capacity was kept constant, except for the comparison between 3 MW to 6 MW. Since waste water with a temperature of around 10 °C is also available in winter, it is a good source all year round, even without storage. However, the higher the power is extracted from the WWHS, the lower the discharged waste water temperature. Because water is used on the source side of the heat exchanger, temperatures below 0 °C must be prevented due to freezing risks. These low temperatures are only reached during times of peak demand. However, Waste Water Heat Source (WWHS) can only be operated until a certain power limit. We have therefore defined the heat demand at which the grid return temperature falls below the freezing point as the demand above which an ice storage tank is necessary. This demand threshold depends on multiple aspects of our simulations: 1) source type, 2) DHW/SH ratio, and 3) source capacity. Above the demand threshold, even small ice storage systems suffice to cover power peaks. These small storages can easily be regenerated due to the high winter source temperature.

The optimal ice storage sizes for the WWTP and CTS appear at heat demands between 6 GWh to 18 GWh (see Section 2.7.1). Below this threshold, the analysed waste heat sources have capacity even in winter to serve a 5GDHC network without an ice storage. However, even if they could supply a lot of energy, they have a limited power, which restricts the size of the connected network. In such grids, ice storage systems can take over peak loads and enable further grid expansion. For both cases using a 6 MW source power the ice storage sizes become significant $>$ 20 GWh with small ice storage volume needs $<$ 0.2 m^3/MWh. For the WWTP capacity of 3 MW, the picture looks quite different compared to the 6 MW source cases. This small source capacity is not able to provide all demands in winter periods and needs substantially larger ice storages with growing volume as demand increases.

The ambient air and solar heat have very low source temperatures in winter and therefore always need an ice storage (our simulations do not provide an alternative source to deal with this period). In both cases, the required ice storage volume is strongly dependent on the dimensioning of the energy source. For very low heat demands, the piping network can take over part of the storage function, which results in smaller specific ice storage volumes (storage size per demand). Nevertheless, the ice storage sizes at very low demands e.g. between 2.5 GWh to 5 GWh, should be taken with caution. The DH network is sized for a larger grid ($\sim$10 GWh) and is thus able to act as a seasonal storage, which allows it to partially cover the role of the ice storage for low demands. However, such low demands are not realistic for DH networks and therefore they are only used to: 1) show-case that solar and air sources will need an ice storage even at low demands and 2) identify how behavior with ice storages differs from behavior without storages.

With increasing demands, the required specific storage volume increases for solar and air sources, but then remains almost constant for both heat sources, when a specific and not an absolute sizing of the sources is used (absolute source size increases with the demand). With large air heat exchangers, a storage volume of approx. 0.6 m^3/MWh is sufficient to prevent complete freezing through the winter. With a generously dimensioned solar system (2 m^2/MWh), approx. 0.7 m^3/MWh is required for higher demands to prevent freezing of the ice storage. Results of the ambient air source show that from a sizing of the ambient air heat exchanger to 1000 FLH (at a temperature difference of 5 K), an increase in size has little benefit. A lower number of full load hours means a higher nominal output of the air heat exchanger at the same temperature difference or the same nominal output at a lower temperature difference. If the heat exchanger is designed smaller, the storage requirement increases. For example, with a typical design for other applications of 2000 full load hours, the storage requirement increases to almost 1 m^3/MWh. On the other hand, if the solar field is reduced to 1 m^2/MWh, the storage requirement even increases to almost 2 m^3/MWh.

As explained before, there is a conceptual difference between the Waste Water Heat Source (WWHS) such as the WWTP and CTE compared to the solar and air sources. The WWHS are used to expand the grid and therefore are only used to cover an additional demand while both air and solar sources need an ice storage right at the beginning. Thus, plotting all these sources on the same Q_d does not give the right perspective of their needs. Fig. 56 shows the ice storage volumes required to increase the heat demand by a specific value, which we call $Q_{add,demand}$.

For air and solar $Q_{add,demand}$=Q_{demand}, while for WWTP and CTS the results from Fig. 55 are shifted to the left in Fig. 56, which simplifies the comparison between sources. Similar additional ice storage volumes are needed to support the 3 MW WWTP and the 1.5 m^2/MWh solar cases for $Q_{add,demand} < 12$ GWh. However, the linear increase of m^3_{lat}/MWh as a function of $Q_{add,demand}$ for the 3 MW WWTP source suggests massive ice storages for $Q_{add,demand}$ in the range of 30 GWh. Increasing the capacity to 6 MW for both the WWTP and the CTS massively reduces the required ice storage as a function of $Q_{add,demand}$, also when compared to solar and air. Since the additional ice storage volumes increase linearly for both WWTP and CTS, while the solar and air values tend towards a constant, the differences between these sources reduces with increasing additional demand.

Fig. 57 shows the required ice storage volumes in absolute terms in m^3_{lat}. (Note that Fig. 56 is the derivative with respect to $Q_{add,demand}$ of Fig. 57.) For a grid with a demand of approx. 10 GWh, a storage size around 6000 m^3_{lat} is required, with a design source of 1000 FLH for air and 2 m^2/MWh for solar thermal, to prevent freezing through the whole winter. Presented results do not include any back-up such as fossil fuel burners or electrical resistance.

We advise caution when assuming that the DH network piping and surrounding ground can be used as seasonal energy storage for low DH demand cases. Our example network is based on the EZL network in Jona, which is dimensioned for a DH demand of 10 GWh. We do not scale the network with the demand and thus it is oversized for demands < 10 GWh. Using a smaller network for low demands would result in slightly smaller storage contributions from the network and thus, an additional need of ice storage volume. On the other hand,

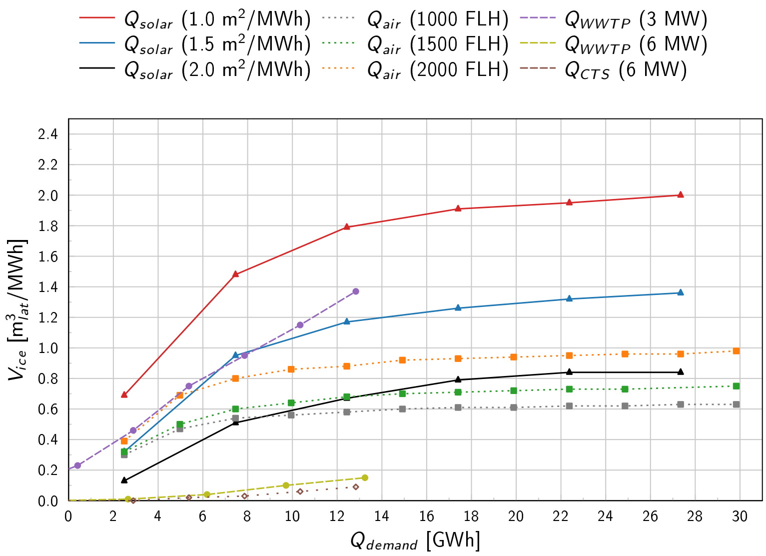

Figure 56: Additional ice storage volumes as function of the additional heat demand that can be covered thanks to an ice storage. Cases simulated with all sources.

a larger DH network for higher demands (e.g. 27.3 GWh) would result in a slightly higher contribution to seasonal demand shifting by the ground and piping. This in turn would allow for smaller ice storage sizes. Thus, the optimal ice storages sizes we present need to be slightly adjusted for different network sizes. However, the contribution of the piping network is less than 1/20th the size of the contribution of the ice store for these cases. An underestimation of the piping contribution, and with it the required reduction in ice storage size, is thus expected to be in the low percentage range.

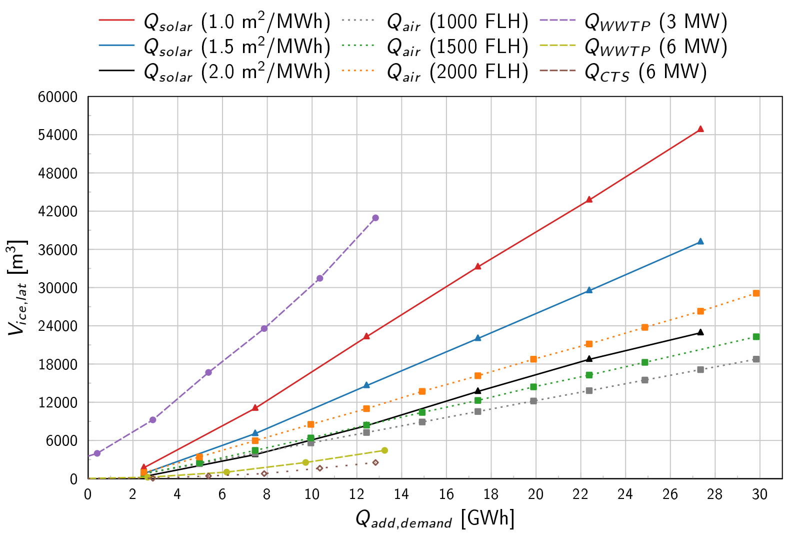

Figure 57: Absolute ice storage needs as function of the additional heat demand that can be covered thanks to an ice storage. Cases simulated with all sources.

4.2 Yearly efficiency of distributed heat pumps

The phase transition of water at 0 °C defines the operating temperature of the heat pumps in systems with ice storage tanks when the latent heat is extracted. The efficiency of the heat pumps is strongly dependent on the source temperature and the duration of the latent heat extraction from the ice storage. The SPF of all the distributed heat pumps together is shown in Fig. 58.

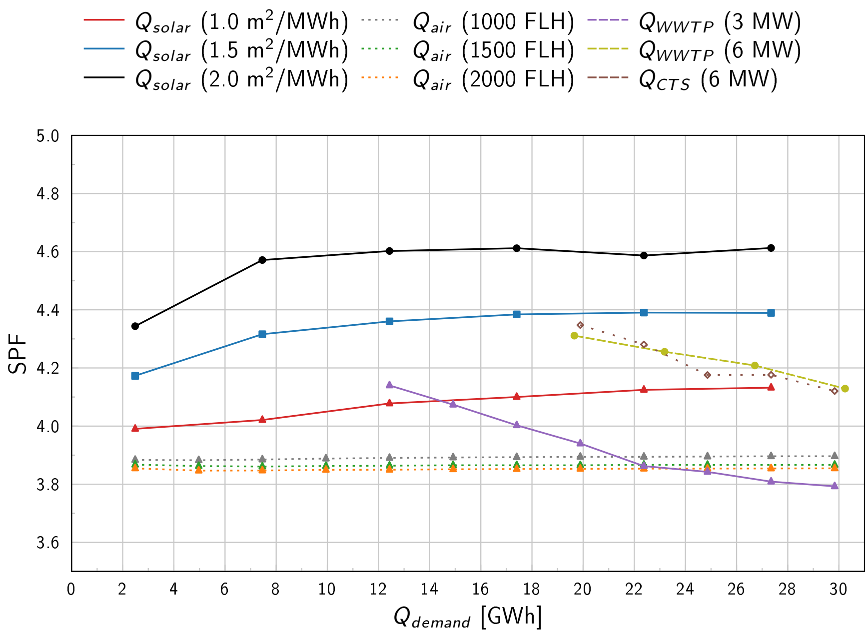

Figure 58: SPF as function of the overall DH heat demand. Cases simulated with all sources.

As described above, the SPF of the system mainly depends on the operating temperatures. The lowest SPF values correspond to the AWHX, which makes sense, as these are the ones that operate the system with the lowest temperature (also see Fig. 52b). For both air and solar, the SPF values are relatively constant with increasing demand. This relates to the scaling factors we used to increase the source capacity as Q_d increases. For the WWTP and CTE, the source capacity does not scale with Q_d and thus, as demand increases, the storage size in m^3_{lat}/MWh increases with demand, subsequently leading to colder DH network temperatures and thus lower SPF values. The highest SPF values are obtained using a solar source with a collector field $\geq$ 1.5 m^2/MWh. Despite the high temperatures achieved by solar, a large part is lost along the uninsulated piping network.

Fig. 59 displays the SPF as a function of $Q_{add,demand}$. As $Q_{add,demand}$ increases, the SPF values for both the WWTP and the CTS decrease. In comparison, higher and constant SPF values are achieved by the solar cases. Operating WWHS at higher temperatures would lead to higher coefficients of performance. In such a case, however, the use of an ice store will decrease the energetic efficiency. Growing demand due to grid expansion can be covered to a certain extent by further cooling of the waste heat source, which requires protection against freezing. This reduces the grid temperature and therefore also the efficiency of the connected heat pumps. If the demand is further increased while an ice storage is integrated, this drop in heat pump efficiency continues. Although the integration of an ice store hinders further temperature reductions below 0 °C, it also extends the time during which the network is operated near 0 °C. Thus, even if an ice store can significantly increase the demand a given source can meet, it also somewhat reduces the efficiency of the connected heat pumps.

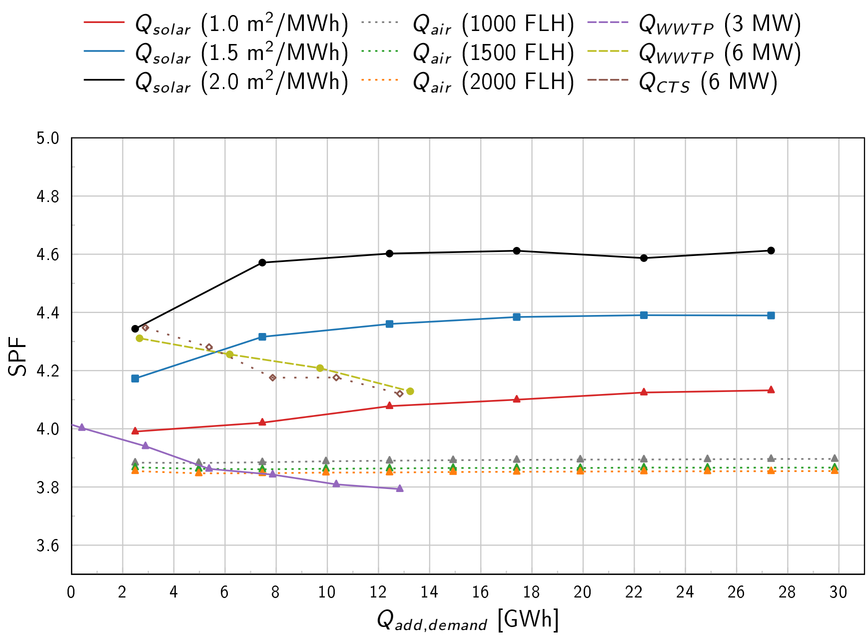

Figure 59: SPF as function of the additional DH heat demand. Cases simulated with all sources.

4.3 Cost analysis

Cost assessments are based on the annuity method presented in section 2.6.2. The main assumptions for the economic analysis are given in Table 4.

Table 4: Assumptions for calculation of heat generation costs.

Rate of interest	1.0 % p.a.
Analysis period	30 years
Yearly Maintenance	1 % of investment costs
Lifetime of all components	Analysis period
Electricity costs (incl. VAT)	Variable costs: 20 Rp./kWh
Increase of electricity costs	1.5 % p.a.

The first part of this Section provides the investment cost for all components. The second part consists of the calculation of the levelized cost of heat for all sources as a function of the heat demand and ice storage volume.

4.3.1 Cost assessment of individual components

The components included in our estimations are: i) solar thermal collectors ii) air-to-water heat exchanger with ventilator and iv) ice storage. For ice storages we use two types of costs: 1) **ice-on-coil** where the cost of vessels filled with capillary mats as available solution as considered, and 2) **ice slurry** where the cost of ice slurry technology with supercooling method to analyse the potential for future usages are considered. Since the ice slurry storages have no heat exchangers inside the vessel, conventional large scale storage tanks can be used. For this case, the cost of the required ice crystallizer is included too.

Cost of solar thermal collectors

The specific cost for the solar thermal field using uncovered selective collectors is about 400 CHF/m^2 for collector fields targeting areas above 20 000 m^2 gross area, which is a common range of DH systems simulated here.

$$\text{Cost for installed uncovered selective collectors (CH)} = 400\,\text{CHF/m}^2 \tag{18}$$

Cost of AWHX

The specific cost for ambient air to water heat exchanges are estimated to be:

$$\text{Cost for installed large scale AWHX} = 225\,\text{CHF/kW (@5K temperature difference)} \tag{19}$$

where about one third of the cost are coming from the device itself, another third from the connection to the system and the last third for planning and installation.

Cost of ice-on-coil storages

The cost of state-of-the-art ice-on-coil storage is split into two parts, namely the casing and the heat exchangers. It is assumed that the casing is made either of a steel container or concrete vessel where excavation is considered to accommodate the ice storage underground. Fig. 60 shows the cost of the storage's concrete casing including excavation for volumes up to 12 000 m^3. Our cost calculation is based on a piece-wise linear model separated into three sections.

All the points in Fig. 60 were collected from different offers and publications. We divided these data into three sets, from which we got the following a piece-wise linearization model:

$$\begin{aligned}
\text{Cost of concrete storages } [CHF] &= 21\,967 + 325 \cdot \text{V}_{\text{ice}}\,[\text{m}^3] \text{ for V}_{\text{ice}} \leq 1\,263\,\text{m}^3 && (20)\\
&= 93\,534 + 191.36 \cdot \text{V}_{\text{ice}}\,[\text{m}^3] \text{ for } 1\,263\,\text{m}^3 \geq \text{V}_{\text{ice}} \leq 2\,462\,\text{m}^3 && (21)\\
&= 297\,390 + 108.59 \cdot \text{V}_{\text{ice}}\,[\text{m}^3] \text{ for } 2\,462\,\text{m}^3 \geq \text{V}_{\text{ice}} \leq 12\,000\,\text{m}^3 && (22)
\end{aligned}$$

For the heat exchangers inside the storage, several offers were collected for capillary mats with a price range that depends on the manufacturer. The cost including installation and engineering is provided as a function of the ice storage volume including the uncertainty due to different offers:

$$\text{cost Hx ice storage} = 450^{+50}_{-50}\,\text{CHF/m}^3 \tag{23}$$

Cost of ice slurry storages

For the ice slurry, we have used the cost associated with pit storages for the vessel costs. For the crystallizer, the costs depend on the needed power and not on the storage volume. Pit storage cost can be used for ice slurry vessels because the slurry technology does not need heat exchangers to keep the ice under water. Thus, the vessel only needs to withstand the forces of water, as a conventional pit storage does. However, pit storages use in insulation that would not be necessary for ice slurry. Thus, costs could even be lower than estimated here. The same strategy explained for the concrete vessels has been used to estimate the cost of the pit storages. Results for two data sets have been plot in Fig. 61.

$$\begin{aligned}
\text{Cost of pit storages } [CHF] &= 292\,628 + 59.497 \cdot \text{V}_{\text{ice}}\,[\text{m}^3] \text{ for V}_{\text{ice}} < 36\,843\,\text{m}^3 && (24)\\
&= 2\,000\,000 + 13.156 \cdot \text{V}_{\text{ice}}\,[\text{m}^3] \text{ for V}_{\text{ice}} \geq 36\,843\,\text{m}^3 && (25)
\end{aligned}$$

The comparison between both storage vessel cost models is shown in Fig. 62 using the piece-wise linear models presented from both cases above. For ice slurry technology, the storage vessel does not need to be insulated

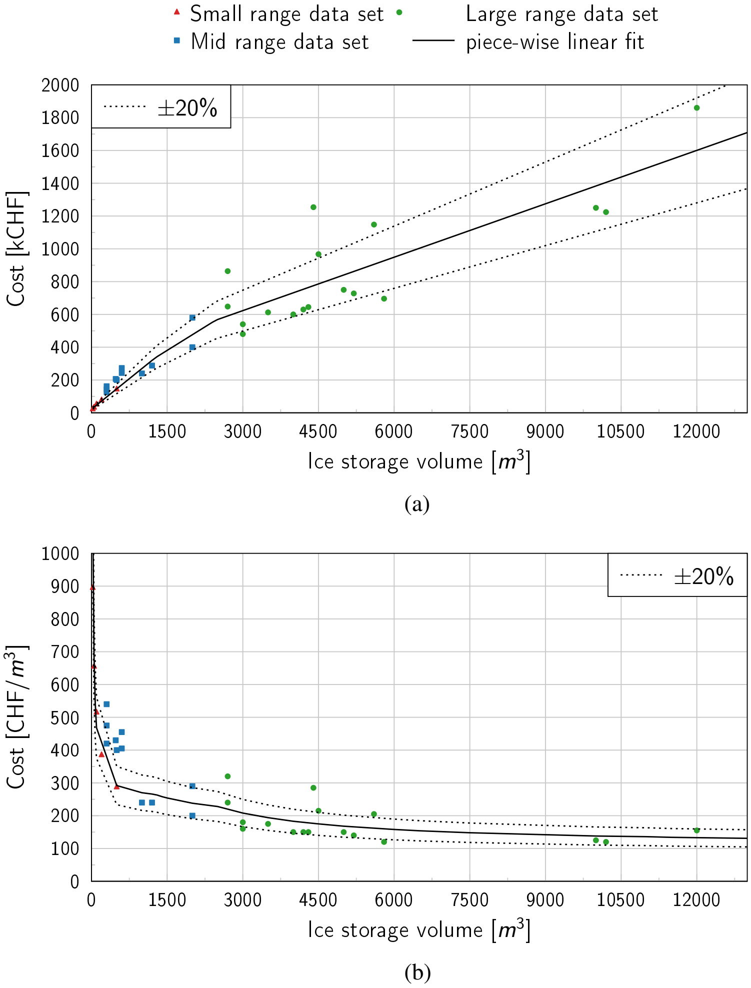

Figure 60: Costs of storage (concrete) casing including excavation as a function of storage volume. **a)** absolute cost, **b)** cost per m^3

leading to significantly overestimated costs for very small storages. Thus, to assess the cost of the ice slurry the lowest cost between the concrete and the pit storage will be used. As a simplification, the cost of concrete storage will be used for storage volumes $< 1400\,\mathrm{m}^3$, while the cost of pit will be used otherwise.

The cost used for the ice slurry vessel is then a combination of that of the concrete tank for small storages $\leq 1400\,\mathrm{m}^3$ and the cost for pit storages for volumes $> 1400\,\mathrm{m}^3$:

$$
\begin{aligned}
\text{Cost of ice slurry vessel } [CHF] &= 21\,967 + 325 \cdot \mathrm{V_{ice}}\,[\mathrm{m}^3] \text{ for } \mathrm{V_{ice}} \leq 1\,400\,\mathrm{m}^3 && (26)\\
&= 292\,628 + 59.497 \cdot \mathrm{V_{ice}}\,[\mathrm{m}^3] \text{ for } 1\,400\,\mathrm{m}^3 > \mathrm{V_{ice}} < 36\,843\,\mathrm{m}^3 && (27)\\
&= 2\,000\,000 + 13.156 \cdot \mathrm{V_{ice}}\,[\mathrm{m}^3] \text{ for } \mathrm{V_{ice}} \geq 36\,843\,\mathrm{m}^3 && (28)
\end{aligned}
$$

For ice slurry technology with supercooling method, an in-stream ice crystallizer is also necessary, which is a device that scales with the power unit for discharging the storage (solidification process). For melting the ice storage, the crystallizer is not necessary. Ice is melted directly by flowing warm water inside the storage achieving a very high extraction power due to the large amount of surface area between slurry particles and

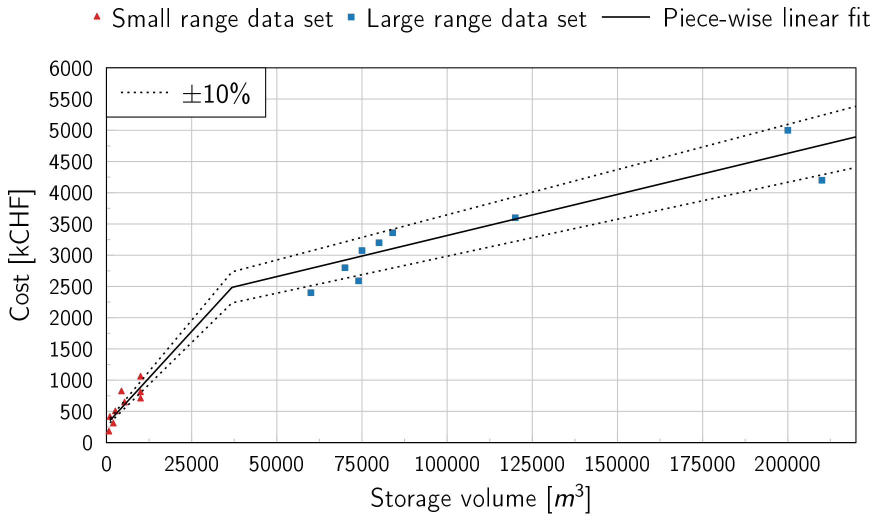

(a)

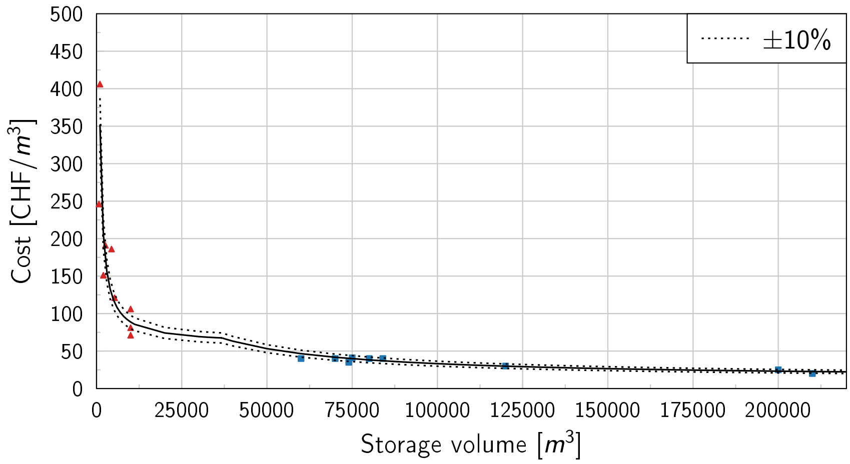

(b)

Figure 61: Costs of pit storage including excavation as a function of storage volume . **a)** absolute costs, **b)** costs per m^3

flowing water. For very large powers in the range of MW, the cost of the ice crystallizer is assumed to be:

$$\text{Cost of in-stream ice crystallizer} = 75^{+25}_{-25}\ \text{CHF/kW} \tag{29}$$

The ice crystallizer should be sized using the nominal heat demand power, which is linked to the source power for cases such as WWTP or CTS. However, for small ice storages $< 2000\,\text{m}^3$ such as those used for WWTP, the nominal source power of e.g. 6 MW is too large for the volume of the storage. The simulations in this report have been carried out using the ice-on-coil technology, in which the heat exchanger area and storage volume are inter-linked and therefore power and capacity are coupled. Thus, our simulations are carried out with a extraction power limited by the ice storage volume. Using well packed coils, an average extraction power of $3\,\text{kW/m}^3$ can be achieved. Thus, the ice crystallizer is sized as the minimum between the average extraction power as function of ice storage volume and the nominal power source. Summarising, the size of

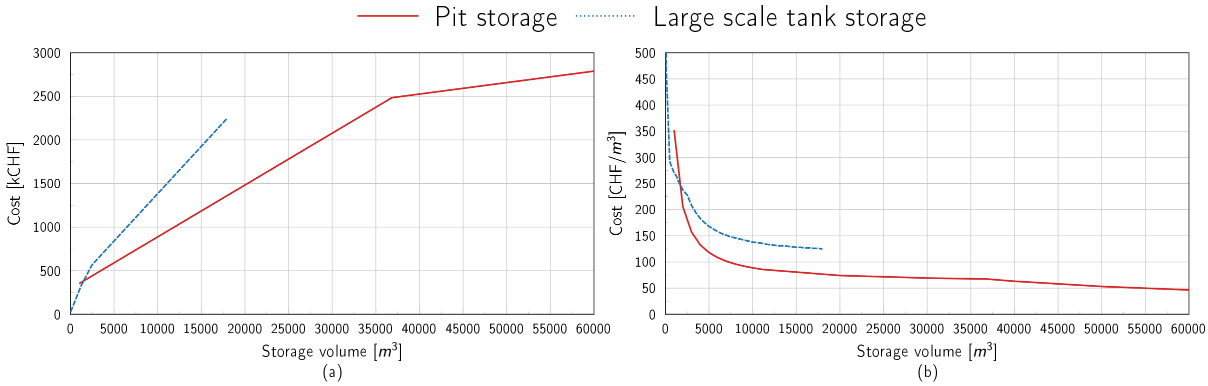

Figure 62: Costs of pit and large scale storages using the piece-wise linear models. **a)** absolute, **b)** per m^3

the in-stream ice crystallizer is obtained by:

$$\text{In-stream ice crystallizer size} = \min(3\ \text{kW/m}^3 \cdot \text{V}_{\text{ice}}, \text{kW}_{\text{nom,source}}) \tag{30}$$

4.3.2 Cost analysis results

Fig. 63 shows the levelised costs of heat over the system's life time for all the sources as a function of the additional heat demand that can be provided thanks to the use of the ice storage. For these calculations, we only consider the cost of the ice storage, the solar field, and the AWHX. The costs of the DH grid are the same for all cases and thus can be disregarded for relative comparisons. Moreover, the ice storage for all WWHS are used to extend the DH network. Thus, it is assumed that a DH network exist and has capacity to provide a higher heat demand, but the current source cannot provide higher demands unless it is possible to store energy either from a seasonal perspective or to cover short periods with more continuous cycling. For these cases, only the ice storage cost including installation and engineering is considered. For solar and air cases we can either consider these heat sources as a way to expand an existing DH network without the possibility or need to extend the existing source or simply consider that the whole DH network is supplied by these renewable heat sources only. In our studies, only the latter case has been simulated. Thus, investment cost of the AWHX and solar field are included in their corresponding cases.

Fig. 63a shows the costs associated to the integration of the ice-on-coil ice storage technology into the DH network for several heat sources.

Integrating an ice storage into an existing WWHS, when the source is large enough or properly sized (e.g. 6 MW for our heat demand cases), allows a grid expansion by up to 12.5 GWh, which enables to deliver between 1.7 to 2 times more demand that what can be covered without an ice storage, at an annualised cost of 5 Rp./kWh to 6 Rp./kWh or 50 CHF/MWh to 60 CHF/MWh. In these cases, the ice storage is mainly used to cover winter peaks when the power of the source is unable to deal with them. However, when the source is too small, e.g. WWTP at 3 MW, the costs increase to the range of 20 Rp./kWh to 22 Rp./kWh.

For the simulated AWHX cases, the costs increase with the heat exchanger size. The cost using an AWHX with a size of 2000 FLH is clearly higher than those using 1000 FLH and 1500 FLH for the ice-on-coil technology. Cost differences between the 1000 FLH and 1500 FLH are relatively small with levelised heat costs in the range of 8.5 Rp./kWh to 9.5 Rp./kWh. The costs remain relatively constant with increasing demand.

For the simulated solar cases, we can observe that the costs decrease as the solar field increases. Perhaps, costs could be reduced further by increasing the solar field above 2 m^2/MWh, where heat costs are in the range of 11 Rp./kWh to 13 Rp./kWh. The costs tend to slightly increase with increasing demand.

Fig. 63b shows the costs associated with the ice slurry storage technology. For these cases, the storage size has been increased to consider the lower $M_{\text{fice,max}}$ of 0.5 possible for the slurry case in comparison to the

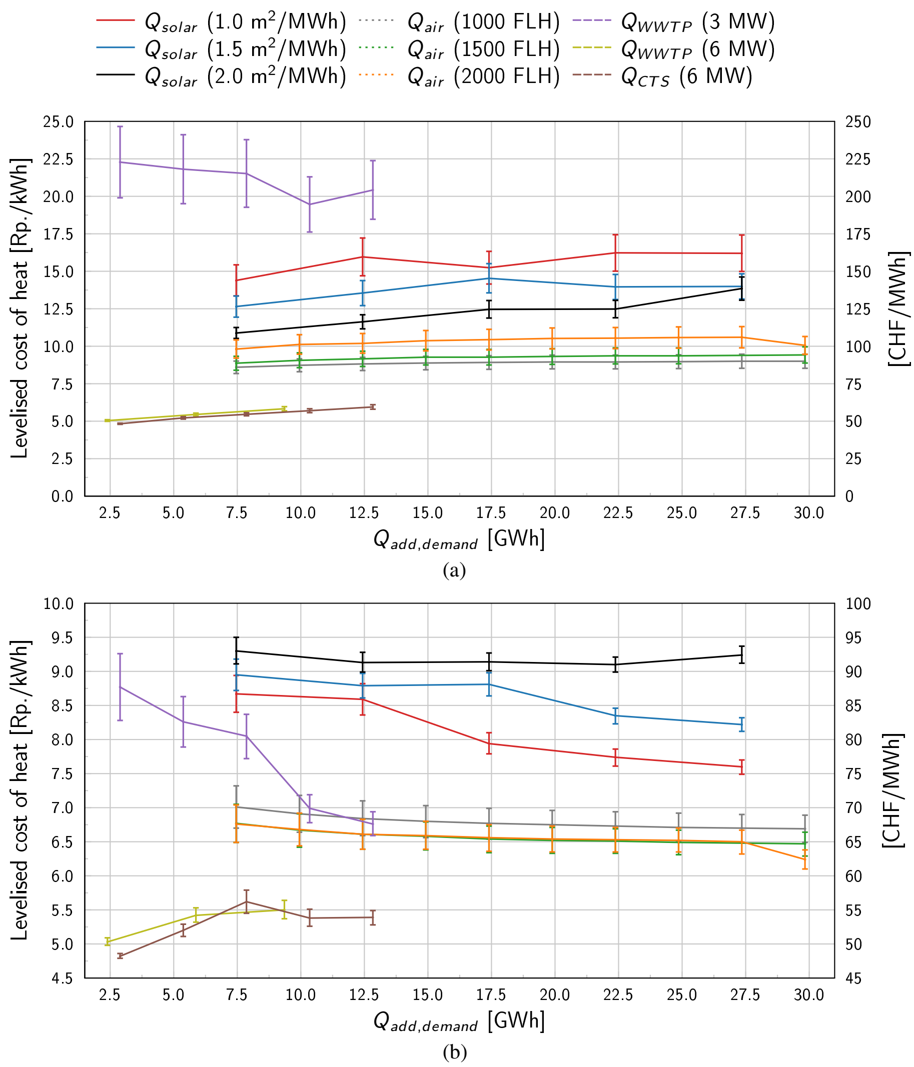

Figure 63: The levelised cost of heat for the different renewable heat sources. Costs include uncertainties and are displayed as a function of the additional DH demand provided thanks to the use of **a)** conventional ice-on-coil and **b)** ice slurry storage technologies.

$M_{fice,max}$ assumed for the ice-on-coil of 0.8. Nevertheless, the levelised cost of heat decreases strongly when using an ice slurry for air and solar sources, where the ice storages are relatively larger than those needed for the WWHS of 6 MW.

The relationship between cost and solar field for the ice slurry case are reverted compared to ice-on-coil, i.e. cost increase by increasing collector field. The main difference between the two ice storage technology is the cost share of the ice storage respect to the total cost. For example, for 1 m^2/MWh and 27 GWh demand, the cost share of the ice storage is 24 % for the ice slurry and 78 % for the ice-on-coil respect to the total investment cost.

Fig. 64 displays the costs separately for each source including both ice slurry and ice-on-coil results on the same plot. In this plots it is easier to compare cost differences better between the two ice storage technologies. Costs for the cheapest solar case decrease from the 9.6 Rp./kWh - 13.8 Rp./kWh range to the 7.6 Rp./kWh - 9.4 Rp./kWh one when switching from ice-on-coil to ice slurry. In average, the ice slurry with supercooling

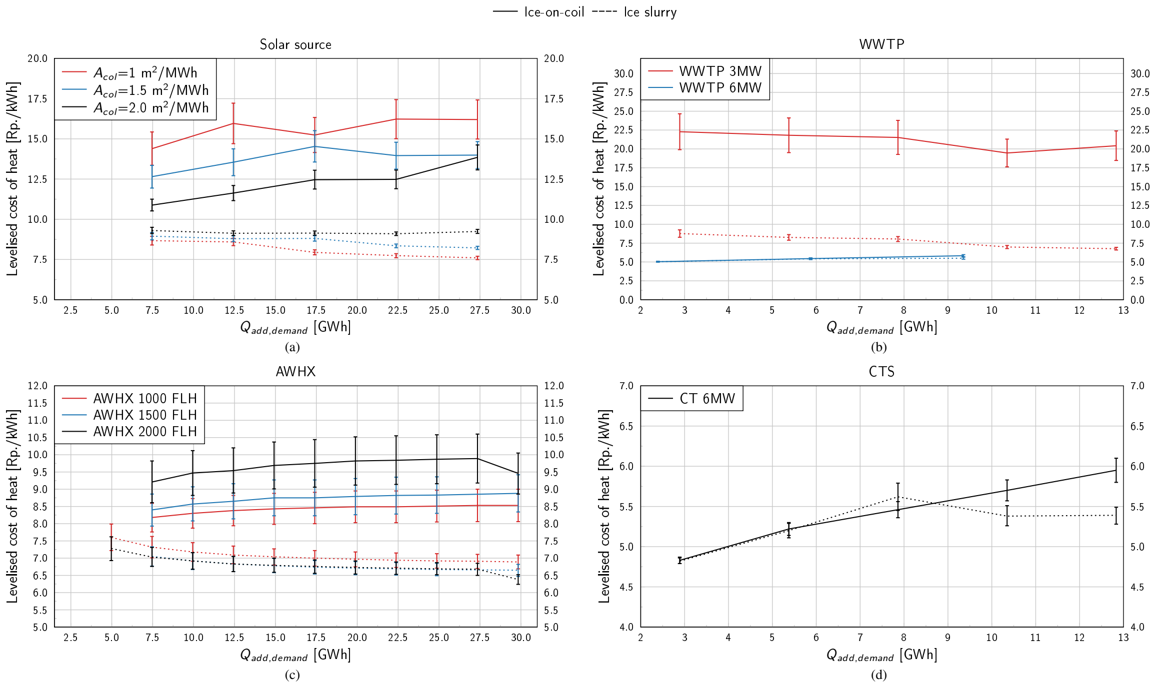

Figure 64: Comparison of the levelised cost of heat between slurry and ice-on-coil technologies as function of the additional heat demand for the different renewable heat sources: **a)** solar **b)** WWTP **c)** AWHX **d)** CTS.

technology can reduce the levelised heat cost by 32 % respect to the ice-on-coil for solar sources.

The average heat cost of the most economic AWHX size reduce from 8.7 Rp./kWh using an ice-on-coil to 6.9 Rp./kWh when employing an ice slurry. Averaging all results for the three AWHX sizes, the ice slurry technology can reduce cost by 24 % compared to ice-on-coil.

Cost of 3 MW WWHS are reduced by 61 % by using ice slurry technology, decreasing the average cost from 21.1 Rp./kWh to 7.8 Rp./kWh. Costs of the 6 MW WWHS cases are not significantly affected by the technology switch since the storage volumes are relatively small.

Fig. 65a) and c) displays the cost as a function of the specific ice storage latent volume. Results from Fig. 65a) shows that cost of ice-on-coil technology tends to follow a linear increase with increasing ice storage volume for solar and air sources. For clarity some overlapping values having the same $V_{\text{ice,lat}}$ have been omitted except two cases for the AWHX when switching from 1000 FLH to 1500 FLH around 0.6 m^3/MWh to show that cost remain similar regardless of the heat exchanger size. For the air source the linear trend is composed by the three AWHX sizes with larger heat exchangers sizes for smaller ice storage volumes. For the solar case the cost also increases linearly with ice storage volume. Higher storage volumes are necessary for lower solar fields. Thus, the points to compose the linear trend are formed by results using the three solar fields. The solar field of 2 m^2/MWh covers the range of ice storage volumes below 0.9 m^3_{lat}/MWh, the middle size of 1.5 m^2/MWh covers the range between 0.9 m^3_{lat}/MWh and 1.4 m^3_{lat}/MWh and the smallest collector fields of 1 m^2/MWh need ice storage volumes $>$ 1.5 m^3_{lat}/MWh.

Fig. 65c) shows that cost of ice slurry technology trends are difference from those obtained using the ice-on-coil. The costs tend to decrease with increasing ice storage volume. The costs for the solar source also show a kind of linear trend, but a linear fit would lead to less accurate fitting results due to several points moving away from the linear function. For the AWHX cases, the cost are linear for 1000 FLH and 1500 FLH, but for the 2000 FLH size, the cost do not follow a linear trend with increasing ice storage volume.

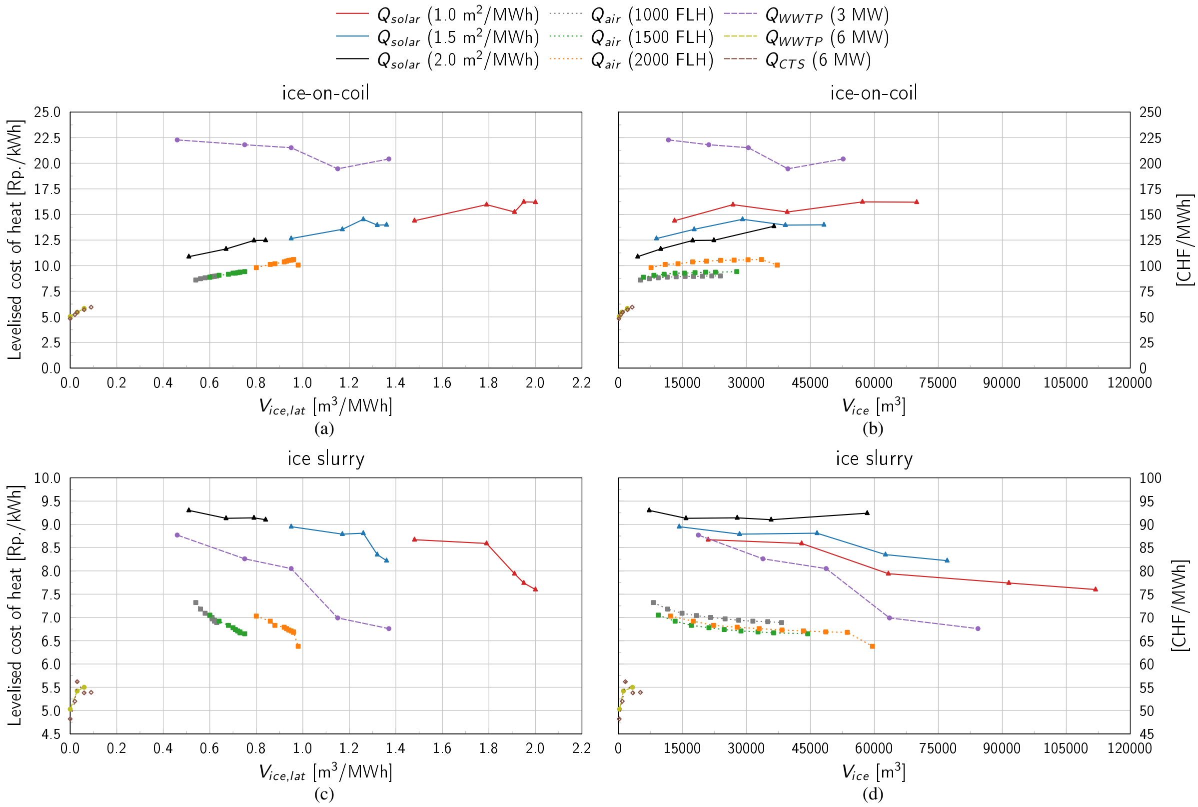

Figure 65: The levelised cost of heat as function of specific and absolute storage volume provided thanks to the use of ice storage technologies for the different renewable heat sources. **a)** and **b)** refer to conventional ice-on-coil and **c)** and **d)** refer to ice slurry technology.

Fig. 65b) and d) display the cost as a function of the absolute ice storage volume, where it can be observed the ice slurry cases need higher absolute volumes. The needs of ice storage capacity for WWTP 6 MW are significantly lower compared to the rest of heat sources leading to significant lower heat costs with absolute storage volumes $< 2050\,\mathrm{m}^3$ for ice-on-coil and $< 2600\,\mathrm{m}^3$ for ice slurry. For AWHX cases the ice storages range from $1.3 \times 10^5\,\mathrm{m}^3$ to $3.3 \times 10^6\,\mathrm{m}^3$. For solar cases absolute storages volumes range from $2.1 \times 10^5\,\mathrm{m}^3$ to $7 \times 10^6\,\mathrm{m}^3$ For the ice slurry cases absolute values are assumed to be 1.6 times larger than those from the ice-on-coil.

5 Conclusions

- **The open-source extensions to both TRNSYS/pytrnsys**[13] we have developed in this project simplifying the modelling of 5GDHC. An adaptation of the double pipe model and its parameterisation for non-insulated pipes was validated using measurement data from the FGZ network. The corresponding drag-and-drop features in the pytrnsys GUI simplify the creation of custom hydraulic diagrams using buried double pipes, and connections between legs of double pipes, or between double pipes and a set of single pipes. Moreover, it is now possible to solve mass flows in complex bidirectional network hydraulics. To shorten simulation times for such complex hydraulics, we introduced simple connector types to couple the network with sources or consumers. These simple types connect components hydraulically without the CPU cost of modelling pipes. These new features are now available to a growing community of pytrnsys users, simplifying the creation of DH network simulations (from standard networks to decentralised bidirectional 5DGHC networks).

- **A direct integration of an ice storage in a 5DGHC** network is possible when an anti-freeze heat transfer fluid is used in the network. The combination of ice storage with a water-based waste heat source also poses a challenge for frost-protected grids, because ice storage systems must naturally operate below the freezing point of water, while freezing of the waste heat source must be prevented. To integrate an ice store directly into a network, the return temperature of the DH must be several Kelvins below the freezing point. However, the outlet temperature of the storage tank is always raised close to the freezing point during operation. With re-circulation, the inlet temperature to the waste heat source can be kept above the freezing point as long as the ice store is not completely frozen. To do this, the ice store must be connected to the network centrally, before the waste heat source. The integration proposed here can be carried out without an additional central heat pump.

- **The integration of an ice storage allows a significant extension of the demand met by existing sources**. Water-based waste heat sources usually provide a relatively constant capacity throughout the year. However, since water should not be cooled below the freezing point, the extraction capacity is limited by the highest demand on cold winter days. By integrating an ice storage system, such power peaks can be covered, allowing significantly larger grids to be served with the same waste heat source. An additional pump by-passing the network and actively regenerating the ice storage allows the full capacity of a waste heat source to be used during periods of lower network demand. This means that the ice store can be regenerated much faster than with passive integration, which would only use the flow rate of the decentralised pumps. For WWHS, relatively small ice storage systems <0.15 m^3_{lat}/MWh can cover short-term power peaks of relatively small source powers (e.g. < 5000 full-load hours) for a very low share of DHW/SH of 0.1. For more common shares of DHW/SH >0.2, ice storages <0.05 m^3_{lat}/MWh can be used for power sources < 5000 full load hours. With these heat sources, the demand met by the DH grid can be doubled with an added cost around 5 Rp./kWh to 6 Rp./kWh when considering ice-on-coils technology. As an example, an ice storage volume of 2050 m^3 with a WWTP heat source of 6 MW was enough to extend the DH demand by 9.3 GWh (leading total demand of 26.3 GWh) at a cost of 5.8 Rp./kWh.

- **In combination with scalable sources like ambient air or solar thermal collectors, ice storage volumes of at least 0.6 m^3_{lat}/MWh are needed**. The combination of solar collectors or ambient air with an ice storage can cover the demand of a 5GDHC network at temperatures around 0 °C and higher for the whole year. In places where no other heat sources are available, these combinations represent an opportunity to provide renewable heat at a moderate cost. The specific ice storage volume needs of AWHX with 1000 FLH increase with the DH demand to an asymptotic value of 0.6 m^3_{lat}/MWh. For the solar cases, the asymptotic value using a collector field of 2 m^2/MWh is around 0.8 m^3_{lat}/MWh for DH demands > 18 GWh. For DH demands between 10 GWh to 18 GWh the ice storage volume range from 0.6 m^3_{lat}/MWh to 0.8 m^3_{lat}/MWh. Thus, if these two sources are generously dimensioned similarly sized ice storage tanks around 0.6 m^3_{lat}/MWh are required to provide full coverage in winter

[13] https://github.com/SPF-OST/pytrnsys_gui

at reference DH demands of 10 GWh. For a demand of 12.4 GWh, a solar source field with 24 860 m^2 needs an ice storage with a volume of 9900 m^3. For the same demand, an AWHX with an equivalent size of 1000 FLH, requires an ice storage of 9300 m^3. Systems based on solar thermal collectors will deliver DH demands up to 27 GWh at costs of around 9.6 Rp./kWh to 13.8 Rp./kWh. The combination of ambient air and ice storage leads to cost of around 8 Rp./kWh to 9 Rp./kWh.

- **Switching from ice-on-coil to ice slurry technology using the supercooling method can provide very large cost savings in the range of 25 % to 60 % for cases with large ice storages**. The use of ice slurry technology has been considered to assess the potential benefits of this promising technology being developed at our institute. Ice slurries have the benefit of eliminating the heat exchangers inside the vessel reducing cost significantly. However, due to the lower mass of ice that can be iced they are expected to be 1.6 times larger. Despite larger sizes, cost are reduced by 32 % for solar applications and by 24 % for air sources. Due to the low specific volumes for WWTP using a 6 MW source, the additional benefits of using an ice slurry storage are marginal. However, for WWTP of 3 MW, the cost reduction of the ice slurry raise up to 60 %. Basically, the larger the ice storage, the larger the benefit of switching from ice-on-coil to ice slurry. However, we advise caution when interpreting the cost of the ice slurry technology. First of all, cost of ice slurry are only valid for the supercooling technology and not for the state-of-the-art commercially available scraped-surface ice slurry devices. Moreover, the ice slurry technology with the supercooling method is still on development stage with cost savings and reliability still to be demonstrated in the field. Thus, despite its theoretical benefits, the ice-on-coil technology, which is very robust and mature, should be taken as reference for feasibility studies in the next five years.

6 National and international cooperation/Publications

The new extensions in TRNSYS/pytrnsys are shared with the pytrnsys community via publication on git. A validation of the uninsulated pipe model was presented at the Eurosun conference (Schubert et al., 2022). The project and the combination of ice storage with WWTP was also presented at the SPF Symposium Solar Energy and Heat Pumps (November 2, 2023, Rapperswil).

The project involves cooperation with several industrial partners. The main collaboration during 2023 was with EZL, which operates the Jona heating network, with whom we exchanged a lot of useful information and had fruitful discussions. Interim results from the project were repeatedly presented and discussed at meetings as part of the SWEET project "DeCarbCH" (within work package 3).

Cooperation is also taking place with SPF's own BigStoreDH project. In BigStoreDH, the extensions of pytrnsys developed here were used to simplify the simulation of classic heating networks. On the other hand, the methods for creating typical load profiles developed in BigStoreDH were used in this project. The extension of the pytrnsys GUI developed in the project for DH networks was announced both nationally (to the DeCarbCH partners) and internationally (at IEA-SHC Task 68).

References

Arenas-Larrañaga, M., Gurruchaga, I., Carbonell, D., and Martin-Escudero, K. (2024). Performance of solar-ice slurry systems for residential buildings in european climates. *Energy and Buildings*, 307:113965.

Buffa, S., Cozzini, M., D'antoni, M., Baratieri, M., and Fedrizzi, R. (2019). 5th generation district heating and cooling systems: A review of existing cases in Europe. *Renewable and Sustainable Energy Reviews*, 104:504–522.

Bédécarrats, J. P., Strub, F., Falcon, B., and Dumas, J. P. (1996). Phase-change thermal energy storage using spherical capsules: performance of a test plant. *International Journal of Refrigeration*, 19(3):187–196.

Caputo, P., Ferla, G., Belliardi, M., and Cereghetti, N. (2021). District thermal systems: State of the art and promising evolutive scenarios. A focus on Italy and Switzerland. 65:102579.

Carbonell, D., Battaglia, M., Daniel, D. P., and Haller, M. Y. (2017a). *Ice-Ex - Heat Exchanger Analyses for Ice Storages in Solar and Heat Pump Applications*. Institut für Solartechnik SPF for Swiss Federal Office of Energy (SFOE), Research Programme Solar Heat and Heat Storage, CH-3003 Bern.

Carbonell, D., Battaglia, M., Philippen, D., and Haller, M. (2018). Numerical and experimental evaluation of ice storages with ice on capillary mat heat exchangers for solar-ice systems. *International Journal of Refrigeration*, 88:383 – 401.

Carbonell, D., Daniel, D. P., and Haller, M. Y. (2017b). *Slurry-Hp - A feasibility study on the use of a super-cooling ice slurry heat pump for solar heating applications*. Institut für Solartechnik SPF for Swiss Federal Office of Energy (SFOE), Research Programme Heat Pumps and Refrigeration, CH-3003 Bern.

Carbonell, D., Granzotto, M., Battaglia, M., Philippen, D., and Haller, M. Y. (2016a). Experimental investigations of heat exchangers in ice storages for combined solar and heat pump systems. In *11th ISES EuroSun Conference*, Palma (Mallorca), Spain. International Solar Energy Society (ISES).

Carbonell, D., Philippen, D., Dudita, M., Schmidli, J., Schubert, M., and Erb, K. (2020). *Slurry-Hp II - Development of a supercooling ice slurry heat pump concept for solar heating applications*. Institut für Solartechnik SPF for Swiss Federal Office of Energy (SFOE), Research Programme Heat Pumps and Refrigeration, CH-3003 Bern.

Carbonell, D., Philippen, D., Granzotto, M., and Haller, M. Y. (2016b). Simulation of a solar-ice system for heating applications. System validation with one-year of monitoring data. *Energy and Buildings*, 127(0):846 – 858.

Carbonell, D., Philippen, D., and Haller, M. Y. (2016c). Modeling of an ice storage buried in the ground for solar heating applications. Validations with one year of monitored data from a pilot plant. *Solar Energy*, 125:398–414.

Carbonell, D., Philippen, D., Haller, M. Y., and Frank, E. (2015). Modeling of an ice storage based on a de-icing concept for solar heating applications. *Solar Energy*, 121:2–16.

Carbonell, D., Schubert, M., and Neugebauer, M. (2021). *Big-Ice - Assessment of solar-ice systems for multi-family buildings*. Institut für Solartechnik SPF for Swiss Federal Office of Energy (SFOE), Research Programme Solar Heat and Heat Storage, CH-3003 Bern.

Carbonell, D., Shubert, M., Frandsen, J. R., Erb, K., Laib, L., and Munari, M. (2022). Development of supercoolers for ice slurry generators using icephobic coatings. *Internationa Journal of Refrigeration*, 144:90 – 98.

Gurruchaga, I., Carbonell, D., Arenas, M., Anton, X. P., and Alonso, L. (2023). TRI-HP Deliverable D7.10 - Potential benefits of TRI-HP systems around Europe. Technical report, SPF Institute for Solar Technology, Eastern Switzerland University of Applied Sciences (OST).

Haller, M. and Ruesch, F. (2019). Fokusstudie "Saisonale Wärmespeicher - Stand der Technik und Ausblick".

Hangartner, D. and Ködel, Ködel, K. (2021). Liste "Thermische Netze". Technical Report Energie Schweiz.

Hangartner, D., Ködel, Ködel, K., Mennel, S., and Sulzer, M. (2018). Grundlagenpapier Thermische Netze. Technical Report Hochschule Luzern.

Kauffeld, M., Wang, M. J., Goldstein, V., and Kasza, K. E. (2010). Ice slurry applications. *International Journal of Refrigeration*, 33(8):1491–1505.

Kozawa, Y., Aizawa, N., and Tanino, M. (2005). Study on ice storing characteristics in dynamic-type ice storage system by using supercooled water.: Effects of the supplying conditions of ice-slurry at deployment to district heating and cooling system. *International journal of refrigeration*, 28(1):73–82.

MacPhee, D. and Dincer, I. (2009). Thermal modeling of a packed bed thermal energy storage system during charging. *Applied Thermal Engineering*, 29(4):695–705.

Nussbaumer, T., Thalmann, S., Hurni, A., and Mennel, S. (2021). Faktenblatt Thermische Netze.

Nussbaumer, T., Thalmann, S., Jenni, A., and Ködel, J. (2017). Planungshandbuch Fernwärme. Technical report.

Philippen, D., Haller, M. Y., Logie, W., Thalmann, M., Brunold, S., and Frank, E. (2012). Development of a heat exchanger that can be de-iced for the use in ice stores in solar thermal heat pump systems. In *Proceedings of EuroSun*, Rijeka and Opatija, Croatia. International Solar Energy Society (ISES).

Ruesch, F. and Haller, M. (2022). Jahresbericht 2022, bigstoredh. Technical report.

Santa, G. D., Peron, F., Galgaro, A., Cultrera, M., Bertermann, D., Mueller, J., and Bernardi, A. (2017). Laboratory Measurements of Gravel Thermal Conductivity: An Update Methodological Approach. *Energy Procedia*, 125:671–677.

Schubert, M., Neugebauer, M. J., Birchler, D., Ruesch, F., and Carbonell, D. (2022). Buried Twin Pipe Model Validation for System Simulations of Ice Storage Tanks in 5GDHC networks. In *EuroSun 2022 Proceedings (submitted)*, Kassel, Germany. International Solar Energy Society.

Sres, A. and Nussbaumer, B. (2014). Weissbuch Fernwärme Schweiz - VFS Strategie.

A Appendix

A.1 Re-validation of double pipe type and optimal parameters

In the course of the project, after the validation of the double pipe type but before starting the simulations of the full DH network a "bug" (i.e. a software error) was discovered in the Fortran code of the double pipe type. This error was corrected and the simulations whose results are discussed in this report were conducted using the corrected version. However, the re-validation of the type with the correction included and the determination of the optimal parameters with regards to the measured data provided by our partners was not done until after the simulations of the whole DH network. A re-evaluation resulted in similar parameters and we expect only minor influences on the interaction of the pipe with the ground and thus a negligible influence on the overall results. However, *the parameters used in this project and reported in table 3 are not the parameters that we recommend using for future simulations.*

Instead, the following parameters are recommended:

Description	Symbol	Value	Unit
Inner pipe diameter	$d_{p,inner}$	0.4028	m
Outer pipe diameter	$d_{p,outer}$	0.429	m
Thermal conductivity of pipe material	k_p	140	kJ /(h m K)
Centre-to-centre spacing of pipes	l_{c2c}	1.37	m
Diameter including casing	d_{casing}	1.800	m
Thermal conductivity of casing	k_{casing}	20	kJ /(h m K)
Thickness of pipe insulation	-	0 (i.e. not insulated)	m
Buried depth	l_{depth}	1.27	m
Thermal conductivity of soil	k_{soil}	7	kJ /(h m K)
Heat capacity of soil	-	1.0	kJ /(kg K)
Density of ground	-	1800	kg /m^3
Fluid	-	Water	-

Table 5: Parameters used for double pipes

Figure 66 shows the geometry of the double pipe type with regards to the parameters in table 5.

For most of the parameters, we propose thus very similar values as in the first evaluation. However, the values for the centre-to-centre spacing of the pipes and the thermal conductivity are noticeably different from the values in table 3. These two deviations compensate each other and lead to a similar thermal resistance between the two pipes. This deviation from physically realistic parameters is due to geometric constraints of the TRNSYS type which had to be overcome and were not accounted for in the previous validation. For the purposes of computing the thermal conductance from the fluid carrying pipes to the soil via the casing, the double pipe TRNSYS TESS type lumps the two fluid carrying pipes together. This "lumped pipe" is assumed to have an "equivalent diameter" of $d_{p,equiv} = \sqrt{2 d_{p,outer} l_{c2c}}$. The lumped model is illustrated in figure 67. The casing layer thickness is then defined by

$$l_{casing} = d_{casing} - d_{p,equiv} \tag{31}$$

At the same time, the TRNSYS type enforces the following constraint:

$$d_{casing} \geq d_{p,outer} + l_{c2c} \tag{32}$$

Plugging the inequality 32 into equation 31 we arrive at the following inequality:

$$l_{casing} \geq d_{p,outer} + l_{c2c} - d_{p,equiv} \tag{33}$$

In FGZ's network the centre-to-centre pipe spacing is around 0.77 m and the casing layer thickness around 0.2 m.

The right hand side of inequality 33 computes to 0.39 m which is already greater than the real casing layer width of 0.2 m. Hence, due to the TRNSYS type's geometric constraints it cannot not directly represent the desired geometry that we wanted to model.

We set d_{casing} to the minimum $d_{p,outer} + l_{c2c}$. Since this will lead to a layer thickness different from the desired thickness of 2 m the thermal conductivity of the casing needs to be converted to an equivalent conductivity for a casing layer thickness of 2 m, to be comparable to, e.g., literature values.

The following formula is used to transform the casing conductivity used in the simulation k_{casing} for a thickness l_{casing} as defined in equation 31 to a "reference conductivity" $k_{casing,ref}$ at the "reference layer thickness" of $l_{casing,ref} = 0.2$ m:

$$k_{casing,ref} = k_{casing} \frac{\log(1 + l_{casing,ref}/d_{p,equiv})}{\log(1 + l_{casing}/d_{p,equiv})} \tag{34}$$

Computing the corresponding reference conductivity for the values in table 5 we find a value of 6.69 kJ/(h m K) which is not dissimilar to the value given in table 3.

To find the optimal values for the parameters in table 5 which minimised the root mean square (RMS) error of the monthly pipe losses, the heat conductivity of the pipe mantles, the casing and the soil and the centre-to-centre spacing were varied. The simulated losses obtained with the parameters given in table 5 are shown together with the measured losses in figure 68. It has to be noted here that uncertainty of the temperature measurements, and therefore also the measured losses, is quite high (on the order of 0.5 K). The relative RMS error over the whole year and both pipes in figure 5 was found to be 33%.

A.1.1 Outlook

Varying the centre-to-centre pipe spacing (l_{c2c}) at the same time as the thermal conductivity of the casing (k_{casing}) might not have been necessary as varying the one can counteract the effect of varying the other. In addition, because the casing conductivity is converted to a reference conductivity anyway, it would be more straight-forward to keep l_{c2c} at its true value of 0.77 m but vary k_{casing} more finely.

Another option would be to replace the constraint 32 with the possibly more meaningful

$$d_{casing} \geq d_{p,equiv} \tag{35}$$

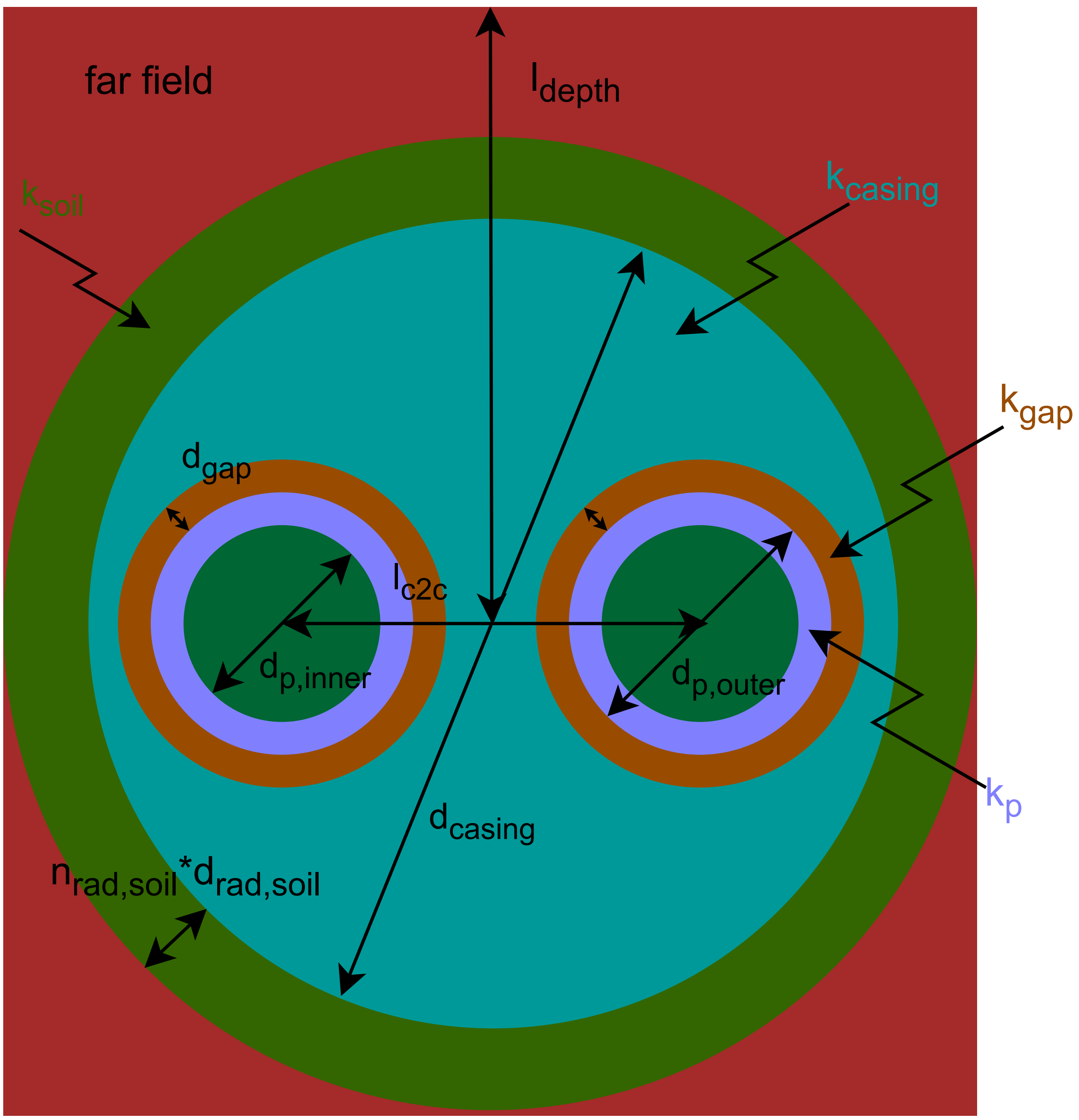

Figure 66: Geometry and parameters of double pipe model.

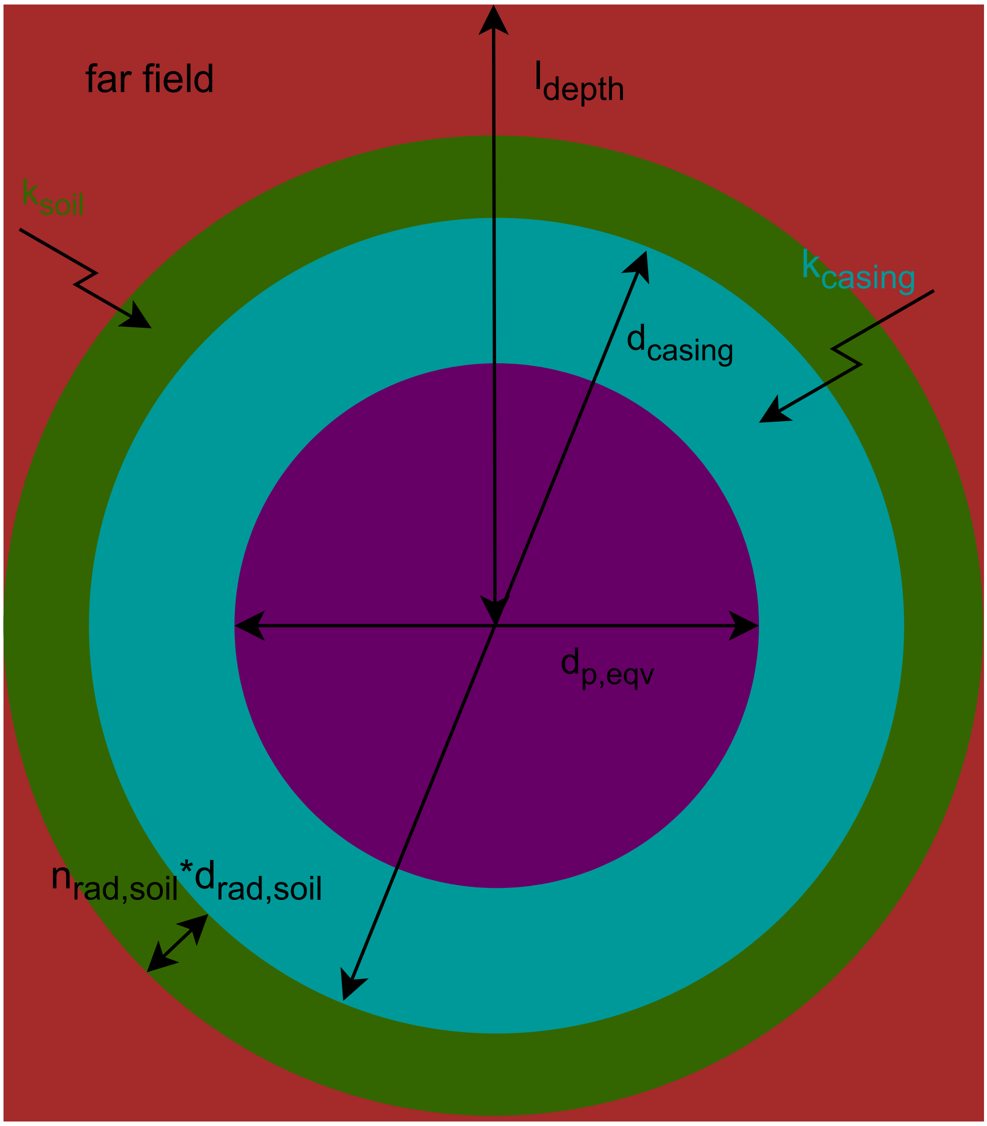

Figure 67: Geometry of the double pipe model with regards to the thermal conductance of the lumped-together pipes towards the soil.

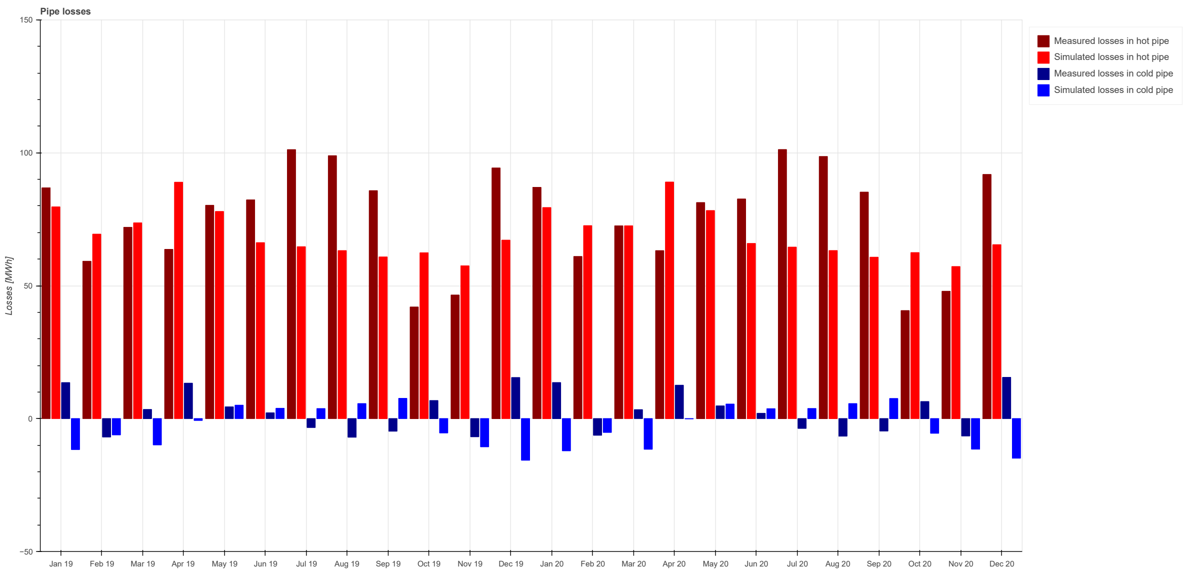

Figure 68: Measured and best matching simulated losses with the new parameter set.